JPL Publication 93-31

Flight- and Ground-Test Correlation Study of BMDO SDS Materials: Phase I Report

Shirley Y. Chung
David E. Brinza
Timothy K. Minton
Albert E. Stiegman
James T. Kenny
Ranty H. Liang

December 1993

Prepared for

Ballistic Missile
Defense Organization

Through an agreement with

National Aeronautics and
Space Administration

by

Jet Propulsion Laboratory
California Institute of Technology
Pasadena, California

The research described in this publication was carried out by the Jet Propulsion Laboratory, California Institute of Technology, and was sponsored by the Ballistic Missile Defense Organization (BMDO) through an agreement with the National Aeronautics and Space Administration.

ABSTRACT

The NASA Evaluation of Oxygen Interactions with Materials-3 (EOIM-3) experiment served as a testbed for a variety of materials that are candidates for Ballistic Missile Defense Organization (BMDO) space assets. The materials evaluated on this flight experiment were provided by BMDO contractors and technology laboratories. A parallel ground exposure evaluation was conducted using the FAST atomic-oxygen simulation facility at Physical Sciences, Inc. The EOIM-3 materials were exposed to an atomic oxygen fluence of approximately 2.3 x 10^{20} atoms/cm^2. The ground-exposed materials' fluence of 2.0 - 2.5 x 10^{20} atoms/cm^2 permits direct comparison of ground-exposed materials' performance with that of the flight-exposed specimens. The results from the flight test conducted aboard STS-46 and the correlative ground exposure are presented in this publication.

ACKNOWLEDGEMENTS

The authors appreciate the support received for this work from Lt. Col. Michael Obal, who obtained funding for this activity as part of the Space Environment and Effects Program of the Ballistic Missile Defense Organization (BMDO) Innovative Science and Technology Directorate's (DTI's) Materials and Structure Program. We also acknowledge Dr. Lubert J. Leger, Branch Chief, Materials Directorate at NASA Johnson Space Center, for providing space on the Evaluation of Oxygen Interactions with Materials Experiment-3 (EOIM-3) platform for this BMDO Experiment.

The authors would like to thank all the BMDO EOIM-3 co-investigators for their participation and valuable contributions to this experiment. Special thanks go to Brian Blakkolb and his team at TRW; Tim Gillespie, Robert Wendt, and their Martin Marietta team; and Linda Johnson and her Naval Air Warfare Center (NAWC) colleagues for their excellent work.

Special thanks go to the following JPL employees: James Soldi for all his assistance in making this program a success, Daniel Taylor for advice on thermal vacuum conditioning and Richard Vasquez in producing the numerous ESCA spectra.

TABLE OF CONTENTS

TABLE OF CONTENTS (continued)

TABLE OF CONTENTS (continued)

Tables | Page

TABLE OF CONTENTS (continued)

Figures | Page

Appendices

1.0 EXECUTIVE SUMMARY

A group of 82 strategic materials of relevance to the Ballistic Missile Defense Organization (BMDO) was tested to determine material performance and reliability under hyperthermal atomic oxygen (AO) exposure characteristic of a low-Earth-orbit (LEO) space environment. In this first phase of what will be a comprehensive testing and evaluation program, both ground-based testing and exposure in space aboard NASA's Evaluation of Oxygen Interactions with Materials Experiment-3 (EOIM-3) were carried out.

The experimental data obtained from this program have allowed an assessment of the performance and longevity characteristics of a number of important but not previously flight qualified materials. In general, a majority of the materials survived the AO environment with their performance tolerances maintained for the duration of the exposure. Optical materials, baffles, and coatings performed extremely well as did most of the thermal coatings and tribological materials. The radiator, threat shielding, and structural materials showed significant degradation for a few candidate materials. Notably, many of the coatings designed to protect against AO erosion of sensitive materials performed this function well.

The results obtained from both the flight and ground-based exposure, for a given material, were correlated and used to devise a ground-based testing protocol. This protocol will permit future materials to be assessed in a rapid, cost-effective manner by ground-based testing. Finally, all data collected in these experiments will be incorporated in a database to assist in future design processes.

2.0 INTRODUCTION

This report describes the space flight and ground-based elements of a recently completed AO experiment. It contains the data generated from 82 samples and provides some general discussion, conclusions, and recommendations. The experiment was a cooperative effort between JPL and nineteen industry and government agency organizations with each organization performing its own functional test(s) and providing data to JPL for insertion into the BMDO Space Environments and Effects (SEE) database. Their executive summaries are included in Appendix A of this report. Final reports from the co-investigators and photographs of all the materials are archived at JPL.

The general conduct of the experiment is shown in the flow chart of Figure 1. The nineteen organizations involved in the experiment provided test materials for both the flight and ground-based elements. They performed the bulk of the laboratory evaluations of material properties to determine the extent of interaction of the materials with the AO environment. JPL integrated the materials into the space flight mission and directed the ground-based exposure. JPL also performed some pre- and post-exposure characterization of the materials. The samples were separated into ten material classes and their experimental results and discussions are contained in Section 3.8.

2.1 Background

BMDO initiated a SEE Program in fiscal year (FY) 1989 to address technology issues and voids associated with deploying and operating Space Defense System (SDS) assets in the natural space environment. The objectives of the program are to (1) define and prioritize the SEE technology issues and voids that represent risk to the long duration operation of SDS assets in space, (2) provide access to space for SDS systems developers to generate space heritage for new materials, (3) develop design data for development of SDS systems, and (4) capture the design data and maintain it in a database accessible by spacecraft developers.

A secondary objective of the program is to start the methodical development of ground-based testing protocols. The protocols are meant to reduce and eventually eliminate the aerospace industry's dependency on space-flight testing of materials. The ground-based testing is to be an affordable alternative to expensive space-flight testing.

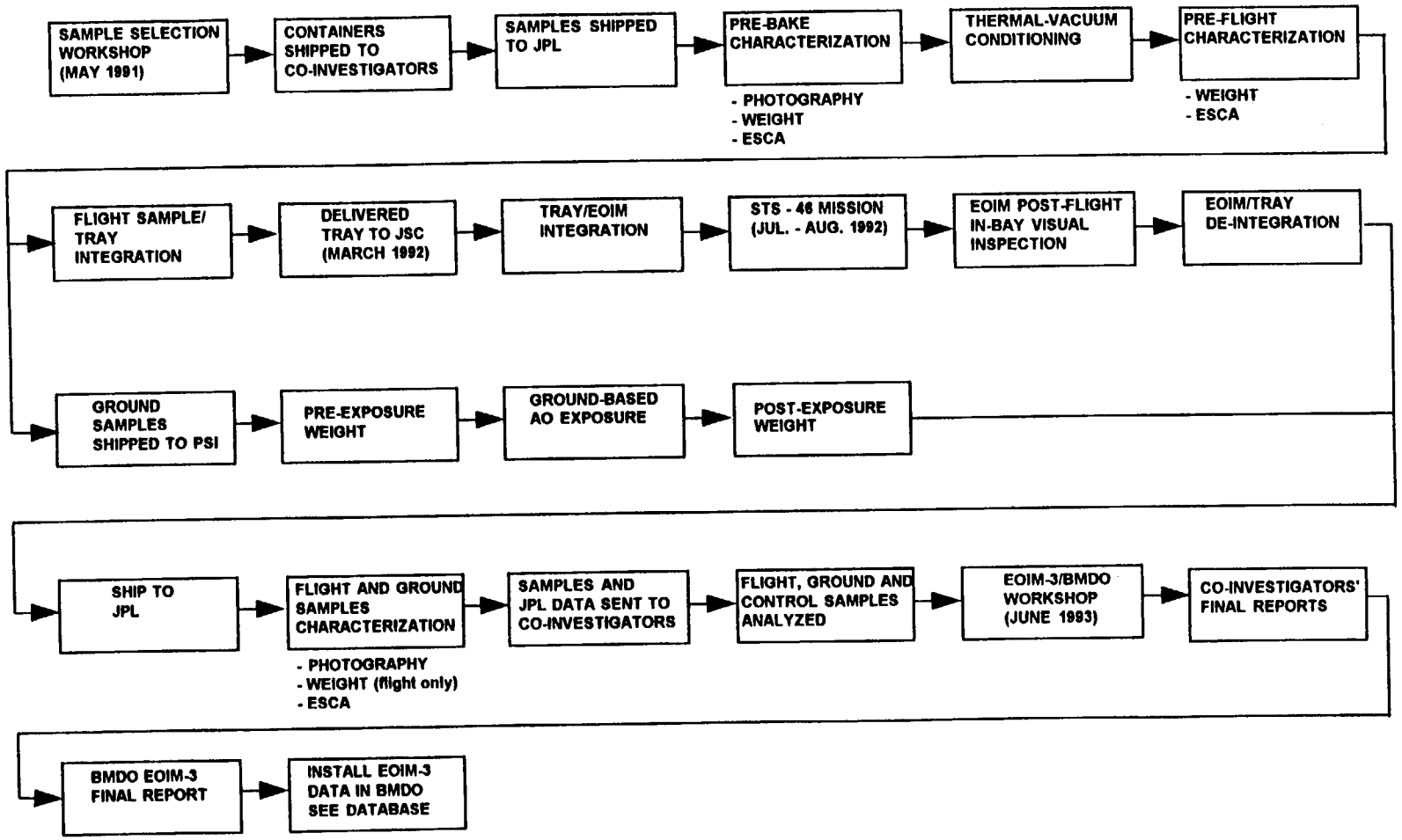

Figure 1. EOIM-3 sample-flow diagram.

To meet the SEE Program objectives, a series of experiments has been planned to coordinate flight opportunities with complementary ground-based testing. The first phase of this program is made up of the recently completed EOIM-3 flight experiment and concomitant ground-based testing. Upcoming flight opportunities which will constitute the other phases of this program include:

- Phase II. MATLAB, Wake Shield facility. Scheduled launch date: January 1994.
- Phase III. Space Testing Experiment Platform (STEP-3)/Space Active Modular Materials Experiments (SAMMES). Scheduled launch date: October 1994.
- Phase IV. Shuttle Pallet Satellite (SPAS-3)/Materials Degradation Experiment (MDE). Scheduled launch date: March 1995.

This report summarizes the results of Phase I of this program. The aim of Phase I, the EOIM-3 experiment, was not only to characterize specific materials for the Brilliant Pebbles (BP) and the Neutral Particle Beam Programs, but to provide a controlled comparison of material degradation in space versus a ground-based facility. EOIM-3 is the first experiment to provide an opportunity to correlate flight and ground-based AO effects with identical sets of materials. The correlation of the results provided information necessary for the assessment of ground-based AO testing. A preliminary ground-based atomic oxygen testing protocol, planned to be published in January 1994, relies on a proven, straightforward correlation between space- and ground-based data to produce a valid ground-based test. As the protocol matures in the future, development activities will be able to quickly evaluate AO interactions with new materials and components under accelerated conditions.

Ground-based testing will also allow investigators to perform in situ measurements prior to, during and after AO exposure. Flight experiments, without the aid of expensive monitoring systems, provide only a look at the end-of-mission effects. Samples returned to laboratories for evaluation are exposed to the terrestrial atmosphere which can alter or conceal AO effects on the materials.

In addition, ground-based exposures provide a capacity for accelerated testing to simulate a long duration mission. Today, short duration flight experiments conducted in the lower realm of LEO ($\leq$250 km) are able to expose materials to the equivalent of 1 to 3 years of fluence at higher LEO altitudes ($\geq$350 km). Since short duration is the mission extent that is typically

available to co-investigators, the effects must be extrapolated from the accelerated 1 to 3 year results to predict 5, 10, 15, or 20 year mission end-of-life properties.

Since hyperthermal AO effects were first discovered on early Shuttle flights, AO interactions have been extensively investigated. These investigations primarily focused on performance evaluation of selected materials and quantified the spatial and temporal AO environments. As a result, a wealth of AO performance data exists on state-of-the-art materials. Several reliable AO models, such as the Electrical Power System Analysis Tool (EPSAT), exist and are available for predicting AO effects during LEO missions. But since the time of AO interaction discovery, no programs have specifically attempted to develop a ground-based facility test procedure to duplicate LEO AO conditions, interactions, and effects. Therefore, no reliable ground-based test procedure exists. As new materials develop, their AO performance has to be evaluated by means of space exposure to obtain reliable design data. As a result, the need exists for a ground-based test procedure as an affordable alternative to space testing.

2.2 Objectives

The objectives of the BMDO-Phased AO Experiments are to:

- develop engineering design data for long duration application of selected SDS candidate materials in the natural LEO environment
- provide access to space and ground-based facilities in order for SDS developers to evaluate new candidate materials for SDS applications
- make the experiment's scientific and engineering data available to all SDS developers
- correlate the experiment's flight and ground-based data and make them available for development of a ground-based testing protocol
- make the experiment's engineering data available for integration into a desktop analysis tool

2.3 Scope

The BMDO-Phased AO Experiments involve the exposure of selected materials to hyperthermal atomic oxygen in space flight and in a ground-based facility. The space- and ground-based AO exposures are conducted with identical sets of materials. The scope of the work covered by the task includes:

- the space-flight and ground-based AO exposure of SDS candidate materials
- characterization of the selected materials before and after AO exposure
- the analysis of exposure results to determine AO effects on the selected materials
- the correlation of flight and ground-based AO exposure effects

The 82 materials listed in Table 1 constitute the materials evaluated by the experiment.

2.4 Approach

NASA provided a tray to the BMDO SEE Program for conducting experiments on-board NASA's EOIM-3 Platform flown on Shuttle Atlantis as part of the STS-46 mission. The space was provided to SDS developers as an opportunity to fly new materials and evaluate their AO performance. SDS developers interested in flight exposure of material samples secured sample space allocation on the BMDO passive tray by agreeing to analyze the effects of ground and space exposures and to provide their data to BMDO for all SDS developers to use. Co-investigators provided identical sets of flight, ground, control, and spare samples. JPL integrated the flight samples into the EOIM-3 mission, arranged the ground-based AO exposure of the ground samples and provided general characterization of the material samples before and after AO exposures.

3.0 EXPERIMENT

3.1 Materials

Eighty-two engineering materials relevant to the BMDO SDS Program were selected for studying AO exposure effects. These developmental materials (mostly new), intended for specialized engineering functions, had no space flight heritage. These selected materials were provided to JPL by SDS contractors and agencies (see Table 1). The organizations and co-investigators that provided the materials are listed in Table 2. A directory listing their names, addresses, and phone and fax numbers is contained in Appendix B.

3.2 Sample Design

The BMDO EOIM-3 Passive Tray design provided space for 82 disk-shaped samples: 27 one-inch diameter disks and 55 one-half-inch diameter disks. The co-investigators supplied

Table 1. BMDO EOIM-3 passive tray materials list.

Material ID Code	Material
1A1	MoS_2-Ni lubricant on steel, Ovonic
1A2	MoS_2-Ni lubricant on steel, Ovonic
1A3	MoS_2-SbO_x lubricant on steel, Hohman
1A4	MoS_2-SbO_x lubricant on steel, Hohman
1B1	SiO_2-doped Al_2O_3/SiO_2 multilayer on fused SiO_2
1B2	TiN (1000 Å) on fused SiO_2
1K3	Four coatings* on Al/PVDF: A: Ni/PbTe B: $Ni/Si/SiO_2$ C: Ni/SiO_2 D: $Ni/ZnS/PbF_2/ZnS$
1K4	Four coatings* on Al/PVDF: A: $Mo/Si/SiO_2$ B: $Ni/TiO_2/Al_2O_3/TiO_2$ C: $Mo/TiO_2/Al_2O_3/TiO_2$ D: Bare
1K8	Al_2O_3/Carbon foil on sapphire, Al holder
1K9	SiO_x/Carbon foil on sapphire, Al holder
1L1	TiC-coated carbon/carbon
1L2	Glass fiber/Teflon composite
1M9	CVD diamond brazed to a ZnS window
1M10	$(SiC/SiO_2)^6/Si$, MWIR-tuned reflector
1M11	$(Si_3N_4/Al_2O_3)^6/Ag$/fused silica, beam splitter
1M12	Al_2O_3/Al half-coated on β-SiC
1M13	Uncoated HIP I-70 beryllium, broadband reflector
1M14	$(Si_3N_4/Al_2O_3)^2/Al/Si$, MWIR-tuned reflector
1M15	AlN/SiH/CVD diamond/ZnS
1M16	$(Si/SiO_2)^4/Al/Si$, MWIR-tuned reflector

* A=upper right, B=lower right, C=lower left, D=upper left.

Table 1. BMDO EOIM-3 passive tray materials list (continued).

Material ID Code	Material
1N4	Beryllium (black-etched) on beryllium foam
1N5	Boron (plasma sprayed) on beryllium
1N6	Martin Black on aluminum
1P2	Tungsten/graphite cloth/carbon foam
1P5	Solar cell
K	Kapton HN
MgF_2	MgF_2 on Al mirror, glass substrate
5C1	T300/934 composite, LDEF trailing edge
5C2	T300/934 composite, adjacent to 5C1 on LDEF
5C4	Polyethylene ring/anodized aluminum cover on silver oxide coated aluminum base
5C5	Polyethylene ring/anodized aluminum cover on anodized aluminum base
5D1	3M Y9469 acrylic transfer tape
5E1	HRG-3/AB epoxy silane (HAC)
5E2	HRG-3/AB epoxy silane (vendor)
5F1	Diamond film on silicon wafer
5F2	Diamond film on silicon wafer
5G1	β-cloth, graphite interwoven
5H1	SiC/Al composite, $CaZrO_3$ coating
5H2	SiC/Al composite, Al_2O_3 coating
5H3	IM7/PEEK, Al_2O_3 coating
5H4	IM7/PEEK, BN/Al_2O_3 coating
5K5	Vendor aluminum electrode/PVDF film
5K6	Y-Ba-Cu-O High temperature superconductor, oxygen deficient
5K7	Y-Ba-Cu-O High temperature superconductor, fully oxygenated

Table 1. BMDO EOIM-3 passive tray materials list (continued).

Material ID Code	Material
5L3	β-alumina (.002") coated aluminum
5L4	Silicon carbide ceramic
5L5	Carbon/carbon composite
5L6	Calcium zirconate coated carbon/carbon
5L7	β-alumina on carbon/carbon
5L8	Copper indium diselenide-photovoltaic
5L9	Niobium beryllide, high temperature alloy
5L0	P75/magnesium vacuum cast composite
5M1	CVD diamond on silicon
5M2	$(SiC/SiO_2)(SiH/SiO_2)^5/Si$, MWIR-tuned reflector
5M3	$(Si_3N_4/SiO_2)^6/Si$, MWIR-tuned reflector
5M4	$(AlN/Al_2O_3)^6/Si$, visible-wavelength-tuned reflector
5M5	$(Si/SiO_2)^5/Si$, MWIR-tuned reflector
5M6	$(SiH/SiO_2)^5/Si$, MWIR-tuned reflector
5M7	$(BN/SiO_2)(SiH/SiO_2)^5/Si$, MWIR-tuned reflector
5M8	Unprotected aluminum on silicon, broadband reflector
5N1	Beryllium, diamond turned, on beryllium
5N2	Beryllium, conv. polished, on beryllium
5N3	Beryllium/silicon/silicon carbide
5O1	P-100 fiber/MR 56-2 composite
5P1	Two coatings on Vit-C/SiC substrate upper: Si/Al_2O_3 lower: Si/Al_2O_3/enhanced MLD
5P3	CVD TiC/graphite cloth/carbon foam
5P4	Alumina on aluminum substrate

Table 1. BMDO EOIM-3 passive tray materials list (continued).

Material ID Code	Material
5P6	Al_2O_3/graphite composite
5P7	Germanium/Kapton
5P8	Indium tin oxide/Teflon/VDA/Kapton
5P9	Microsheet/Ag/Y966/Al
5P0	$(Si/SiO_2)/(TiO_2/SiO_2)$/Kapton
5Q1	Aluminum, textured
5Q2	Aluminum, textured
5Q3	Beryllium, textured, 100 μm, on aluminum
5Q4	Beryllium, textured, 100 μm, on aluminum
5Q5	Beryllium, black etched, on beryllium
5Q6	Beryllium, black etched, on beryllium
5Q7	Boron carbide on graphite
5Q8	Boron carbide on graphite
5Q9	Magnesium oxide on beryllium
5Q0	Magnesium oxide on beryllium

Table 2. List of BMDO EOIM-3 co-investigators.

CODE	PROVIDERS	POINT OF CONTACT	PHONE NUMBERS
A	Aerospace/Sandia National Lab	Mike Dugger	(505) 844-1091
C	Boeing	Gary Pippin	(206) 773-2846
D	CSA Engineering	Joe Maly	(415) 494-7351
E	Hughes	Susan Oldham	(310) 616-8784
F	JPL	Yuh-Han Shing	(818) 354-2690
G	JHU/APL TEQ	Jack Sanders	(410) 792-6000 x-3055
H	AMT, Inc.	Richard Bohner	(714) 545-8825
K	LANL	Jon Cross Peter LaDelfe	(505) 667-0511 (505) 667-1597
L	Martin Marietta	Robert Wendt Tim Gillespie	(303) 971-9383 (303) 971-3684
M	NAWC	Linda Johnson	(619) 939-1422
N	ORNL	Roland Seals	(615) 574-0936
O	SPARTA, Inc.	Walter Whatley	(619) 455-1650
P	TRW	Brian Blakkolb	(310) 814-9249
Q	U.S. Army SDC	Gail Lowe Ed Johnson (SPIRE) Al Akerman (ORNL) Pat Lamb (BATTELLE)	(205) 955-1660 (617) 275-6000 (615) 574-4687 (205) 881-0262

their own necessary substrates for their materials per the "Guidelines and Rationale for EOIM-III Passive Exposure Specimens" (see Appendix C). The assembled pre-flight BMDO EOIM-3 passive exposure tray is shown in Figure 2.

3.3 Sample Identification

Six samples of each selected material were provided by the co-investigators. The six included a sample for flight, one for ground-based testing, a control sample, and three spares. A four-character identification code was developed to identify each sample. The code contains the sample diameter, the co-investigator's company or agency, the material number (for co-investigators who provided more than one material), and the sample type. The code was diamond-scribed onto the sample containers. The key for the code follows.

CODE: # X n Y

- # is a numeric character, either 1 or 5, that represents the sample size: 1 for 1 inch diameter and 5 for 0.5 inch diameter.
- X is an alpha character (A to Q) that identifies the co-investigator's company or agency (see Table 2).
- n consists of one or two numeric characters identifying the test material.
- Y is an alpha character (A-F) designating the individual sample type:

  A - Flight
  B - Spare
  C - Ground
  D - Spare
  E - Spare
  F - Control

In the cases where co-investigators only provided triplicate samples, the following codes were assigned:

A - Flight
B - Ground
C - Control

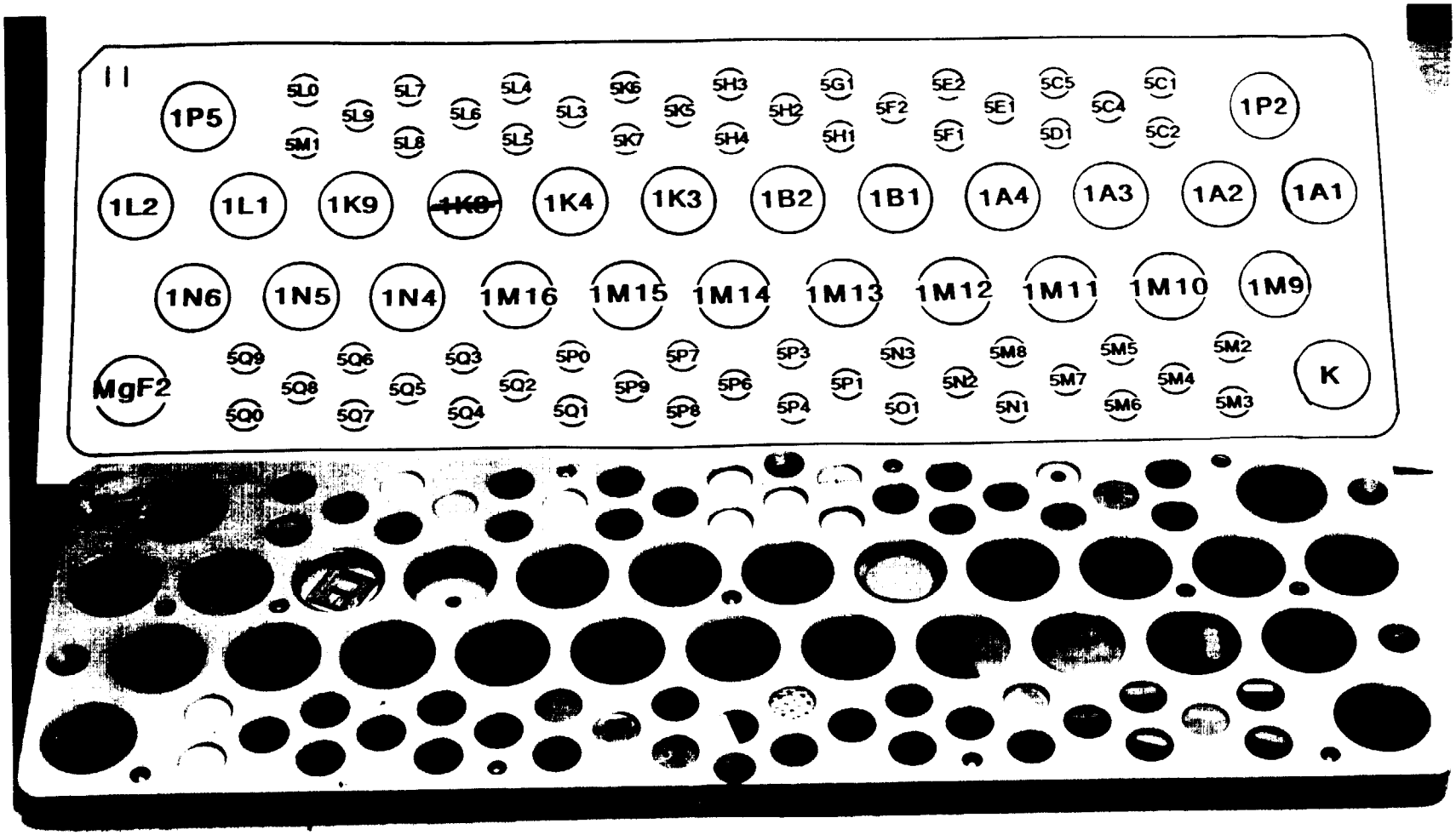

Figure 2. The assembled pre-flight BMDO EOIM-3 passive exposure tray.

3.4 Sample Handling

At JPL, material samples were handled by personnel wearing vinyl, lint-free Class 100 clean room gloves. Samples were maintained in individual Fluoroware containers consisting of polypropylene wafer shippers with polyethylene springs. The containers protected the samples from damage and contamination during shipping and storage. The containers were cleaned with Soxhlet-extracted cloths wet with an azeotrope of 1,1,1-trichloro-ethane (75%) and ethanol (25%). Both the cloths and the solvent were supplied by Thermal Analytical, Inc. and certified by them to have a low non-volatile residue (NVR) of 4 ppm and 2 ppm, respectively. A final rinse with the solvent was used after wiping.

During shipping, the containers, with or without samples inside, were double-bagged in 3M-2110E antistatic reclosable bags. Handling and shipping instructions were provided to each co-investigator to standardize the packaging and shipping methods and to minimize the risk of contamination or damage to the samples. The instructions are contained in Appendix D.

3.5 JPL Sample Characterization

3.5.1 Photography

All specimens were photographed at JPL in a Class 100 clean room. Initially, the samples were photographed in their as-received condition prior to any thermal vacuum conditioning or characterization. For a direct comparison, close-up photographs of each flight-exposed sample adjacent to its control were taken. A third set of photographs was taken of each ground-exposed sample side-by-side with its control.

3.5.2 Electron Spectroscopy for Chemical Analysis

The surface chemistry of each control sample was analyzed with the use of Electron Spectroscopy for Chemical Analysis (ESCA), also known as X-ray Photoelectron Spectroscopy (XPS). The analysis ascertained material surface cleanliness and chemical composition.

ESCA spectra were collected with a Surface Science Instruments SSX-501 Spectrometer with monochromatized Al Kα X-rays (1486.6 eV). The X-ray source produces spot diameters of 150, 300, 600, and 1000 μm. Both 300 and 600 μm diameter spots were used. The chemical composition of the surface is probed to a depth of 100 Å. ESCA can detect all elements except hydrogen. Sample analyses were performed at pressures below 3×10^{-8} torr.

ESCA spectra were taken for control samples before and after thermal-vacuum conditioning. Flight and ground samples were analyzed after the AO exposures and then compared to the control. The results of the comparisons are presented in Section 3.8 ("Results and Discussion").

3.5.3 Weight Measurement

The difference in sample weight before and after exposure provides a method to determine AO effects. A weight loss may indicate erosion. Weight increases may also be observed and could indicate water pickup, contamination, or a more complex interaction such as oxidation.

The flight, ground, and control samples were weighed before and after thermal vacuum conditioning. To account for moisture uptake, prior to each weighing, the materials were conditioned in a 50% relative humidity chamber at room temperature for 24 hours per ASTM E-595 procedures. The chamber used a saturated calcium nitrate solution to maintain the humidity.

Weight measurements were made on a Mettler AE 163 Balance, which has a 0.01 mg sensitivity. The weighing procedure consisted of removing a sample from the humidity chamber and placing it in the balance immediately. The weight was recorded when the reading stabilized, which typically was less than one minute. After weighing, the sample was promptly returned to its Fluoroware container.

3.5.4 Thermal Vacuum Conditioning

Materials were subjected to a thermal-vacuum conditioning to remove any surface molecular contamination in order to reduce the potential of outgassing in a vacuum during space flight or during ground-based testing. The thermal-vacuum conditioning environment was 65°C at 10^{-6} torr for a minimum of 48 hours per NASA Johnson Space Center (JSC) requirements.

Materials were processed in two separate lots. Lot one contained only optical and non-polymeric materials. Lot two contained the balance of the samples including polymeric materials. Each sample set included the flight, ground, and control specimens. The spare samples were not thermal-vacuum conditioned. Lot one was conditioned for 54 hours and lot

two for 62 hours. Samples were supported directly on a pre-cleaned, pre-vacuum-baked stainless steel mesh.

A residual gas analyzer (RGA) monitored the outgassing products during the thermal-vacuum conditioning. Mass numbers greater than 60 (indicating possible hydrocarbon contaminants) were detected at the beginning of the conditioning at a pressure of 3×10^{-6} torr. There was an order of magnitude decrease of all masses by the end of the bake-out.

A Temperature-controlled Quartz Crystal Microbalance (TQCM) monitored the progress of the outgassing during the bake-outs. The amount of outgassing products deposited on the TQCM crystal at 0°C was measured and found to decrease gradually with time.

Post-thermal-vacuum ESCA results showed no significant evidence of contamination. The sensitive ultra-clean optics served as witnesses for contamination. They showed evidence of slight amounts of hydrocarbon accumulation on the surface ($\sim$10-20 Å), which should be removed with a fluence of $< 10^{17}$ atomic oxygen exposure and therefore were not considered to be detrimental.

3.6 Flight Experiment

3.6.1 Tray-Level Integration

NASA Johnson Space Center (JSC) supplied the flight-ready passive sample tray (N-11), assembly hardware and remove-before-flight cover for the BMDO EOIM-3 Experiment. The wavy washers, aluminum disks, and bolts were cleaned at JPL using an azeotrope of 1,1,1-trichloro-ethane and ethanol. The tray was pre-cleaned by NASA Johnson Space Center. The flight sample installation into the tray followed procedures in the NASA JSC "Procedures for Assembly of Disk Sample Specimen into a Passive Sample Carrier" (see Appendix E). After flight sample installation was complete, the tray assembly was photographed. The flight-ready tray assembly is shown in Figure 2. After photography, the remove-before-flight cover was attached to the tray. The tray assembly was triple-bagged in 3M-2100E material and each bag was sealed with Kapton/Y966 tape. The tray assembly was shipped to NASA JSC and then to NASA KSC for integration into the EOIM-3 pallet.

3.6.2 EOIM Pallet-Level Integration

The tray to pallet integration was performed by Lockheed Engineering and Space Co. personnel under the direction of the NASA/JSC experiment manager. The installation took place in the NASA KSC Operations and Configurations (O&C) Building Class 100,000 high bay clean room. The individual remove-before-flight covers remained in place until all 15 EOIM-3 trays were installed. These individual covers were removed prior to the EOIM-3 pallet integration into the orbiter, where the entire EOIM-3 pallet was protected with a large single pallet cover. The EOIM-3 Experiment pallet was installed in Shuttle Bay 12. The EOIM-3 pallet cover was removed during orbiter close-out activities approximately 70 hours before launch. The payload service structure provided a nominal Class 100,000 environment for the orbiter payload prior to closing the payload bay doors 60 hours before launch. A nitrogen purge through the orbiter payload bay continued from 40 hours before launch until just prior to launch.

The location of the BMDO passive tray N-11 on the EOIM-3 pallet is shown in Figures 3-4. The location of the EOIM-3 pallet in the orbiter payload bay is shown in Figures 5-6.

3.6.3 STS-46 Mission

The STS-46 mission included two primary payloads, the European Retrievable Carrier (EURECA) Satellite and the Tethered Satellite System (TSS-1), and two secondary experiments, the Thermal Energy Management Processes Experiment (TEMP 2A-3) and EOIM-3. STS-46 also carried four Get-Away Special canisters which included the Limited Duration Candidate Exposure Experiment (LDCE-1,2,3) and the Consortium of Materials Space Processing Complex Autonomous Payload (CONCAP-II & -III).

3.6.3.1 Mission Time Line

STS-46 was launched on July 31, 1992. Deployment of the EURECA satellite, the first major mission milestone, occurred at a Mission Elapsed Time (MET) of 1 Day, 17 hours and 8 minutes (01/17:08). Deployment occurred at an orbit altitude of approximately 425 km (230 nm). Prior to EURECA deployment, the orbiter orientation maintained the payload bay in a solar inertial configuration (-ZSI) for approximately 12 hours starting at MET 0/23:07, with -Z pointing out of the payload bay (see Figure 5). After EURECA deployment, STS-46 continued in a station-keeping mode with EURECA, providing a minor period of approximately 4 hours

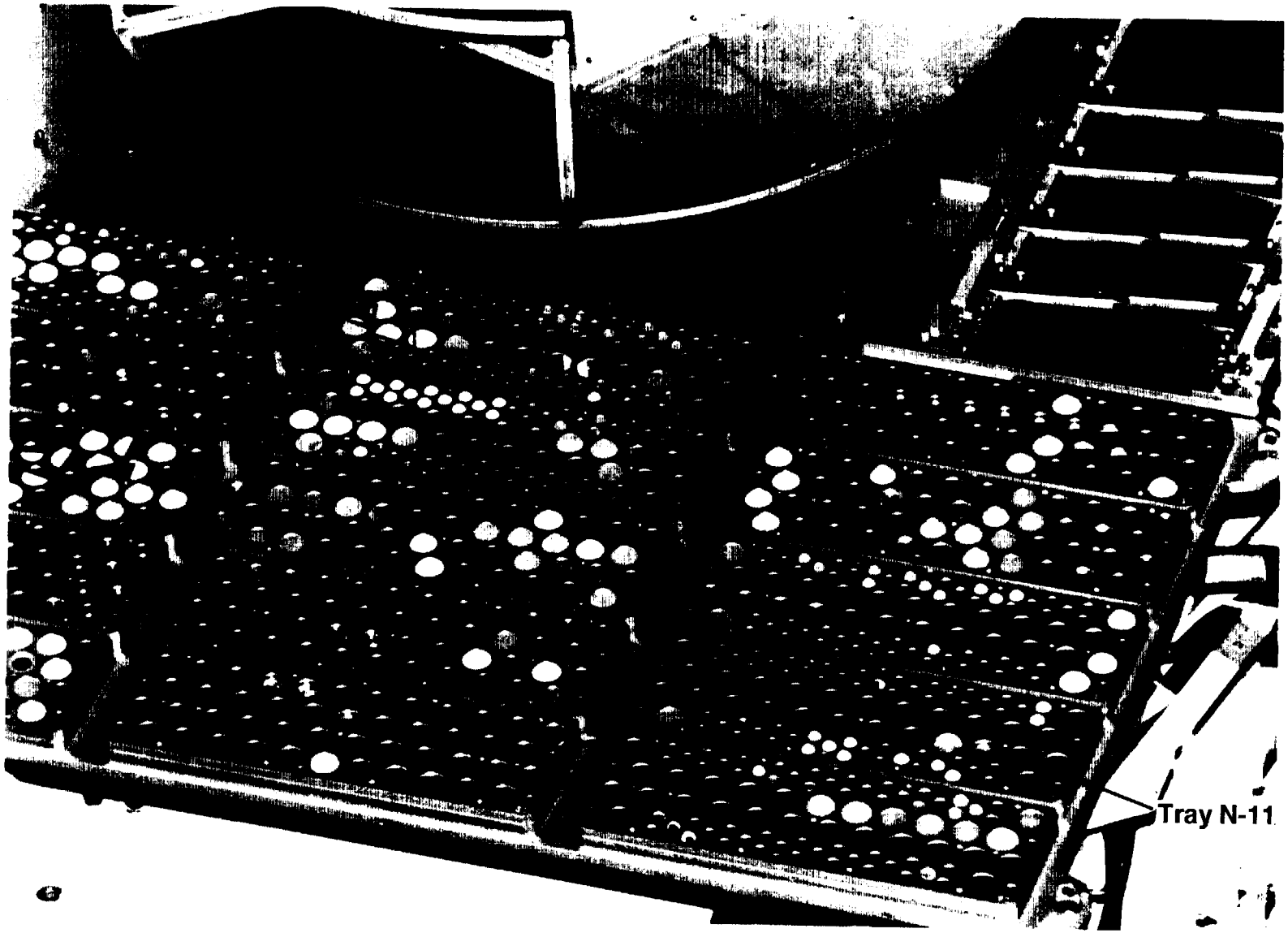

Figure 3. BMDO passive tray (N-11) on the EOIM-3 experiment pallet.

NASA-S-86-03285B

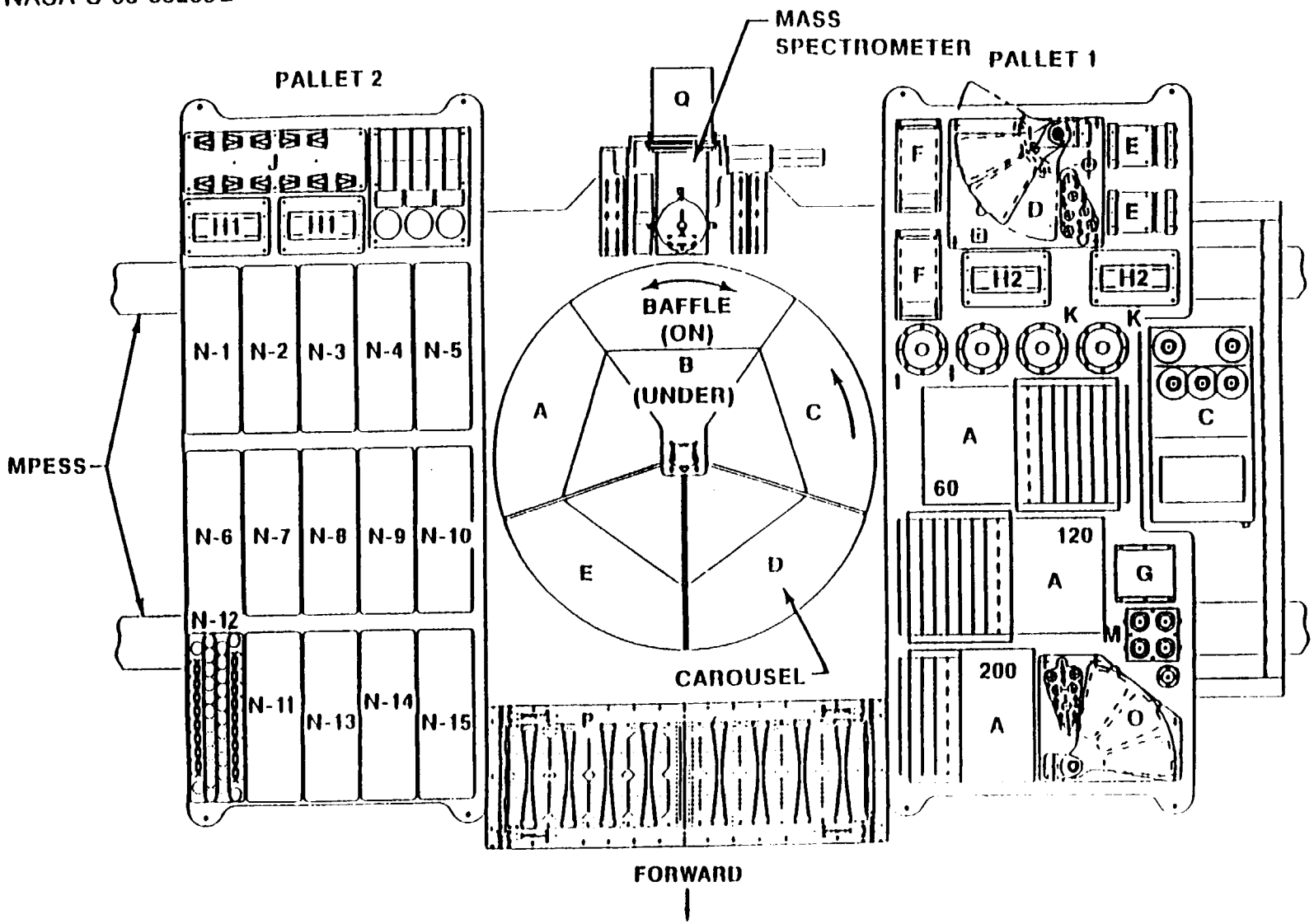

Figure 4. The EOIM-3 experiment pallet.

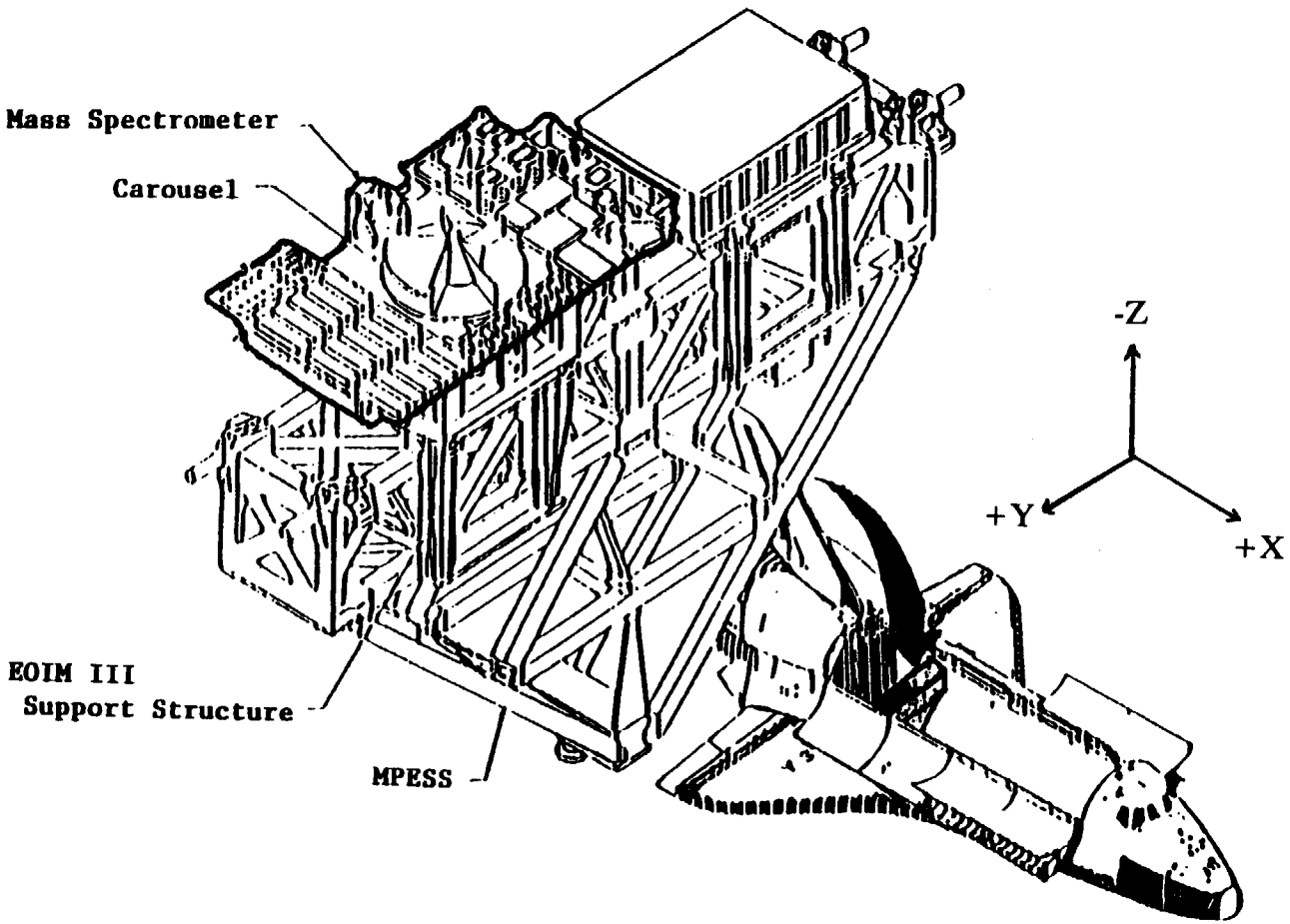

Figure 5. Sketch showing EOIM-3 experiment pallet location in Shuttle Bay 12.

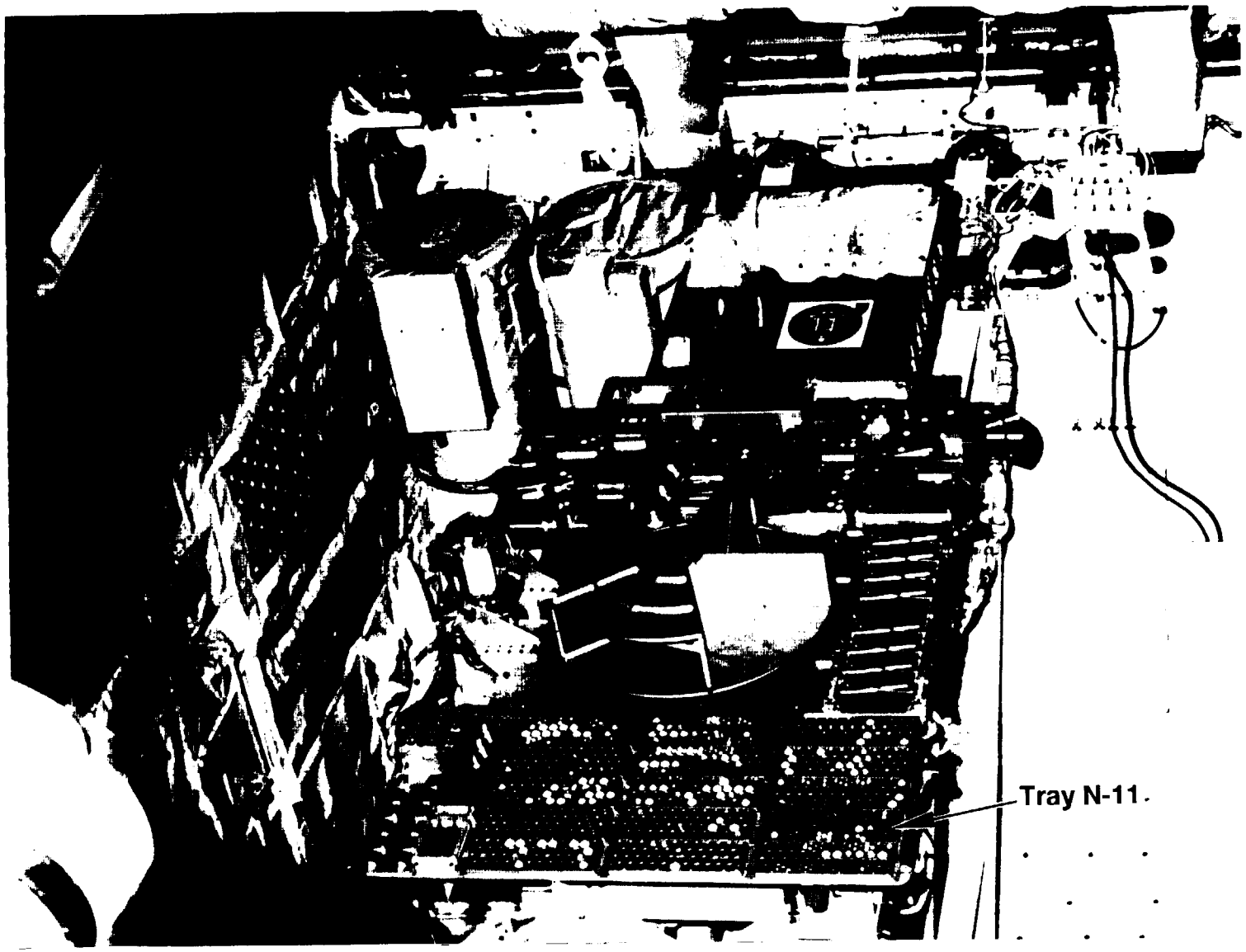

Figure 6. Photograph showing EOIM-3 pallet in the orbiter payload bay prior to removal after mission.

of ram atomic oxygen exposure to EOIM-3. STS-46 then moved into a circular orbit of approximately 300 km (160 nm) at MET 02/20:28 for TSS-1 operations.

The TSS-1 satellite was planned for deployment to a distance of approximately 20 km from the Shuttle and to conduct an electrodynamic experiment. Due to technical problems, TSS-1 was deployed to only approximately 280 meters. Following retrieval and berthing of TSS-1 at MET 05/08:56, the orbiter transferred into a circular orbit of approximately 230 km (124 n.mi.) at MET 05/19:27.

At MET 05/22:30, the payload bay of Atlantis was oriented into the orbital velocity vector (-ZVV), commencing the EOIM-3 atomic oxygen exposure experiment. Thereafter, the orbiter maintained the ram attitude within $\pm 20°$ until MET 07/16:45, at which time the payload bay was reoriented out of the velocity direction and prepared for the de-orbit burn. The total elapsed experiment time was 42.25 hours.

3.6.3.2 Atomic Oxygen Environment

The AO fluence for EOIM-3 is estimated to be 2.2 - 2.5 x 10^{20} atoms/cm^2. Three methods provided estimates of the EOIM-3 atomic oxygen fluence. The first method uses the Mass Spectrometric and Incoherent Scatter (MSIS-86) Thermospheric model along with the National Oceanic and Atmospheric Administration's (NOAA's) reported solar 10.7 cm (F10.7) flux and magnetic indices (Ap, Kp), and the estimated densities for various atmospheric species, including AO. The fluxes were computed with the MSIS-86 model. Fluences were calculated by multiplying fluxes by orbiter velocity and integrating for the exposure periods. Depending on the period for which the solar and magnetic indices were sampled, the estimated AO fluence varied from 2.0×10^{20} atoms/cm^2 to 2.2×10^{20} atoms/cm^2. The second AO fluence estimate is based on the erosion of Kapton polyimide film. Numerous Kapton samples were located on various passive trays on the EOIM-3 pallet. Erosion was determined by mass loss, Scanning Electron Microscopy (SEM) and profilometry measurements. Based on a reaction efficiency of 3.0×10^{-24} cm^3/AO atom, the EOIM-3 fluence was calculated to be between 2.3×10^{20} atoms/cm^2 and 2.5×10^{20} atoms/cm^2. The weight losses varied with sample location and gave rise to the calculated fluence range. The third AO fluence estimate is based on data from the Air Force Phillips Laboratory mass spectrometer. The on-board spectrometer provided a mission fluence

estimate of $2.2 \pm 0.4 \times 10^{20}$ atoms/cm^2. The estimated AO fluence from each of the three sources is summarized below.

AO Fluence Estimate	Method
$2.2 - 2.4 \times 10^{20}$	MSIS/NOAA model
$2.3 - 2.5 \times 10^{20}$	Kapton erosion
$2.2 \pm 0.4 \times 10^{20}$	Mass spectrometer

3.6.3.3 Solar UV Environment

NASA JSC provided the EOIM-3 solar UV exposure estimate. Their estimate is based on integration of the sun angle, orbiter attitude, and ephemeris over the entire mission. The estimate does not account for shadowing from payloads and orbiter structure but is thought to be accurate within $\pm 20\%$. The estimate is 22 equivalent solar hours' (ESH) exposure.

3.6.3.4 Thermal Environment

The EOIM-3 pallet provided twelve temperature sensors as part of the state-of-health and engineering data system. Figure 7 shows the on-orbit temperature history for an aluminized Kapton film bonded on a thin aluminum disk to which one of the temperature sensors was mounted. The various phases of the mission are indicated along the base of the plot. During the EURECA operations, the payload bay was held in a solar inertial attitude for approximately 12 hours. The Kapton film reached a temperature in excess of 70°C during this period. Later, during the EOIM-3 exposure phase of the mission, the same sensor temperature cycled between +20°C and +45°C. Figure 8 shows the temperature history of the mounting location for tray N-11. This temperature history is representative of the temperature for the BMDO EOIM-3 tray and the more massive test specimens within the tray. The tray temperature excursions were damped considerably as compared to the aluminized Kapton specimen temperature excursions. The peak temperature during the solar inertial phase reached +55°C, and temperatures cycled between +5°C and +20°C during the EOIM-3 exposure period.

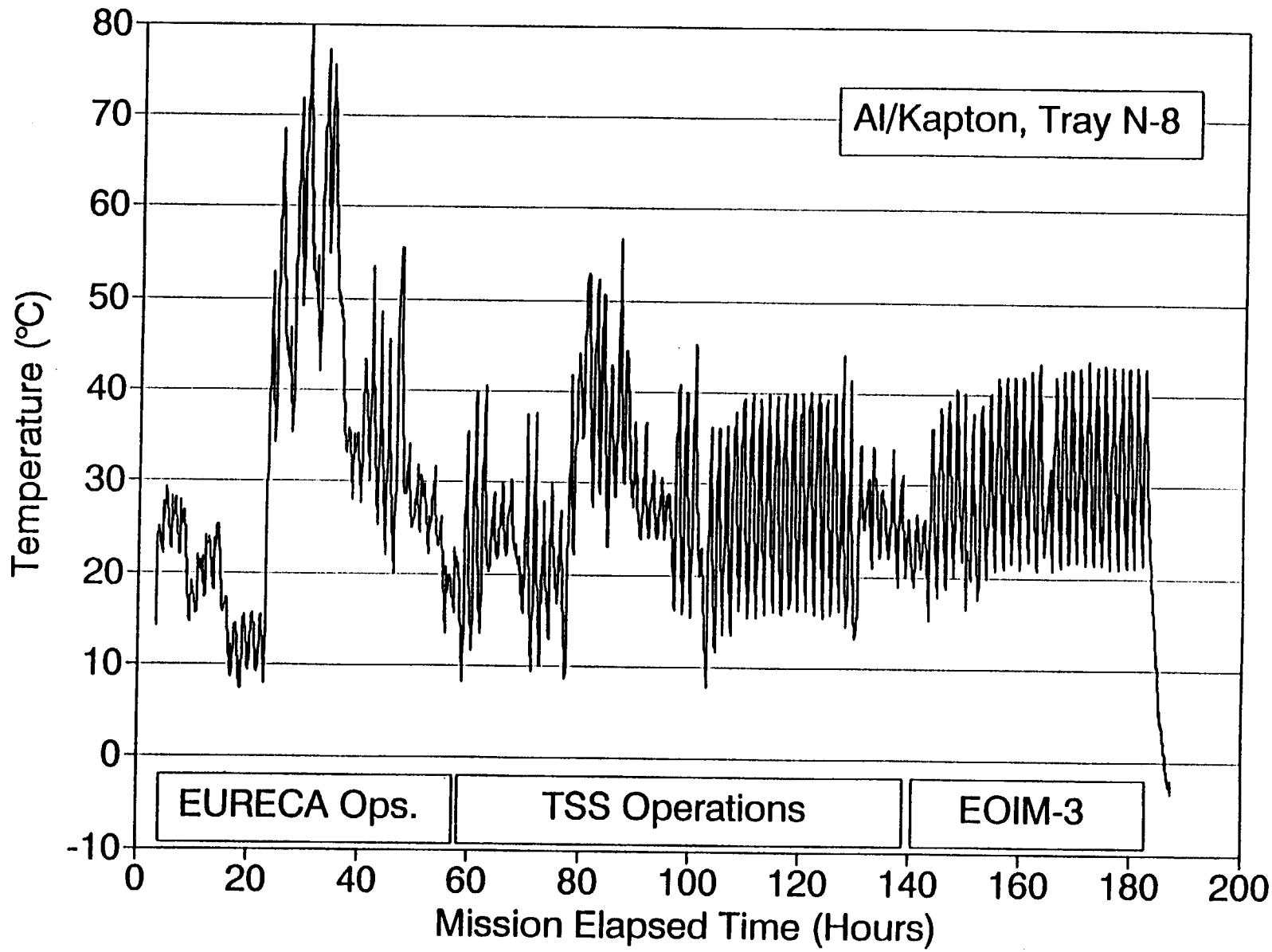

Figure 7. Temperature history of passive tray N-8.

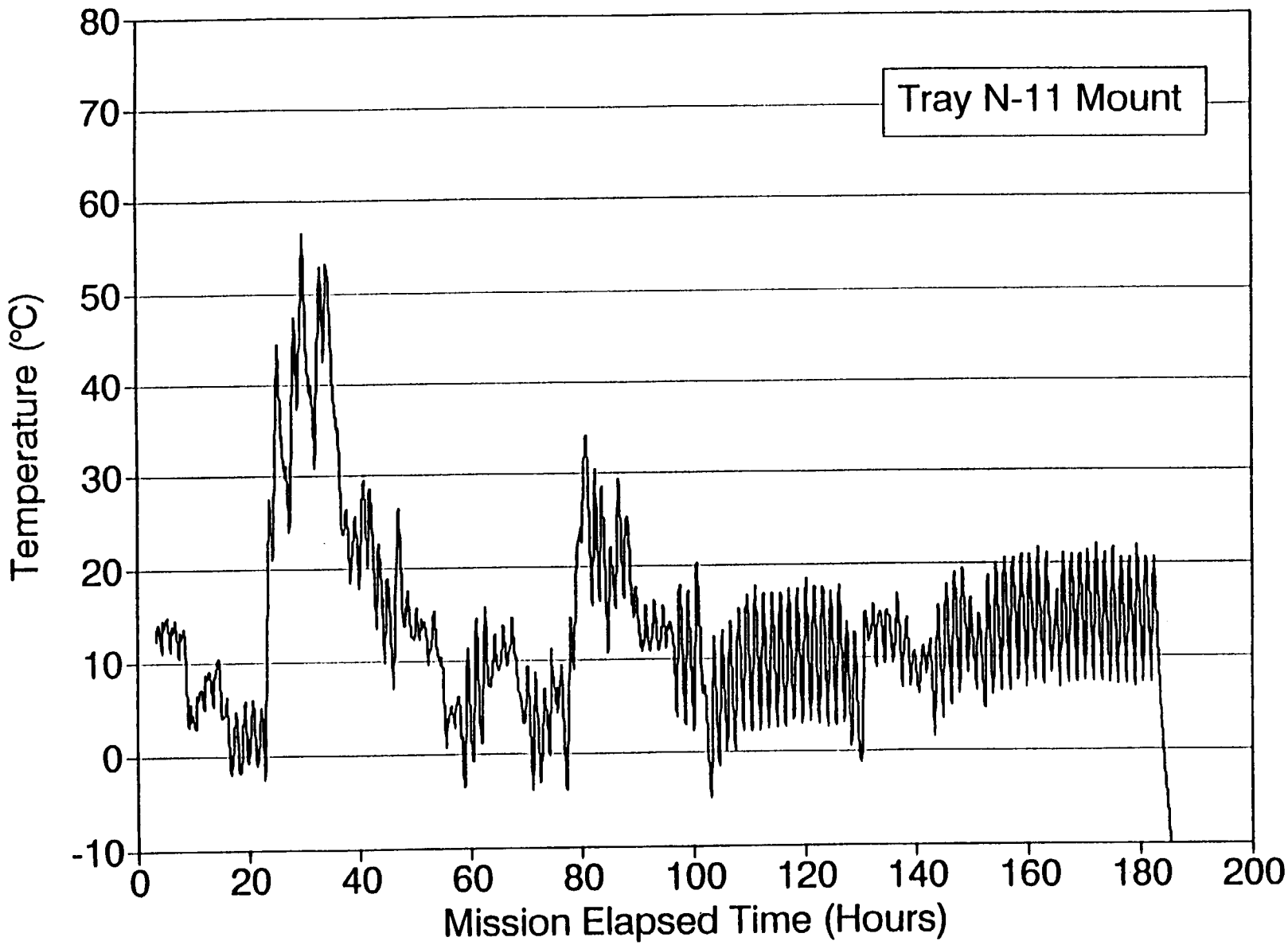

Figure 8. Temperature history of the mounting location for tray N-11.

3.6.3.5 Flight Contamination

After the mission, surface chemical analyses revealed a small percentage of silicon present on all flight samples. Materials readily eroded by atomic oxygen contained 2-3 atom percent silicon on the surface. The more stable or resistant materials contained 9-12 atom percent silicon on the surface. The stoichiometry indicated that a thin film of SiO_2 had formed on these specimens. For the stable materials, which had received a heavier accumulation of silicon, this film is on the order of 20 Å thick.

The NAWC polycrystalline diamond on silicon (5M1A) flight sample contained a visibly distinct "crescent" feature on the surface near the tray retaining lip. ESCA showed the crescent region to be completely free of silicon. The rest of the sample surface had nearly 10 atom percent silicon. The sample contained a gold strip which was visible in tray photographs. The strip oriented the crescent area with respect to the tray and the orbiter. From a geometrical analysis of the crescent feature and the height of the retainer lip, it is theorized that the contamination source was located in the aft portion of the orbiter and could not extend more than 30° above the plane of the BMDO EOIM-3 tray top surface. Figure 9 shows the geometrical relationship between the test sample, the tray, and the orbiter. The theory is that the contamination source was either at the top of the aft bulkhead surface or extended along the entire aft bulkhead surface.

It is not clear whether the forward surfaces of the OMS pods were in the field-of-view of the NAWC sample. Since a silicone-based waterproofing agent is applied to the shuttle thermal protection system (TPS) tiles, the tiles are a potential source of silicone contamination. The aft bulkhead is covered with a multi-layer insulation blanket with an outer layer of Beta-cloth. Beta-cloth is a woven glass fabric encapsulated in a fluorocarbon resin. In the manufacturing process, the glass fabric is treated with a silicone oil prior to encapsulation to improve the handling characteristics of the material. In the thermal vacuum environment of space, this silicone oil can slowly diffuse from within the fabric, migrate to the surface, and outgas. Yellowing of the Beta-cloth liner is commonly observed and is associated with environmental aging of the silicone film. Silicone oil could outgas and be transported via line-of-sight to sensitive EOIM-3 surfaces.

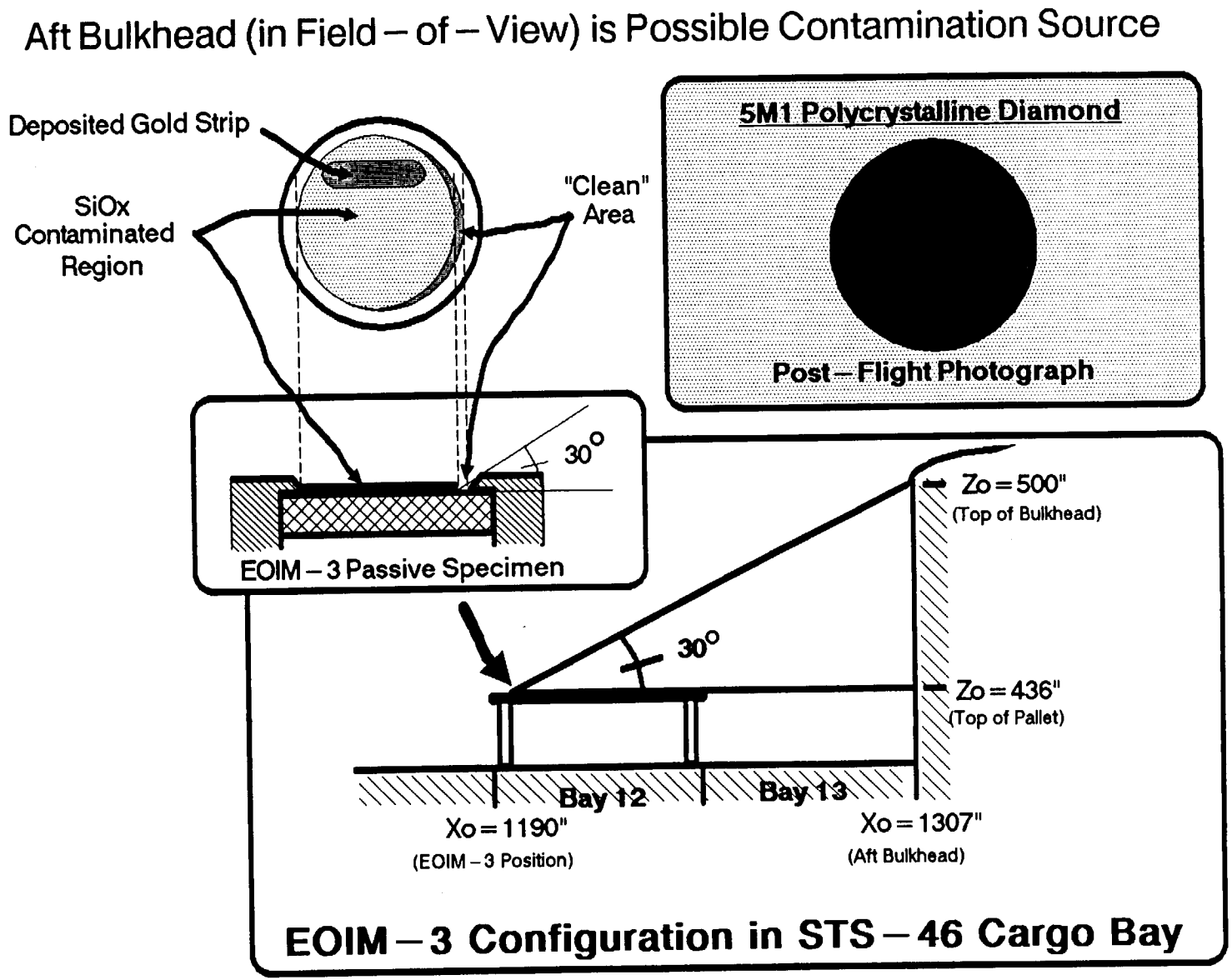

Figure 9. Line-of-sight shadow on BMDO EOIM-3 test specimen.

3.6.4 Post-Flight Inspection

A team of EOIM-3 co-investigators and the Mission Manager inspected EOIM-3 in the orbiter payload bay when Atlantis returned to Orbiter Processing Facility Bay 2. The inspection objectives were to assess overall hardware condition, examine hardware and experiments for evidence of contamination, and direct the photographic documentation of EOIM-3. The inspection team members were:

Bruce Banks	NASA Lewis Research Center
David Brinza, BMDO Investigator	NASA Jet Propulsion Laboratory
Rachel Kemenetzky	NASA Marshall Space Flight Center
Jack Triolo	NASA Goddard Space Flight Center
Michael Richardson, Mission Manager	NASA Johnson Space Flight Center

The team performed two visual inspections of the EOIM-3 hardware and experiments while EOIM-3 was in the bay. The first inspection was performed from the Level 7 platforms approximately 15 feet above and 20 feet outboard of the payload bay. The second inspection occurred from the Level 13 platforms located adjacent to the payload bay door hinges.

The first inspection provided an overall perspective of the hardware in relationship to the orbiter structures and other payloads in the bay. No obvious regions of contamination were observed during this inspection. The EOIM-3 hardware itself appeared to be in good condition. The passive trays appeared normal.

The second inspection permitted a physically closer evaluation of the experimental hardware and surrounding support structure. The BMDO EOIM-3 passive tray showed no visibly apparent contamination. The JPL Kapton witness appeared non-specular and the MgF_2 witness appeared clean. The mirror materials from the Naval Air Warfare Center (NAWC) appeared visually clean as did other protective coatings.

3.6.5 De-Integration

The EOIM-3 pallet was removed from Atlantis on August 15, 1992, and transferred to the Operations and Checkout (O&C) Building. Tray level de-integration began on August 25, 1992. The BMDO EOIM-3 tray was removed on August 26, packaged in 3M-2100E bagging

material and returned to JPL on August 27, 1992. The tray assembly was photographed (see Figure 10) and the individual samples were removed from the tray and installed in their individual Fluoroware containers.

3.7 Ground-Based Experiment

Seventy-seven material samples, identical to those flown on the BMDO EOIM-3 passive tray, plus ten witness samples, were exposed to atomic oxygen in the ground-based facility located at Physical Sciences, Inc. (PSI) in Andover, MA. Although the passive tray contained 82 samples, three samples, 5P5, 1K8, and 1K9, were one-of-a-kind, and two were Kapton and magnesium fluoride control samples. While no spare samples of magnesium fluoride existed, numerous Kapton witness samples accompanied the ground-based materials during exposures to provide a good measurement of the Kapton-equivalent fluences. In addition, germanium-coated Kapton samples, which do not erode upon exposure to atomic oxygen, were included in the ground-based test as monitors of the contamination levels in the chamber and in the O-atom beam. All samples were delivered to PSI in December of 1992. PSI weighed the samples before and after exposure. The samples were exposed in two batches, and each batch was returned to JPL after exposure was completed, in February and March 1993, respectively. The first batch consisted of samples from co-investigators L, M, and P. The second batch contained the balance of the samples. At JPL, photographs were taken of the exposed samples and control samples together. The control samples had been in storage at JPL. Also, survey ESCA analyses were carried out on the exposed samples. The samples were then returned to the co-investigators for further analyses and comparison to the flight samples.

3.7.1 Facility

Central to the PSI Fast Atom Sample Tester (FAST-1) facility is an atomic oxygen beam source developed at PSI under the Small Business Innovation Research Program with PSI and NASA funds. The key elements of the source are a pulsed molecular beam valve, coupled to an expanding conical nozzle, and a 14 J/pulse CO_2 TEA laser. The pulsed valve introduces a burst of oxygen gas into the conical nozzle. As the gas expands into the nozzle, the CO_2 laser is fired, and the light pulse is focused down into the cone where it initiates a plasma and heats

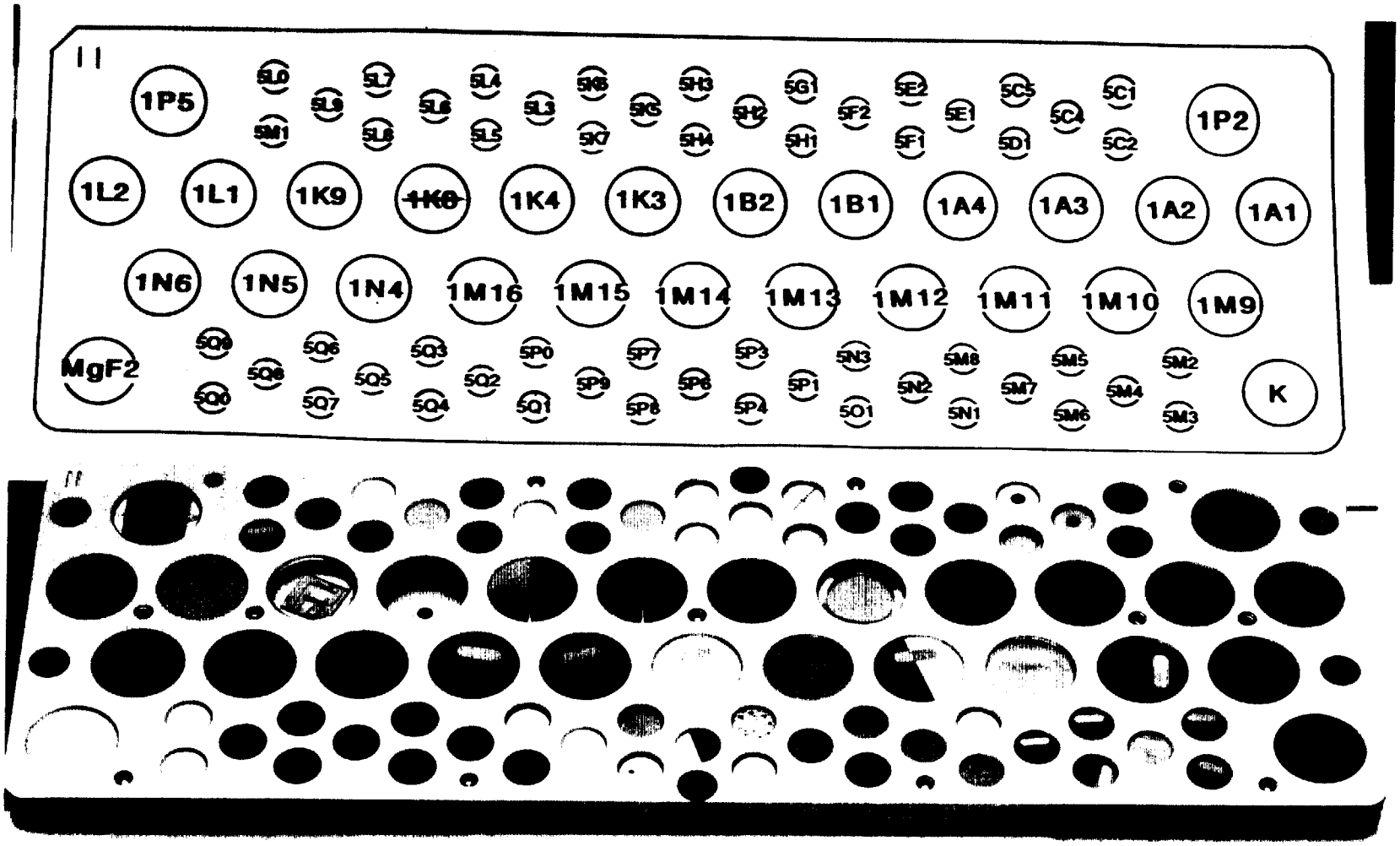

Figure 10. Photograph of BMDO EOIM-3 passive exposure tray assembly after flight.

it to over 20,000 K. The high temperature, high pressure plasma expands rapidly into the diverging cone following the detonation and engulfs much of the remaining cold gas. The local densities in the nozzle are sufficient to allow for electron-ion recombination, but by the time the atoms formed in the plasma have cooled enough to recombine, the termolecular collision rate has dropped so low that the atoms are, in effect, frozen in the emerging beam. The resultant beam from the nozzle consists predominantly of fast neutral atoms with small ion and molecular components all traveling at hyperthermal velocities. There is still a large thermal component of unprocessed O_2 gas. The source conditions are typically adjusted such that the mean O-atom velocity in the beam is 7.8 km/sec with a velocity spread similar to that encountered in LEO. Under these conditions, PSI has measured an O/O_2 ratio of about 4 (in the hyperthermal component of the beam) and a total ion content of one percent. The UV/VUV irradiances generated by the source are about one incident photon per 10^4 incident O-atoms, which is comparable to the level encountered in LEO. Thermal heating of samples either through energy accommodation of the hyperthermal atoms or through scattered laser radiation is negligible at the (50 cm) distance from the source that the samples were placed. A chart illustrating the facility and capabilities has been provided by PSI and is shown in Figure 11. The reader is referred to PSI for more details of the facility.

3.7.2 Sample Mounting

JPL provided a preliminary sample pallet design which PSI redimensioned to accommodate mounting rods in the FAST-1 apparatus. The sample pallet was machined from 0.5 inch thick aluminum plate. A central hole of 1 inch I.D. is located in the pallet center to allow for laser access. For each sample position on the pallet, a throughbore, 1/16 inch less than the sample O.D., is counterbored to within 1/32 inch of the front surface with an I.D. 0.01-0.02 inch larger than the sample O.D. Each sample is backed with a 1/8 inch thick aluminum disk and held in place with a 1/16 inch diameter oversized Viton O-ring. A cross section is shown in Figure 12. The layout of the pallet is shown in Figure 13. The large circles represent holes for 1 inch diameter samples and the small circles represent holes for 1/2 inch diameter samples. The pallet was mounted 50 cm from the small end of the nozzle cone. At this relatively large distance, the whole pallet can be exposed, with an O-atom fluence variation of not more than 20 percent. Although the exposure area is relatively large, only about half the

PSI FAST™ ATOM SOURCE

- Simulate erosive LEO environment in ground-based facility
  - Atomic oxygen energies from 2 to 14 eV
  - Atomic oxygen flow velocity from 5 to 14 km/s
  - Fluxes to 10^{16}/s at 8 km/s over 300 cm^2
  - Fluence to $10^{21}/cm^2$ routine

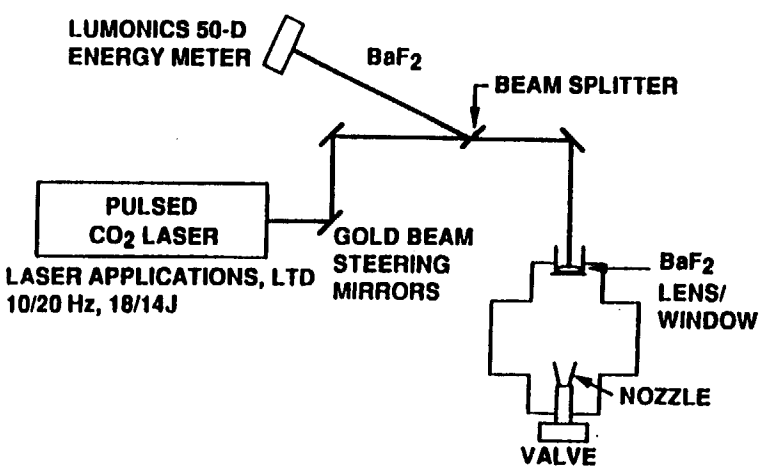

U.S. Patent 4,894,511 Foreign Patents Pending

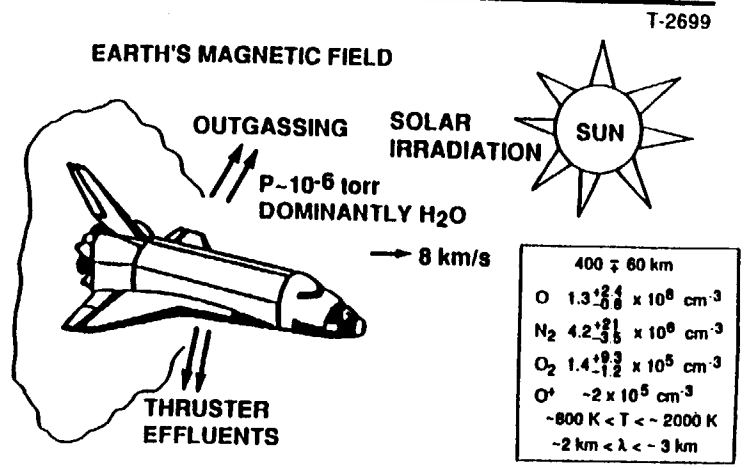

The LEO Environment

- Material studies for government and industry
  - Mass loss
  - Surface modification
  - Energy accommodation
  - Spacecraft qualification
- Sales and licensing of technology
  - European Space Agency
  - French Space Agency

Figure 11. Illustration of PSI's facility and capabilities.

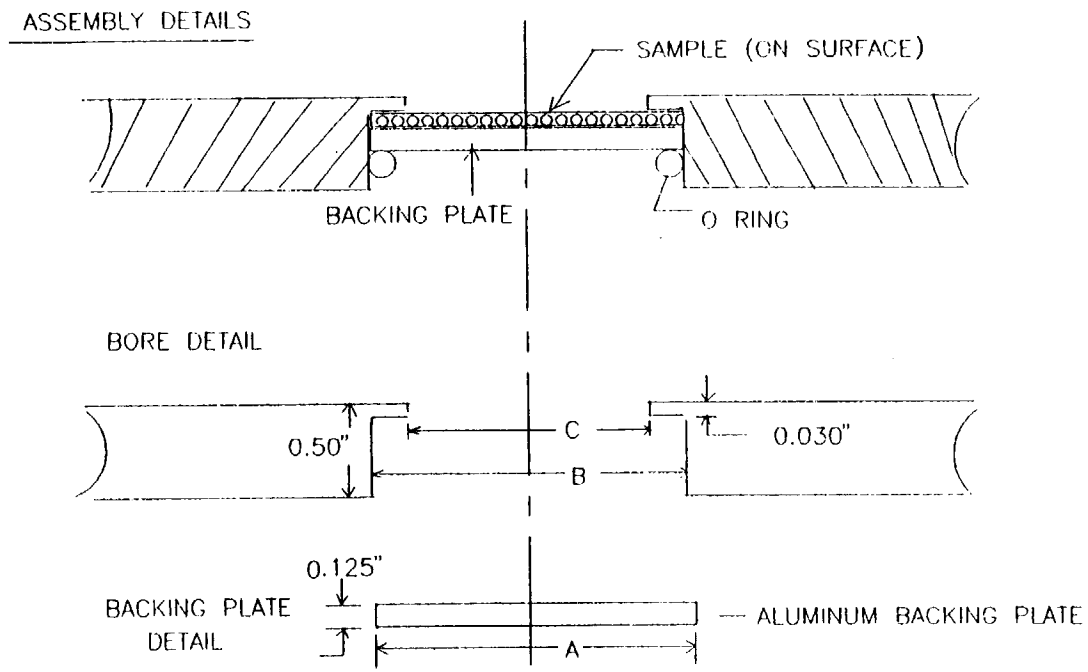

	A	B	C	O-RING
1" DISK	1.000 $^{+.000}_{-.005}$"	1.020 $\pm$ .005	0.875 $\pm$ .010	1.062" O.D.
1/2" DISK	0.500 $^{+.000}_{-.005}$	0.520 $\pm$ .005	0.437 $\pm$ .010	0.563" O.D.

Figure 12. Sample pallet bore dimensions.

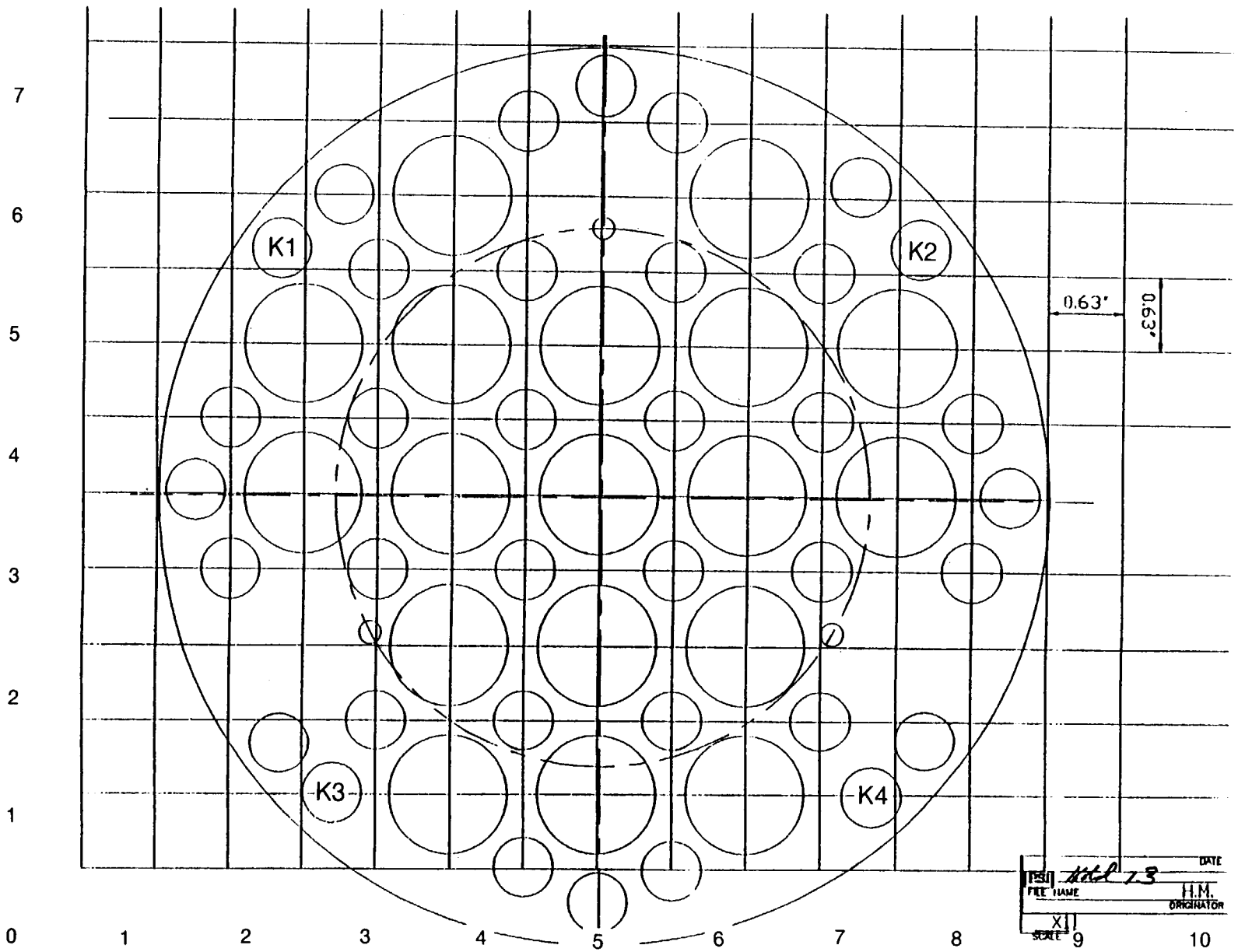

Figure 13. Layout of the exposure pallet.

samples could be exposed in one batch, so two batches were run. For each batch, four Kapton witness samples were mounted at various positions on the pallet in order to determine the exposure fluence and to verify exposure uniformity (see Figure 13).

3.7.3 Sample Weighing

All samples were weighed before and after AO exposure. Most samples were weighed on a Mettler analytical balance with a sensitivity of ± 0.1 mg. Samples weighing less than 0.2 g were weighed on a Cahn microbalance with a sensitivity of ± 1 μg. The samples were degassed in the vacuum chamber in their containers (Fluoroware) overnight prior to weighing and sample mounting. After degassing, the samples were stored in a desiccator until weighing. Once a sample was removed from the desiccator, a stopwatch was started. Weights were recorded every minute for four minutes, and the recorded weight was extrapolated back to the weight at the time the sample was removed from the desiccator. This procedure reduced the uncertainty in mass that resulted from water adsorption by the samples. The same weighing procedure was followed after exposure in the vacuum chamber.

Although steps were taken to account for water uptake by the samples, germanium-coated Kapton witness samples showed that some mass loss occurred during handling. These samples, which should not have been eroded by O-atoms, exhibited a 20 μg mass loss, indicating that complete desiccation of the hygroscopic samples might not have been attained. This fact should be taken into consideration when one is attempting to draw conclusions about the O-atom reactivity of a tested material.

3.7.4 Environment

Four Kapton witness specimens were exposed in each batch. Based on the weight loss of these samples and a Kapton reactivity of 3.00×10^{-24} cm^3/atom, the average fluences of each batch were 2.46×10^{20} atoms/cm^2 and 1.97×10^{20} atoms/cm^2, respectively. The fluence variation across the sample pallet for the first batch was 2.30-2.78×10^{20} and that for the second batch was 1.88-2.13×10^{20}. Both batches were exposed for the same amount of time, 25 hours, at a 3 Hz pulse rate. The fluence difference for the two batches provides an idea of the ability to control the fluence from test to test without an in situ monitor. The target fluence was 2.0×10^{20} atoms/cm^2, which was the best estimate of the EOIM-3 mission fluence at the time of the

ground-based exposure. Subsequent estimates adjusted the EOIM-3 flight fluence upward to $\sim 2.5 \times 10^{20}$ atoms/cm^2. Given the uncertainties in the EOIM-3 fluence and in the ability to predict an actual ground-based exposure fluence, the ground-based exposures can be considered to be equivalent to the EOIM-3 fluence. Tables 3a, 3b, 4a, and 4b summarize the results for the exposure of the samples at PSI.

3.7.5 Ground-Based Facility Contamination

Survey ESCA analyses were performed on all samples subjected to ground-based exposure. One objective of the analyses was to determine if the surface chemistry was the same for both ground and flight samples. The results will be discussed in Section 3.8. The second objective of the ESCA analyses, which will be discussed here, was to assess the contamination generated by the facility on the samples that were exposed in the ground-based facility.

Germanium-coated Kapton (Ge/K) witness samples accompanied both batches of samples. ESCA analyses of these witness samples were performed at JPL before shipping them to PSI. Although the germanium coating can oxidize, it has been shown to erode negligibly, if at all. Therefore, Ge/K can serve as a valid witness for contamination that is deposited on a surface and does not erode away.

The first exposure batch contained a Ge/K sample that sampled the ambient environment of the vacuum chamber. It was placed out of the direct line of sight of the O-atom beam. Table 5 shows the ESCA analysis of the sample before and after exposure. The only change observed was in the relative amounts of carbon and oxygen on the surface. The increase in atom percent of O is likely the result of increased oxidation on the surface from scattered O-atoms in the chamber. There is no evidence for contamination arising from the ambient chamber environment.

One Ge/K sample (5P7C) served as the witness sample in the beam for the first batch. Two spots were examined after exposure (see Table 6). Again, the relative oxygen content of the surface increased, presumably as a result of oxidation. In addition, there is evidence for contamination arising from the exposure. In particular, the surface acquired silicon (Si), fluorine (F), copper (Cu), and sodium (Na). The fluorine is generated from laser ablation of the Teflon poppet in the pulsed valve in the source, and the copper comes from ablation of the adjacent copper nozzle. The origins of the Si and Na are unclear.

Table 3a. Conditions for first-exposure batch.

Target fluence	2.00×10^{20} atoms/cm^2
Actual fluence	2.46×10^{20} atoms/cm^2
Beam velocity	7.8 km/s
Average pulse rate	3.03 Hz
Test duration	25.17 hours
Number of pulses	274,560

Table 3b. Fluence determination, first-exposure batch.

Sample	Exposed Area (cm^2)	Pre-test Mass (g)	Post-test Mass (g)	Δ(g)	Fluence (atoms/cm^2)
Kapton-C	4.45	0.033665	0.028385	-0.005280	2.78×10^{20}
Kapton-1	0.97	0.009232	0.008255	-0.000977	2.36×10^{20}
Kapton-2	0.97	0.022883	0.021795	-0.001088	2.63×10^{20}
Kapton-3	0.97	0.009222	0.008298	-0.000924	2.24×10^{20}
Kapton-4	0.97	0.022992	0.022041	-0.000951	2.30×10^{20}

Table 4a. Conditions for second-exposure batch.

Target fluence	2.00×10^{20} atoms/cm^2
Actual fluence	1.97×10^{20} atoms/cm^2
Beam velocity	7.8 km/s
Average pulse rate	3.02 Hz
Test duration	25.28 hours
Number of pulses	274,560

Table 4b. Fluence determination, second-exposure batch.

Sample	Exposed Area (cm^2)	Pre-test Mass (g)	Post-test Mass (g)	Δ(g)	Fluence (atoms/cm^2)
Kapton-1	0.97	0.009020	0.008244	-0.000776	1.88×10^{20}
Kapton-2	0.97	0.022821	0.022020	-0.000801	1.94×10^{20}
Kapton-3	0.97	0.008717	0.007914	-0.000803	1.94×10^{20}
Kapton-4	0.97	0.022921	0.022043	-0.000878	2.13×10^{20}

Table 5. ESCA analysis of Germanium-coated Kapton sample, Ge/K-1, chamber witness.

Element	Pre-test (atom %)	Post-test (atom %)
Ge	37.73	37.45
C	18.85	10.60
O	40.76	49.49
Na	2.66	2.46

Table 6. ESCA analysis of Germanium-coated Kapton sample, 5P7C, that served as a witness for the first-exposure batch.

		Post-test	
Element	Pre-test (atom %)	Area 1 (atom %)	Area 2 (atom %)
Ge	27.41	23.77	18.49
Si	-----	4.48	6.20
C	38.48	7.50	22.92
K	-----	3.25	-----
O	34.11	44.80	41.91
F	-----	11.06	5.34
Cu	-----	-----	1.46
Na	-----	5.14	3.69

Table 7. ESCA analysis of Germanium-coated Kapton sample, Ge/K-2, that served as a witness for the second-exposure batch.

		Post-test		
Element	Pre-test (atom %)	Area 1 (atom %)	Area 2 (atom %)	Area 3 (atom %)
Ge	37.69	23.25	22.10	23.34
Si	-----	4.73	4.04	5.11
C	19.34	9.83	10.62	10.62
O	40.96	56.88	54.22	52.98
F	-----	-----	3.78	3.23
Cu	-----	3.42	3.50	3.45
Na	2.02	1.89	1.75	1.27

The Ge/K witness in the beam for the second exposure batch showed similar results (see Table 7). For this sample, three areas on the surface were examined by ESCA after the exposure, thus providing a good indication of the variability of the surface. Although the fluorine contamination appears to be lower for the second batch, examination of the test samples shows that both batches had similar fluorine contamination levels. It appeared that sample surfaces acquired an extra 3 to 20 atom percent F as a result of the exposure. The wide variability suggests that the measurement is strongly dependent on the area of the surface that is examined. Contamination from the other three elements, Si, Cu, and Na, did not appear to be so severe, as they were typically present at atom percentages of 5 or less.

3.8 Results and Discussion

The results based on analyses of the materials evaluated in the BMDO EOIM-3 flight exposure and ground test are summarized in this section. Discussions of the data are presented in Sections 3.8.1 through 3.8.10, while the actual data are summarized in Tables 8 through 17. Materials' properties which underwent significant changes due to atomic oxygen exposure are highlighted in the tables with gray shading. For certain materials, entries are marked "N/A," indicating that the measurement is not applicable for the particular specimen configuration. Other entries are marked "TBS," indicating that the data were not available at the time this report was prepared. The discussions and tables are arranged according to categories corresponding to typical applications for the materials. There are two rows of data per sample: the top row represents flight exposure data and the bottom row represents ground exposure data.

Visual changes are seen by side-by-side comparisons of flight, ground, and control photographs and on observational notes taken during de-integration and analyses.

Mass changes were considered insignificant if the change was 0.1 mg or less. In general, changes of less than 0.5 mg are of little significance, especially for thick specimens, since moisture uptake can appreciably affect specimen weights. Conclusions from mass changes for thin coatings on thick substrates should be drawn with care.

The criteria for denoting a "yes" in the "ESCA change" column for the flight test specimens included significant atom percent changes in elements other than silicon. This is due to the ubiquitous presence of silicon contamination at low levels. Materials which were highly reactive to atomic oxygen received an approximately 2 to 3 atom percent coverage of silicon in

the flight exposure. Stable materials received a significantly higher 9 to 12 atom percent coverage of silicon. This latter value corresponds to a roughly 20 Å thick layer of SiO_2 deposited on non-reactive surfaces. A "yes" in the "ESCA change" column for the ground test specimens indicates significant atom percent changes in elements other than fluorine, which was generated by the testing in the ground-based facility (see Section 3.7.5).

Data in the columns on the right were provided by the co-investigators and represent the critical functional properties for the test materials. For further details regarding these measurements, the final reports from the co-investigators should be consulted. The executive summaries of those reports are contained in Appendix A, and a co-investigators' directory is listed in Appendix B.

Mass and ESCA data are included in Appendix F. The first row of mass data pertains to the flight sample, while the second row of mass data (measured at PSI) pertains to the ground sample. The as-received and post-bake ESCA data were measured on the control specimen, whereas the post-flight and post-ground columns pertain to the flight and ground samples, respectively.

Materials evaluated by the co-investigators were logically categorized by their functional class. The class names provide the top-level definition for the SEE Program's AO database. The parameters evaluated for each material class provided a list and structure of attributes to be included in the database for each material. Photographs, taken before and after AO exposures, will be scanned into the database (see Appendix G) and available to database users to view on-line.

The AO experiments' effects data for individual materials will be integrated into a desktop system-analysis tool. With the tool, users can input a mission time line, orbital parameters and spacecraft orbital orientation, build a low-fidelity, 3-dimensional model of spacecraft surfaces and associate a material or materials with the surfaces. The model will provide predictions, based on the materials' effects data, of the materials' durabilities.

3.8.1 Advanced Radiator, Threat Shielding, and Structural Materials

Nine advanced radiator, threat shielding, and structural materials were evaluated, and the data are summarized in Table 8. Significant erosion occurred in the unprotected carbon/carbon composite (5L5) as compared to the tungsten (1P2) or titanium carbide, (5P3, 1L1) overcoated

Table 8. Advanced radiator, threat shielding, and structural materials.

Material Specimen	Sample Code	Visual Change	Mass Change (mg)	ESCA Change	α		ε	
					Pre	Post	Pre	Post
Tungsten/graphite cloth/carbon foam	1P2A	Delaminated	No	No	0.696	0.729	0.093	0.113
	1P2C	Cracked	-0.7	YES	0.696	0.707	0.093	0.084
CVD TiC/graphite cloth/carbon foam	5P3A	No	-0.6	No	0.661	0.671	0.274	0.270
	5P3C	No	-0.2	No	TBS	TBS	TBS	TBS
TiC-coated carbon/carbon	1L1A	No	No	No	0.55	0.56	0.14	0.15
	1L1C	No	No	YES	0.55	0.56	0.15	0.15
Carbon/carbon composite	5L5A	Blackened	+2.6	No	0.82	0.97	0.57	0.75
	5L5C	Blackened	-0.7	No	0.82	0.99	0.57	0.69
T300/934 composite, LDEF trailing edge	5C1A	Blackened	+1.3	No	N/A	N/A	N/A	N/A
	5C1B	No	-0.2	No	N/A	N/A	N/A	N/A
T300/934 composite, adjacent to 5C1	5C2A	Blackened	+1.0	YES	N/A	N/A	N/A	N/A
	5C2B	No	-0.6	YES	N/A	N/A	N/A	N/A
P-100/MR56-2 composite	5O1A	Blackened	+0.2	YES	N/A	N/A	N/A	N/A
	5O1C	Blackened	-0.3	YES	N/A	N/A	N/A	N/A
P75/Mg vacuum cast composite	5L0A	No	+0.5	No	N/A	N/A	N/A	N/A
	5L0C	No	No	No	N/A	N/A	N/A	N/A
Niobium beryllide high temperature alloy	5L9A	Pits	No	No	0.62	0.57	0.12	0.12
	5L9C	Cracked,Peeled	No	No	0.62	0.57	0.12	0.13
3M Y9469 Acrylic transfer tape	5D1A	Blackened	-0.8	YES	N/A	N/A	N/A	N/A
	5D1C	Darkened	-0.7	No	N/A	N/A	N/A	N/A

Table 9. Optical baffle materials.

Material Specimen	Sample Code	Visual Change	Mass Change (mg)	ESCA Change	Reflectance		BRDF Change
					Pre	Post	
Beryllium (black etched) on beryllium foam	1N4A	No	-0.6	No	0.26	0.12	No
	1N4D	No	-0.7	No	0.26	0.21	No
Boron (plasma) on beryllium	1N5A	No	N/A	No	No change		No
	1N5C	No	No	No	No change		No
Martin Black on aluminum	1N6A	No	No	YES	No change		No
	1N6C	No	-0.3	YES	No change		No
Aluminum, textured	5Q1A	No	No	No	0.029	0.034	Minor
	5Q1C	No	-0.2	No	0.03	0.03	No
Aluminum, textured	5Q2A	No	No	No	0.028	0.029	Minor
	5Q2C	No	No	No	0.03	0.03	No
Beryllium, textured, 100 μm, on aluminum	5Q3A	No	No	No	0.009	0.010	Minor
	5Q3C	No	-0.2	No	0.01	0.01	No
Beryllium, textured, 100 μm, on aluminum	5Q4A	No	No	No	0.009	0.010	No
	5Q4C	No	-0.2	No	0.01	0.01	No
Beryllium, black etched, on beryllium	5Q5A	No	No	No	No change		No
	N/A	----	----	----	------		----
Beryllium, black etched, on beryllium	5Q6A	No	No	No	No change		No
	5Q6B	No	No	No	No change		No

Table 9. Optical baffle materials (continued).

Material Specimen	Sample Code	Visual Change	Mass Change (mg)	ESCA Change	Reflectance		BRDF Change
					Pre	Post	
Boron carbide on graphite	5Q7A	No	No	YES	No change		No
	5Q7B	No	No	YES	No change		No
Boron carbide on graphite	5Q8A	No	No	YES	No change		No
	N/A	----	----	----	----		----
Magnesium oxide on beryllium	5Q9A	No	No	YES	TBS		Improved
	5Q9C	No	No	YES	TBS		No
Magnesium oxide on beryllium	5Q0A	No	No	YES	TBS		Improved
	5Q0C	No	No	YES	TBS		No

Table 10a. Optical reflector materials.

Material Specimen	Sample Code	Visual Change	Mass Change (mg)	ESCA Change	TIS* (x 10^{-4})		Reflectance*	
					Pre	Post	Pre	Post
$(SiC/SiO_2)(SiH/SiO_2)^5/Si$ (tuned MWIR)	5M2A	No	N/A	YES	8.6	16.8	0.9914	0.9921
	5M2B	No	No	YES	11.1	10.2	0.9919	0.9926
$(Si_3N_4/SiO_2)^6/Si$ (tuned MWIR)	5M3A	No	N/A	YES	N/A	N/A	0.9646	0.9622
	5M3B	No	No	YES	N/A	N/A	0.9648	0.9624
$(AlN/Al_2O_3)^6/Si$ (tuned visible)	5M4A	No	N/A	YES	N/A	N/A	N/A	N/A
	5M4B	No	No	YES	N/A	N/A	N/A	N/A
$(Si/SiO_2)^5/Si$ (tuned MWIR)	5M5A	No	N/A	YES	8.8	13.9	0.9968	0.9976
	5M5B	No	-0.2	YES	9.3	11.6	0.9967	0.9973
$(SiH/SiO_2)^5/Si$ (tuned MWIR)	5M6A	No	N/A	YES	2.8	17.0	0.9966	0.9974
	5M6B	No	-0.3	YES	3.9	4.9	0.9965	0.9973
$(BN/SiO_2)(SiH/SiO_2)^5/Si$ (tuned MWIR)	5M7A	Darkened	N/A	YES	7.8	30.3	0.9967	0.9511
	5M7B	No	-0.3	YES	5.7	9.2	0.9954	0.9683
Unprotected Al on silicon (broadband)	5M8A	No	N/A	No	2.3	11.0	0.9556	0.9559
	5M8B	No	-0.2	No	2.6	6.9	0.9560	0.9562
$(SiC/SiO_2)^6/Si$ (tuned MWIR)	1M10A	No	N/A	YES	10.8	20.1	0.9937	0.9943
	1M10B	No	-0.2	YES	14.6	15.2	0.9938	0.9939
Uncoated HIP I-70 beryllium (broadband)	1M13A	No	N/A	No	6.7	10.0	0.9540	0.9533
	1M13B	No	No	No	9.5	10.2	0.9535	0.9532

*TIS was measured at 3.39 μm; reflectance was measured in MWIR.

Table 10a. Optical reflector materials (continued).

Material Specimen	Sample Code	Visual Change	Mass Change (mg)	ESCA Change	TIS (x 10^{-4})		Reflectance	
					Pre	Post	Pre	Post
$(Si_3N_4/Al_2O_3)^6$/Ag/ fused silica	1M11A	No	N/A	YES	~6	~8	0.9101	0.9109
	1M11B	No	No	YES	~6	45±10	0.9158	0.9169
Uncoated half of β-SiC (UV reflector)	1M12A-SiC	No	N/A	YES	0.6	1.0	N/A	N/A
	1M12B-SiC	No	N/A	YES	1.6	6.0		
Al_2O_3/Al-coated half of β-SiC (broadband)	1M12A-Al	No	N/A	No	6.4	6.5	0.9482	0.9479
	1M12B-Al	No	N/A	No	6.1	12.3	0.9497	0.9464
$(Si_3N_4/Al_2O_3)^2$/ Al/Si (tuned MWIR)	1M14A	No	N/A	YES	2.5	6.0	0.9823	0.9828
	1M14B	No	-0.4	YES	2.5	81.7	0.9815	0.9818
$(Si/SiO_2)^4$/Al/Si (tuned MWIR)	1M16A	No	N/A	YES	14.4	17.7	0.9962	0.9971
	1M16B	No	No	YES	14.2	18.0	0.9965	0.9966

Table 10b. Optical coatings and mirrors.

Material Specimen	Sample Code	Visual Change	Mass Change (mg)	ESCA Change	Reflectance	BRDF
SiO_2-doped Al_2O_3/ SiO_2 multilayer on fused SiO_2	1B1A	No	No	TBS	No change	No change
	1B1C	No	No	TBS	Decreased	More scatter
TiN (1000 Å) on fused SiO_2	1B2A	Pits	No	TBS	TBS	No change
	1B2C	No	No	TBS	TBS	More scatter
Beryllium, diamond turned, on beryllium	5N1A	Edge: pits	No	No	No change	No change
	5N1C	No	No	YES	No change	No change
Beryllium, conventional polished, on beryllium	5N2A	No	No	No	No change	No change
	5N2C	No	No	YES	No change	No change
Beryllium/silicon on SiC substrate	5N3A	No	No	YES	No change	No change
	5N3C	No	+0.2	YES	No change	No change
Si/Al_2O_3 on Vit-C/SiC (upper)	5P1A-u	No	N/A	YES	No change	No change
	5P1C-u	No	N/A	YES	No change	More scatter
Si/Al_2O_3/enhanced MLD on Vit-C/SiC (lower)	5P1A-l	No	N/A	YES	No change	No change
	5P1C-l	No	N/A	YES	No change	More scatter

Table 10c. Optical protective coatings.

Material Specimen	Sample Code	Visual Change	Mass Change (mg)	ESCA Change	Recession (Å)	RMS (Å)	
						Pre	Post
CVD diamond on silicon	5M1A	Darkened	N/A	YES	None	1011*	790*
	5M1B	Dark patch	-0.3	YES	2138	1138	1200
CVD diamond brazed to a ZnS window	1M9A	Darkened	N/A	YES	None	54.4	53.3
	1M9B	Turned reddish	-0.3	No	1043	58.6	263
AlN/SiH/CVD diamond/ZnS	1M15A	No	No	No	TBS	N/A	N/A
	1M15B	No	-0.7	No	None	40	43
Diamond film on silicon wafer	5F1A	Darkened	No	YES	TBS	TBS	
	5F1B	Darkened	No	No			
Diamond film on silicon wafer	5F2A	Darkened	No	YES	TBS	TBS	
	5F2B	Darkened	No	YES			

*Measured in crescent-shaped area near edge of sample.

Table 10d. Optical substrate material.

Material Specimen	JPL Code	Visual Change	Mass Change (mg)	ESCA Change	α		ε	
					Pre	Post	Pre	Post
Silicon carbide ceramic	5L4A	No	No	YES	0.76	0.78	0.61	0.61
	5L4C	No	No	YES	----	0.77	----	0.62

Table 11a. Thermal control coatings.

Material Specimen	Sample Code	Visual Change	Mass Change (mg)	ESCA Change	α		ε	
					Pre	Post	Pre	Post
SiC/Al composite, $CaZrO_3$ coating	5H1A	No	No	YES	0.57	0.58	0.82	0.81
	5H1C	No	No	YES	----	0.58	----	0.81
SiC/Al composite, Al_2O_3 coating	5H2A	No	No	YES	0.30	0.31	0.81	0.81
	5H2C	No	No	YES	----	0.31	----	0.81
IM7/PEEK, Al_2O_3 coating	5H3A	No	No	YES	0.35	0.32	0.82	0.82
	5H3C	No	No	YES	----	0.34	----	0.82
IM7/PEEK, BN/Al_2O_3 coating	5H4A	No	No	YES	0.39	0.37	0.80	0.80
	5H4C	No	No	YES	----	0.39	----	0.80
Beta-alumina (0.002") coated aluminum	5L3A	No	No	No	0.29	0.30	0.90	0.90
	5L3C	No	No	No*	----	0.29	----	0.90
Calcium zirconate coated C/C	5L6A	No	+2.7	No	0.59	0.59	0.82	0.82
	5L6C	No	-0.3	No*	----	0.59	----	0.82
Beta-alumina on C/C	5L7A	No	+2.9	No	0.28	0.26	0.90	0.89
	5L7C	No	-0.3	No*	----	0.28	----	0.89

*Specimens were contaminated with fluorine.

Table 11b. Thermal control materials.

Material Specimen	Sample Code	Visual Change	Mass Change (mg)	ESCA Change	α		ε	
					Pre	Post	Pre	Post
Alumina on aluminum substrate	5P4A	No	No	YES	.218	.220	.045	.045
	5P4C	Turned green	No	YES	----	.224	----	.046
Germanium/Kapton	5P7A	No	No	YES	.485	.485	.627	.614
	5P7C	No	-0.3	YES	.482	.465	.616	.634
Indium tin oxide/ Teflon/VDA/Kapton	5P8A	No	No	No	.166	.162	.681	.677
	5P8C	Milky haze	-0.2	YES	.169	.181	.675	.674
Microsheet/Ag/Y966/Al	5P9A	No	No	No	.092	.091	.825	.824
	5P9C	No	-0.3	No	.092	.091	.822	.822
$(Si/SiO_2)/(TiO_2/SiO_2)$ on Kapton	5P0A	No	No	No	.180	.192	.740	.741
	5P0C	No	-0.2	No	.180	.186	.740	.738

Table 11c. Thermal blanket materials.

Material Specimen	Sample Code	Visual Change	Mass Change (mg)	ESCA Change	Erosion
Glass fiber/Teflon composite	1L2A	No	No	No	No
	1L2C	No	No	No	YES
Kapton HN	K-A	Matte finish	-3.0	YES	YES
	K-C	Matte finish	-5.3	YES	YES
Beta-cloth, graphite interwoven	5G1A	No	No	No	No
	5G1C	No	-0.5	No	YES

Table 12a. Protective coatings (curable).

Material Specimen	Sample Code	Visual Change	Mass Change (mg)	ESCA Change	RMS Roughness (nm)	
					Pre	Post
HRG-3/AB epoxy silane (HAC)	5E1A	No	No	YES	105	73
	5E1C	No	No	YES	----	113
HRG-3/AB epoxy silane (vendor)	5E2A	Darkened	No	YES	140	40
	5E2C	No	No	YES	----	374

Table 12b. Plasma-spray protective coating.

Material Specimen	Sample Code	Visual Change	Mass Change (mg)	ESCA Change	Recession (μm)	Erosion Yield (cm^3/atom)
Al_2O_3 coating on graphite composite	5P6A-c	Brownish film	N/A	YES	None	None
	5P6C-c	No	N/A	YES		
Uncoated graphite composite	5P6A-u	Brownish film	N/A	No	2±0.4	1×10^{-24}
	5P6C-u	Blackened	N/A	No	2±0.7	1×10^{-24}

Table 13. Tribological materials.

Material Specimen	Sample Code	Visual Change	Mass Change (mg)	ESCA Change	μ	
					Pre	Post
MoS_2-Ni lubricant on steel, Ovonic	1A1A	Delaminated	No	N/A	0.015	0.084
	1A1C	No	No	N/A	----	0.050
MoS_2-Ni lubricant on steel, Ovonic	1A2A	Delaminated	No	N/A	TBS	TBS
	1A2C	No	No	N/A	----	TBS
MoS_2-SbO_x lubricant on steel, Hohman	1A3A	No	No	N/A	0.025	0.018
	1A3C	No	No	N/A	----	0.021
MoS_2-SbO_x lubricant on steel, Hohman	1A4A	No	+1.6	N/A	TBS	TBS
	1A4C	No	No	N/A	----	TBS

Table 14. High temperature superconductors.

Material Specimen	Sample Code	Visual Change	Mass Change (mg)	ESCA Change	T_c/K	
					Pre	Post
Y-Ba-Cu-O high temperature superconductor, oxygen deficient	5K6A	Darkened	No	No	43	42
	5K6B	No	No	No	43	40
Y-Ba-Cu-O high temperature superconductor, fully oxgyenated	5K7A	No	No	No	87	82
	5K7B	No	+0.2	No	87	82

Table 15. Actinometers.

Material Specimen	Sample Code	Visual Change	Mass Change (mg)	ESCA Change	Norm. Conductance	
					Pre	Post
Al_2O_3/carbon foil on sapphire, Al holder	1K8A	Cracked	N/A	N/A	1.0	0.26
SiO_x/carbon foil on sapphire, Al holder	1K9A	Foil eroded	+0.7	No	1.0	0.7

Table 16. Photovoltaics.

Material Specimen	Sample Code	Visual Change	Mass Change (mg)	ESCA Change	V_{oc}/I_{sc} (v) (A)		P_{mp} (mW)	
					Pre	Post	Pre	Post
Copper indium diselenide-photovoltaic	5L8A	Slight darkening	-0.2	YES	TBS	TBS	TBS	TBS
	5L8C	No	No	YES	TBS	TBS	TBS	TBS
Solar cell	1P5A	No	-0.2	No	.587/ .101	.581/ .101	44	43

Table 17. Pyroelectric detectors.

Material Specimen	Sample Code	Visual Change	Mass Change (mg)	ESCA Change	Spectral	
					Pre	Post
Ni/PbTe/Al/PVDF	1K3A-A	Burn spot	N/A	TBS	No change	
	1K3C-A	Darkened		YES		
Ni/Si/SiO_2/Al/PVDF	1K3A-B	Darkened	N/A	TBS	No change	
	1K3C-B	No		No		
Ni/SiO_2/Al/PVDF	1K3A-C	Darkened	N/A	TBS	No change	
	1K3C-C	No		No		
Ni/ZnS/PbF_2/ZnS/Al/PVDF	1K3A-D	Darkened	N/A	TBS	No change	
	1K3C-D	No		YES		
Mo/Si/SiO_2/Al/PVDF	1K4A-A	No	N/A	TBS	No change	
	1K4C-A	No		YES		
Ni/TiO_2/Al_2O_3/TiO_2/Al/PVDF	1K4A-B	No	N/A	TBS	No change	
	1K4C-B	No		No		
Mo/TiO_2/Al_2O_3/TiO_2/Al/PVDF	1K4A-C	No	N/A	TBS	No change	
	1K4C-C	No		YES		
Al/PVDF	1K4A-D	No	N/A	TBS	No change	
	1K4C-D	No		No		
Al/PVDF (Vendor Al)	5K5A	No	+0.5	No	No change	
	5K5C	Wrinkles	+0.2	No		

carbon/carbon materials. The TiC coated carbon/carbon materials were slightly oxidized with some loss of carbon. The T300/934 fiber-reinforced polymer composite material (5C1), previously flown on the trailing edge of the Long Duration Exposure Facility (LDEF), was compared to the same material (5C2) flown on LDEF but not exposed to the external solar environment. It was found that the significant fixed silicon contamination (as SiO_2) which occurred during the LDEF mission as regards the exposed material specimen (5C1) affected the specimen's erosion yield for the EOIM-3 experiment. The P-100 fiber-reinforced MR56-2 bismaleimide composite (5O1) showed heavy erosion of the matrix. The P75/magnesium composite (5L0) was unaffected by flight or ground exposure. The 3M Y9469 acrylic tape (5D1) used for passive damping was not analyzed for direct atomic oxygen exposure effects. Sample SD1 was shielded from AO in a sandwiched configuration but showed changes in its loss factors.

3.8.2 Optical Baffle Materials

Thirteen sets of samples, representing eight optical baffle materials, were evaluated in this experiment, and the data are listed in Table 9. Duplicate specimens were flown for five of the eight materials for subsequent evaluation in a nuclear threat environment. The optical baffle materials showed little or no degradation in reflectance or bidirectional reflectance distribution function (BRDF) as a result of flight or ground exposure to atomic oxygen. Magnesium oxide on beryllium flight samples (5Q9A, 5Q0A) experienced a slight improvement in BRDF as a result of AO exposure. Several of the optical baffle materials underwent surface chemical changes due to AO reactions. Martin Black samples (1N6A, 1N6C) experienced substantial loss of surface carbon as a result of flight and ground atomic oxygen exposure. Boron carbide on graphite flight and ground specimens (5Q7A, 5Q7B) also exhibited significant carbon removal, whereas the second flight sample (5Q8A) experienced loss of boron. The flight-exposed samples with magnesium oxide coatings on beryllium (5Q9A, 5Q0A) showed a slight increase in oxygen content. A substantial amount of fluorine was found in the ground-exposed magnesium oxide on beryllium specimens (5Q9C, 5Q0C).

3.8.3 Optical Materials and Coatings

Twenty-seven optical materials and coatings were evaluated in the BMDO EOIM-3 Experiment. Table 10a summarizes the mid-wave infrared (MWIR) reflectance and total integrated scatter (TIS) for fourteen optical reflectors supplied by the Naval Air Warfare Center at China Lake. Table 10b provides reflectance and BRDF data for seven mirror and optical coatings. Table 10c summarizes erosion and surface roughening effects for five optical protective coating samples. Table 10d provides a data summary for a silicon carbide ceramic material. Due to the sensitive nature of the performance measurements for these optics, effects due to molecular and particulate contamination were often important considerations for interpretation of the post-exposure data.

3.8.3.1 NAWC Optical Reflectors

Fourteen developmental dielectric and bare metal reflectors were supplied by the Naval Air Warfare Center Weapons Division (NAWCWPNS) for evaluation on the BMDO EOIM-3 Experiment. Table 10a provides a data summary for these reflectors, including absolute reflectance and total integrated scatter measurements performed by NAWC. With the exception of the boron nitride optic (5M7), the samples showed an insignificant change in the reflectance as a result of exposure to atomic oxygen. Several materials had significant increases in TIS; most of the increases can be attributed to contamination, rather than an atomic oxygen attack of the optical surfaces. The nitride coatings were susceptible to chemical attack by atomic oxygen, which results in substitution of nitrogen by oxygen. The boron nitride (5M7), silicon nitride (5M3, 1M11, 1M14), and aluminum nitride (5M4) optics exhibited the tendency to replace nitrogen with oxygen as a result of flight or ground exposure. The poor performance of boron nitride as an optical coating is attributed to the formation of boron oxides which easily hydrolyze in the terrestrial atmosphere to form volatile boric acid. This mechanism explains the measurable loss of boron in the boron nitride (5M7) samples, and the loss also correlates with the large reflectance change (2-5%) for this coating. The silicon (5M5, 1M16) and silicon hydride (5M6) coatings were oxidized beyond levels consistent with contamination. The silicon carbide coatings (5M2, 1M10) lost carbon due to oxygen attack in both flight and ground exposure tests.

3.8.3.2 Optical Coatings and Mirrors

Seven optical coatings and mirror materials from sources other than NAWC, evaluated in the BMDO EOIM-3 Experiment, are listed in Table 10b. The optical properties of these materials were only slightly affected, if at all, by exposure to atomic oxygen. The slight changes in scattering or reflectance were generally attributed to contamination effects. Most of the coatings did experience changes in surface chemical composition due to atomic oxygen. ESCA measurements were not performed on the silica-doped alumina/silica multilayer optic (1B1) and the titanium nitride on silica optic (1B2) at the request of the supplier, in order to leave the surface unaffected for subsequent threat exposure evaluations. The flight beryllium mirrors (5N1A and 5N2A) did not experience any significant chemical change. The ground-exposed mirrors (5N1C and 5N2C) did oxidize slightly with a substantial loss of carbon. The flight and ground beryllium/silicon on carbide substrates (5N3A and 5N3C) both exhibited a loss of carbon and slight oxidation, with the ground test specimen acquiring a significant amount of fluorine. The silicon/alumina and aluminum-enhanced multi-layer dielectric silicon/alumina coatings on vitreous carbon/silicon carbide substrates (5P1A and 5P1C) showed slight oxidation and loss of carbon for both flight- and ground-exposed specimens.

3.8.3.3 Optical Protective Coatings

Table 10c contains data for five optical protective coating samples. As discussed earlier, the polycrystalline chemical vapor deposited (CVD) diamond film on silicon (5M1) specimen showed unique sensitivity to the molecular contamination environment in the flight experiment. The crescent-shaped region which was protected from the line-of-sight source of silicone contaminants was found to have measurable rms roughness, possibly due to a preferential attack on the edges of the diamond crystallites by atomic oxygen. The flight specimen (5M1A) showed no measurable recession of coating thickness whereas the ground-exposed specimen (5M1B) lost over 2000 Å of the diamond coating. A similar phenomenon occurred for the CVD-diamond on a chalcogenide glass braze over zinc sulfide (1M9). The ground-exposed sample exhibited a 1000 Å erosion of the coating, but no measurable loss was detected in the flight specimen. The ground-exposed aluminum nitride/silicon hydride anti-reflection coating on a CVD diamond on a chalcogenide glass braze over zinc sulfide specimen (1M15B) showed no measurable recession or change in rms roughness. The recession and rms roughness of diamond coatings

on silicon (5F1 and 5F2) were not characterized. The flight diamond coatings showed evidence for oxidation beyond the levels accounted for by silicon oxide contamination films. A slight increase of oxygen content ($\sim 5\%$) was also noted for the ground-exposed diamond materials. The aluminum nitride coating showed a reduction of carbon content, but little evidence of oxygen substitution for nitrogen. This indicates that the aluminum nitride material is exceptionally stable against atomic oxygen attack.

3.8.3.4 Optical Substrate Material

The data for the silicon carbide ceramic optical sample (5L4) are summarized in Table 10d. The material showed no change in solar absorptance or emittance as a result of flight or ground exposure to atomic oxygen. The changes in surface chemical composition were as expected: slight oxidation and a loss of carbon content observed for both the flight and ground-exposed articles.

3.8.4 Thermal Control Materials and Coatings

A total of fifteen thermal control materials and coatings were evaluated in the BMDO EOIM-3 Experiment. Characterization data for the thermal control coatings are discussed in Section 3.8.4.1, with the data summarized in Table 11a. Other thermal control materials are described in Sections 3.8.4.2 and 3.8.4.3, with characterization data listed in Tables 11b and 11c.

3.8.4.1 Thermal Control Coatings

Seven ceramic thermal control coatings over various composite substrates were tested on the BMDO EOIM-3 Experiment. Data are listed in Table 11a. No measurable changes in solar absorptance or hemispherical emittance were measured for any of these coatings after atomic oxygen exposure. Surface chemical analysis for all of these materials shows the typical loss of carbon content due to atomic oxygen reaction. The oxygen content remained stable for the flight samples, but a significant amount of fluorine was noted on all of the ground-exposed materials. It should be noted that sample 5H4 was identified by the supplier as a boron nitride/alumina coating on an IM7/PEEK composite. ESCA analysis revealed no boron or nitrogen present on the surface of this specimen. Further ESCA analysis of this material after sputter removal of

the outer surface did detect boron, indicating that some differentiation of constituents may have occurred during the plasma-spray application of the coating. A discrepancy in flight versus ground test was found in the morphology of the ß-alumina coating on C/C (5L7); it is attributed to formation of sodium fluoride fibers.

3.8.4.2 Thermal Control Materials

Data from five thermal control material samples are shown in Table 11b. **The solar absorptance and hemispherical emittance values for each of these materials remained essentially constant through both the flight and the ground exposures.** The sputter-deposited alumina on aluminum samples (5P4) showed slight color variation among themselves prior to exposure. The color variation is attributed to an interference effect caused by slight variations in coating thickness. The sample composed of an indium tin oxide coating on aluminized FEP bonded to Kapton (5P8) developed a somewhat hazy appearance after atomic oxygen exposure. However, the critical thermo-optical properties were unaffected. Chemical analysis of the surface revealed reduction of carbon content for each of the specimens by atomic oxygen reaction. The germanium/Kapton flight- and ground-exposed specimens (5P7) oxidized, forming an oxide layer estimated to be about 60 Å thick. The chemical composition of the indium tin oxide coating of 5P8A was not significantly altered during flight exposure, but the ground-exposed specimen (5P8C) acquired a significant amount of fluorine during exposure. The surface composition of the silvered-microsheet second-surface-mirror (5P9) was essentially unchanged for both the flight and ground specimens, as was the surface composition of a multi-layer dielectric stack on Kapton material (5P0).

3.8.4.3 Thermal Blanket Materials

Three materials commonly used in multi-layer insulation (MLI) thermal blankets were tested in the BMDO EOIM-3 Experiment. The data are shown in Table 11c. Film specimens of Kapton HN were used as standard atomic oxygen erosion monitors for the flight and ground exposures. Sample K-A represents Kapton HN exposed in flight and K-C represents ground exposure. As determined by weight loss and scanning electron microscopic measurement, approximately 6.4 μm of Kapton were eroded away in the flight exposure. Two samples of Beta-cloth (glass fabric encapsulated in Teflon) were also tested. Slight erosion of the ground-

exposed Beta-cloth was detected for both samples 1L2C and 5G1C, but the flight specimens were not perceptibly affected. Chemical analysis of the surface revealed no significant chemical changes for the Beta-cloth samples, but the oxygen content of the surface of the flight and ground Kapton HN film samples increased slightly. This is consistent with observations in previous exposure studies.

3.8.5 Protective Coatings

Three materials were evaluated as coatings to protect against atomic oxygen on the BMDO EOIM-3 Experiment. Data for epoxy-terminated silanes (5E1 and 5E2) are listed in Table 12a. The effectiveness of a plasma-spray alumina in protecting a graphite-fiber-reinforced thermoplastic composite (5P6) is shown in Table 12b.

The epoxy-terminated silane materials were flown as neat resins cast on a smooth substrate. The original surface roughness was found to be slightly reduced by the flight atomic oxygen exposure. Surface chemical analysis shows the silane epoxies developed a thin silicon dioxide film. This film acts as an effective self-protecting skin to halt atomic oxygen degradation.

Specimen 5P6 was prepared by coating one half of a PEEK composite disk with plasma-spray alumina. The unprotected region was eroded by atomic oxygen to a depth of about 2 μm, whereas no measurable erosion was found in the coated area. Surface chemical analysis in the unprotected region shows little change in composition. The coated region exhibited the typical loss of carbon due to atomic oxygen reaction.

3.8.6 Tribological Coatings

Two dry-film tribological coatings were evaluated on the BMDO EOIM-3 Experiment. The data are shown in Table 13. Samples 1A1 and 1A2 were sputtered molybdenum disulfide/nickel multi-layer films deposited on polished stainless steel substrates. Specimens 1A3 and 1A4 were co-deposited molybdenum sulfide and antimony oxide sputtered from a composite target onto polished stainless steel substrates. Visual inspection readily identified a delamination failure of the MoS_2/Ni multi-layer coating. This delamination was subsequently attributed to an oxide film at the coating to substrate interface which led to debonding as a result of stresses induced by thermal cycling in earth orbit. The MoS_2/SbO_x lubricant film did not suffer from

this delamination problem. Friction testing of the intact MoS_2/SbO_x films resulted in friction coefficients which were essentially unchanged from the pre-exposure values for both the flight- and ground-exposed specimens. The flight MoS_2/Ni multi-layer film (1A1A) had a post-flight coefficient of friction almost a factor of six higher than its pre-flight value, while the ground-test specimen (1A1C) increase was almost a factor of four. Surface composition analysis shows that atomic oxygen readily replaces sulfur, forming an abrasive oxide film that may be self-protecting against further atomic oxygen attack. This oxide film is worn through within about 1000 cycles with a stylus at 1.0 GPa peak contact stress. **Based on these results, the MoS_2/SbO_x films appear to be superior for use in space applications over the MoS_2/Ni multi-layer lubricants.**

3.8.7 High Temperature Superconductors

Two samples of yttrium-barium-copper oxide (1-2-3) high temperature superconductors were tested and the data are shown in Table 14. One specimen (5K6) was supplied as an oxygen-deficient film, prepared by thermal decomposition in argon, while the other specimen (5K7) was fully oxygenated with T_c = 91 K (pre-flight). The transition for the flight exposed fully-oxygenated film occurred at about 85 K. If thermal vacuum cycling degraded the flight specimens in the early part of the mission or during the ground vacuum bake-out process, ram atomic oxygen was able to restore the exposed film almost to its original state. The deoxygenated material did not recover, presumably because oxygen was lost from the bulk of the material during thermal decomposition and the temperature and atomic oxygen fluence were not sufficiently high to replenish the oxygen within the material. Surface chemical analysis did not reveal any significant changes in the oxygen stoichiometry between the exposed and the control values. The differences in composition between the oxygen-deficient and fully oxygenated materials are not obvious from inspection of the pre-flight or post-flight ESCA data.

3.8.8 Actinometers

Two actinometers evaluated thin protective films for the Neutral Particle Beam (NPB) neutralizer foils. The data are listed in Table 15.

3.8.9 Solar Photovoltaics

Two solar photovoltaics were evaluated in the BMDO EOIM-3 Experiment, as summarized in Table 16. Copper indium diselenide (5L8) was evaluated as a candidate thin film photovoltaic system. ESCA showed that carbon was replaced by zinc for both flight and ground specimens. The CVD SiO_2 on an amorphous silicon solar cell (1P5) showed no quantitatively significant difference between pre- and post-flight performance.

3.8.10 Pyroelectric Detectors

Selective-interference absorbers on the pyroelectric detectors were evaluated for their sensitivity to a LEO environment, as summarized in Table 17. No functional differences were found except in the lead telluride design, 1K3A-A. In that design, the spectral response shifted by 3% toward shorter wavelengths, indicating a general thinning of PbTe. The magnitude of this shift was not sufficient to degrade the detector performance.

3.9 Conclusions

The materials, the thermal-vacuum conditioning and the sample handling procedures were chosen to minimize any risk of contamination on the samples. The result was a nominally clean atomic oxygen exposure experiment. The measured mass loss of Kapton agrees with estimates based on the MSIS-86 predictions. Different erosion rates for various materials were observed, as expected. It is important to recall that the total amount of silicone contamination is considered to be small, but it was sufficient to affect the optical performance of some of the optical test samples.

The BMDO samples that were exposed in a ground-based atomic oxygen testing facility produced an **average** flux of O-atoms about twice that encountered on EOIM-3. The concept of peak flux is misleading because the pulse duration is short. The nominal O-atom velocity and the velocity distribution were close to on-orbit O-atom velocities. The O-atom fluence to which all the samples were exposed was the same as the EOIM-3 fluence within the uncertainties associated with measurement of the ground and space fluences for the respective exposures ($\sim$20 percent). Although low levels of contamination were observed on most of the witness samples, these levels should have no bearing on conclusions reached about the correlation of the ground- and space-based exposures. Any differences observed between the EOIM-3 flight samples and

the identical samples that were exposed at PSI should reflect a fundamental difference between the nature of the FAST-1 and LEO environments and not an experimental artifact associated with the ground-based test.

The 82 samples flown by BMDO on the EOIM-3 experiment cover a broad range of material types for a number of specific applications. There was a broad range of atomic oxygen effects from "no effect" to highly deleterious. Given this diversity, only a limited number of general conclusions can be drawn. One of these, which is consistent with previous atomic oxygen testing, is that carbon-containing materials, such as graphite, organic polymers, and carbon fiber composites, are extremely susceptible to erosion, while metals and refractory inorganics are not. For example, structural materials (Section 3.8.1) show significant erosion of bare carbon-carbon and P-100 fiber-reinforced MR56-2 bismaleimide composites. A significant result derived from the BMDO experiments, however, is that protective coatings aimed at protecting these potentially important classes of materials from atomic oxygen work very well. The tungsten-coated and titanium-carbide-coated carbon-carbon composites were resistant to erosion, unlike the bare materials. Similarly, plasma-sprayed alumina effectively protected PEEK composites, while epoxy-terminated silane materials were ultimately protected by the formation of silicon dioxide coating. Interestingly, for some materials such as the Martin Black and boron carbide on graphite optical baffles, removal of carbon occurred without any significant compromise in their primary performance characteristics as indicated by the invariance of their reflectance and BRDF parameters.

Within the specific classes of materials, some generalized comments can also be made. As mentioned previously, the optical baffle materials showed no performance changes even though erosion was observed. Some classes of materials showed no significant change when exposed to atomic oxygen, due to the chemical nature (i.e., relative inertness) of their composition. Among these are the optical materials including the Naval Air Warfare Center reflectors (Sec. 3.8.3.1) and the mirrors and coatings provided by other co-investigators (Sec. 3.8.3.2), which, with a few minor exceptions noted elsewhere, showed no degradation either in their physical or performance characteristics. Similarly, silicon carbide optical substrates showed no changes, though a small amount of oxidation was observed. Of the optical materials investigated, the most notable changes were observed for some of the protective coatings such

as the diamond films; the changes are discussed in Section 3.8.3.3. Likewise, ceramic copper oxide high temperature superconductor materials tested were also unaffected by AO.

Good results were obtained for a majority of the thermal control materials. Coatings for thermal control applications, including ceramic coatings on various composite substrates (7 samples), and several classes of coating materials (4 samples), such as Kapton-based materials (Sec. 3.8.4), showed no significant change in their performance parameters. Their measured absorptivity and emissivity did not change as a function of atomic oxygen exposure. Of the three thermal control blankets, the Beta-cloth and the glass fiber/Teflon composite were unaffected, but the Kapton HN showed the expected erosion.

The advanced radiator, threat shielding, and structural materials showed the most significant degradation. This was especially obvious for unprotected materials with a large organic chemistry component such as bare carbon-carbon composites. Two tribological materials, MoS_2/Ni and MoS_2/SbO_x, were also tested, with the latter giving the superior performance in the space environment.

Overall, the ground and flight correlation was excellent with the exception of fluorocarbons and the plasma-sprayed Beta-alumina on carbon/carbon composite samples. In general, many of the materials tested showed a good resistance to atomic oxygen degradation. As a number of these have no prior flight history, this should facilitate their integration into future flight hardware. More importantly, the ability to duplicate the essential responses of the space-exposed materials with ground-based testing has provided a valuable step toward reliable ground-based testing.

3.10 Recommendations

- Since the Shuttle bay environment may generate a measurable level of silicone contamination, experiments sensitive to even monolayers of silicone may need to consider operating outside the Shuttle bay.
- Co-investigators must characterize their materials prior to exposure and provide sufficient materials of identical pedigree for valid comparisons.
- Weight measurement procedures must be consistent for direct comparison between flight and ground.

- There is a need to perform active experiments and continually monitor environment effects because passive experiments only provide data points at the start and the conclusion of the experiment.

APPENDIX A

CO-INVESTIGATORS' EXECUTIVE SUMMARIES

TABLE OF CONTENTS

TABLE OF CONTENTS (continued)

Tribology and Surface Chemistry of Sputtered MoS_2 Solid Lubricants Exposed to Atomic Oxygen

Michael T. Dugger
Sandia National Laboratories

Executive Summary

Sputtered MoS_2 is a solid lubricant material capable of ultralow friction coefficients (below 0.05) and high load-bearing capacity. Since it possesses low friction and wear rates in vacuum, low outgassing rate, is non-migrating and lacks organic binders, this material is an attractive lubricant for space-based mechanisms. The properties of sputtered MoS_2 even make it a viable replacement for systems which traditionally employ liquid lubricant systems (such as high speed gimbals and momentum transfer devices), but without the payload weight of a liquid delivery and contaminant system. Prior to 1991, these materials contained extensive porosity which provided large surface areas for absorption of atmospheric gases and opportunity for oxidation. At that time, sputtered MoS_2 was notorious for its tendency to oxidize when exposed to water vapor or active oxygen. Recent advances in sputtering technology allow dense films to be deposited, which are much less sensitive to reaction with the environment. In order to exploit these materials to their fullest potential, designers of space-based motion systems will require data on the effects of atomic oxygen exposure on dense, sputtered MoS_2. The purpose of this experiment was to provide data on how the mechanical properties and surface composition of sputtered MoS_2 are affected by exposure to the atomic oxygen in low earth orbit.

The major conclusions of this experiment are:

Proper surface preparation is critical to insure adhesion of sputtered MoS_2 on stainless steel. When oxide films are present at the interface, the lubricant may fracture and debond under the influence of externally-applied stresses. Stress may be generated by thermal expansion coefficient mismatch and temperature cycling, or by surface shear during sliding.

As-deposited and worn surfaces contain a greater atomic fraction of sulfur than molybdenum (i.e. S:Mo ratio greater than 1:1). This is to be expected since the films are close

in stoichiometry to natural molybdenite (MoS_2), and because shear is known to cause reorientation of MoS_2 films so that sulfur-terminated basal planes are parallel to the sliding surface. Exposure to atomic oxygen causes a reduction in the atom fractions of carbon and sulfur, and an increase in oxygen. Interaction of organic materials with atomic oxygen to produce volatile reaction products and erosion is well documented. We conclude that atomic oxygen also produces volatile reaction products with sulfur, causing a depletion of sulfur at MoS_2 surfaces. Increased amounts of oxygen after atomic oxygen exposure probably reflect the formation of molybdenum oxide.

Despite dramatic changes in surface composition sputtered MoS_2 films that are adherent to the substrate retain their excellent tribological properties. This is attributed to confinement of the reactions with atomic oxygen to the near-surface region, which protects the bulk of the film from damage. With use, the affected material is worn away, exposing the underlying MoS_2. This material develops a surface composition in response to sliding which is virtually identical to that developed by lubricant that was never exposed to atomic oxygen. Contacting bodies lubricated with sputtered MoS_2 that are exposed continuously to atomic oxygen while in motion are expected to exhibit higher friction coefficients and wear rates than those not exposed to atomic oxygen.

The primary difference in material response between flight exposed and ground exposed specimens is attributable to the thermal cycling which occurs during flight exposure. A more accurate representation of the flight environment may be produced by artificially ramping the temperature during laboratory atomic oxygen exposures. The contamination of flight exposed samples (with Si and Al) did not produce any changes in the tribological properties measured, compared to ground exposed samples.

LDEF Composite Materials Retest and Recombination Efficiency of Reflecting Surfaces

Roger Bourassa and Gary Pippin
Boeing Defense and Space Group

Six composite specimens and six scatterometers were supplied for the EOIM-3 Test. Data on these specimens is summarized as follows.

Composite Specimens

1. Sample pedigree

   The composite specimens were T300/934, graphite/epoxy composites.

2. Material handling history

   a. The two composite panels from which the six specimens were cut were fabricated by Boeing in 1978.

   b. Following fabrication, the composite panels were incorporated into LDEF Experiment Tray M0003-10, by Aerospace.

   c. The panels were stored by Aerospace from 1978 to 1983.

   d. Both panels were flight tested on LDEF from April 1984 until January 1990. One panel was exposed to the external LDEF, Row-4 environment. The second panel was mounted adjacent to the first panel, but was shielded form the external environment. The environment experience by the exposed panel would be solar radiation. Atomic oxygen exposure was insignificant on LDEF Row-4.

   e. The LDEF was recovered in January 1990. The M0003-10 was removed at the SAEF II Building, KSC and returned to Aerospace. The panel specimens were removed from the Experiment Tray and returned to Boeing in sealed containers.

   f. LDEF tests on the panels, consisting of microscopic examination and tensile strength measurements, were performed by Boeing in 1990.

   g. In 1992, 0.5-inch diameter disk specimens were cut from the remaining composite panel materials. Two disk specimens from each panel were supplied for the EOIM-3 tests.

h. One disk specimen each from the two panels were flown on the STS-46, EOIM-3 test. The remaining two specimens were designated controls and maintained on the ground.

Scatterometers

1. Sample pedigree

   A diagram of the scatterometers is shown in Figure 1.

2. Material handling history

   The scatterometers were fabricated by Boeing in 1992 and were installed on the STS-46, EOIM-3 test flight.

   The two scatterometers differed in the material used for the molecular reflecting surface. The reflecting surface of one scatterometer was CAA anodized aluminum and the other was silver oxide. The receiving surface of both scatterometers was polyethylene (MIL-P-21922, Type I, Class H, Form A).

The data shows considerable increases in contamination on flight samples 5C1A and 5C5A in comparison with both the ground control and ground simulation samples exposed at PSI. In comparison with each post-baked ground control specimen, the corresponding flight and ground exposed specimens show increased elemental % oxygen atoms on the surface. Each flight sample shows a greater increase in oxygen % than its corresponding ground-exposed sample.

Three of the four ground-exposed samples show the appearance of significant quantities of fluorine and sulfur on their surfaces subsequent to the $\sim 2x10^{+20}$ atomic/cm^2 atomic oxygen exposure.

The 5C1 specimens were previously flown exposed to space on the LDEF trailing edge. The 5C2 specimens were flown on the LDEF trailing edge, but shielded from direct solar exposure. All specimens from both sets have silicon based contamination present, with the specimens exposed to LEO environments on LDEF (5C1) having the higher % silicon. The

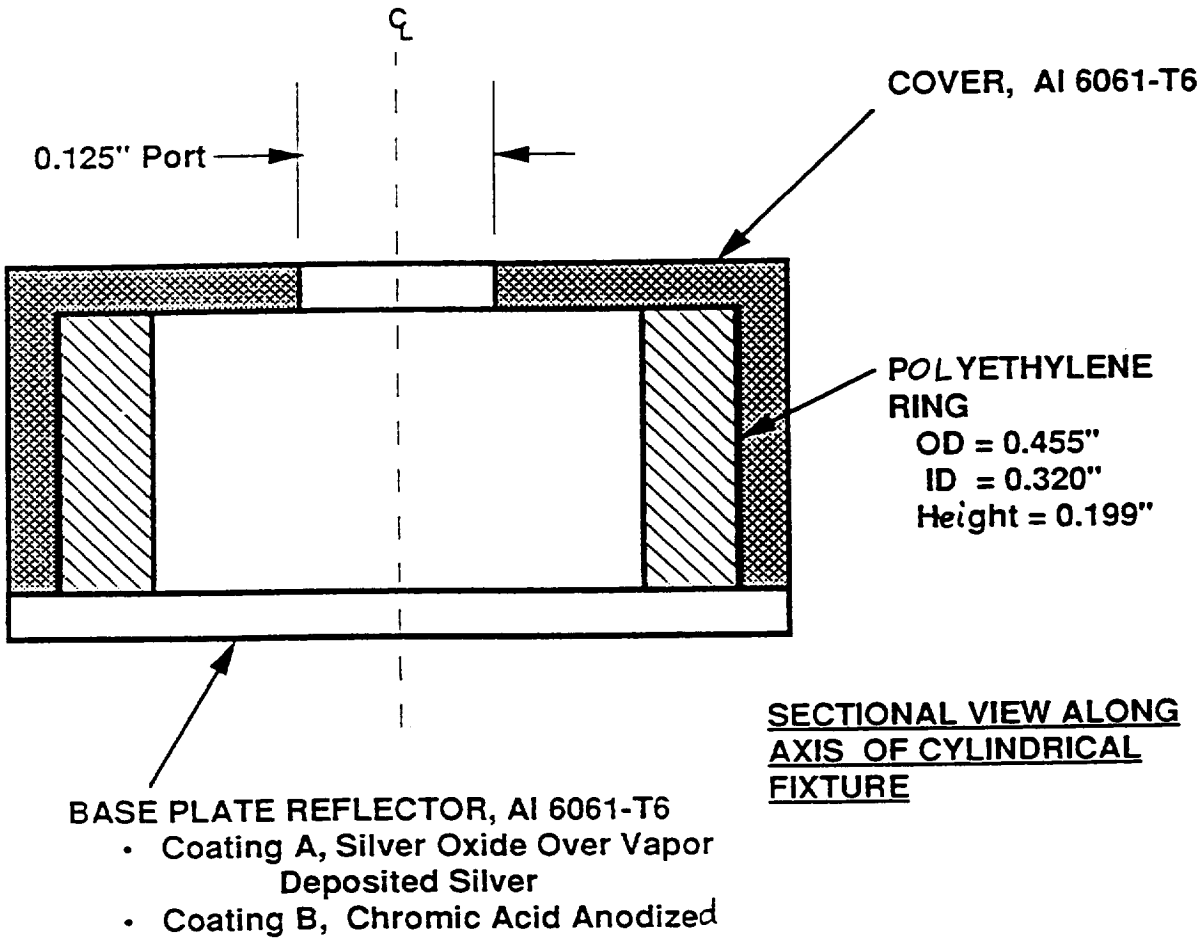

Figure 1. Scatterometer for measuring atomic oxygen reflectance of surfaces.

mass increases measured for the flight composite specimens are likely due to additional contamination during the EOIM-3 flight. The reason for the large amount of F on flight sample 5C2C is not known.

The mass differences on the 3-layer stack specimens, before and after flight, and before and after ground-test, respectively, are not significant.

The ground-test results correlate qualitatively to the flight results but the wide variation in S, F, and Si % from sample to sample rules out meaningful quantitative comparisons. Both oxygen exposures lowered the relative amount of carbon on the surface of the 3-layer stack specimens, as expected if hydrocarbon based contaminants are being oxidized. The carbon to oxygen ratio decreased for each composite post-ground test specimen and for the previously UV exposed (on LDEF) flight specimen (5C1A). Specimen 5C2A, previously flown in a shielded position on LDEF appears to have lost silicon as a result of both the EOIM-3 exposure and the subsequent ground based oxygen atom exposure. The 5C1A specimen was exposed to ~ 11000 hours of solar radiation and underwent post-deposition reactions which adhered the material to the surface. The silicon based material deposited on the 5C2A specimen had no such solar exposure, and as a result was easier to remove under subsequent oxygen exposure. Both flight and ground based oxygen exposure support this conclusion.

AN EXPERIMENT ON THE EFFECTS OF AN ACRYLIC PRESSURE SENSITIVE ADHESIVE

Joseph Maly
CSA Engineering, Inc.

This abstract documents tests that examined the deterioration induced by atomic oxygen (AP\O) exposure on an acrylic pressure sensitive adhesive, 3M Y9469. Two specimens were exposed, one in flight and one in a ground (laboratory) test. Specimens contained two sections of viscoelastic material, one directly exposed and the other indirect. The intent of the layout was to acquire information about the material's integrity under very heavy AO exposure (the directly exposed film), and to provide a more realistic simulation of how the material would actually be used in space (the indirectly exposed section.) AO fluence of the directly exposed section was measured to be approximately $2x10^{20}cm^2$. Exposure was directly incident on a 0.005-inch-thick film; this part of the specimen was examined visually and by an Electron Spectroscopy for Chemical Analysis (ESCA) to determine any surface deterioration. A second material section was sandwiched between two aluminum plates and AO flux was blocked but not sealed from the edges of the sandwiched film.

Different means were used to examine the material degradation of specimen segments. The indirectly exposed material was examined via dynamic mechanical tests, which indicated the shear modulus and loss factor of the viscoelastic material, the two parameters that are key to its damping performance. Examination of the directly exposed viscoelastic indicated visual discoloration only for the laboratory AO test; otherwise, no deterioration was visually apparent. The material maintained its flexibility and tack character without delamination or cohesive failure. ESCA results for the flight test specimen showed a slight increase in oxygen content compared to the control specimen, yet laboratory AO exposure introduced a significant increase in oxygen accompanied by a notable decrease in carbon content compared to the control specimen. Results from the dynamic mechanical tests on the indirectly exposed specimens indicated some change. The average of the shear moduli from both ground and flight tests were approximately that of the control samples. However, the loss factors from both ground and flight tests were lower than those from the control specimens by approximately 20 to 30 percent.

Y9469 appears to be suitable for constrained layer applications in space. Material integrity appeared satisfactory after a very large fluence of AO, yet loss factor deteriorated slightly at a much lower fluence; the extent of this indirect exposure was not quantified. Only one flight specimen was tested and the scope of these tests was quite limited, yet the outlook for the performance of this material as implemented for constrained-layer damping applications looks good.

EOIM-3 PRE- AND POST-EXPOSURE CHARACTERIZATION OF HRG-3 EPOXY-SILANE

Susan Oldham
Hughes Aircraft Company

Executive Summary

Pre-flight and post-flight characterization was performed on two EOIM-3 sample sets of Hughes Aircraft's patented 2,11-bis(3-glycidylphenyl)-2,11-dimethyl-2,11-disiladodecane (HRG-3) cured with 1,3-bis(3-amino-butyl)-1,1,3,3-tetramethyl-1,3-disiloxane (AB). Thermal analysis, outgassing, and ground-based oxygen erosion testing were only performed on the unexposed Hughes and vendor synthesized HRG-3 materials. Ground-based simulation of these HRG-3/AB samples was accomplished both by plasma ashing (at Hughes) and FAST testing (at PSI). Weight determinations, electron spectroscopy for chemical analysis (ESCA), atomic force microscopy (AFM), and optical photography were performed by JPL on pre-flight, post-flight, and post-ground exposure. A summary of the erosion results is shown in Table 1:

Conclusions:

1. Insignificant differences in weight change, surface chemistry, and calculated reaction efficiencies were found between plasma ashed and FAST tested specimens.

2. Significant difference in surface roughness between flight (smoothening) and FAST (roughening) tested specimens.

3. Overall, there is a good correlation between flight and ground.

4. In conclusion, HRG-3/AB appears to be a good LEO protective material.

HRG-3/AB EROSION RESULTS

PARAMETERS	SAMPLE IDENTIFICATION					
	HUGHES SYNTHESIZED RESIN			VENDOR SYNTHESIZED RESIN		
	5E1F (CONTROL)	5E1A (FLIGHT)	5E1C (GROUND TEST)	5E2F (CONTROL)	5E2A (FLIGHT)	5E2C (GROUND TEST)
WEIGHT LOSS (μg)	-	120	+13	-	60	+5
WEIGHT LOSS (%)	-	0.09	+0.01	-	0.05	+0.004
RMS ROUGHNESS (nm)						
20μm scan	217	169	282	170	147	145
5μm scan	105	73	113	140	40	374
FRACTAL ROUGHNESS	2.080 2.162	2.080 2.073	2.098 2.068	2.095 2.015	2.031 2.031	2.110 2.129
SURFACE AREA DIFFERENCE 5μm scan (%)	13.624	5.288	10.439	10.280	3.193	11.267
MAXIMUM EROSION depth (nm)	100	100	100	100	100	100
ESTIMATED REACTION EFFICIENCY (cm^3/atom)						
- BY WEIGHT	-	5×10^{-26}	5×10^{-26}	-	2×10^{-26}	2×10^{-26}
- BY EROSION DEPTH	-	$\leq 5 \times 10^{-26}$	$\leq 5 \times 10^{-26}$	-	$\leq 5 \times 10^{-26}$	$\leq 5 \times 10^{-26}$

* Ground test performed at PSI, using pulsed high flux AO source (FAST)

POLYMER MATRIX BLENDS
EOIM-3 BMDO EXPERIMENT

Jack T. Sanders
Johns Hopkins University
Applied Physics Laboratory

Executive Summary

The Johns Hopkins University, Applied Physics Laboratory provided one material for the Evaluation of Oxygen Interaction with Materials (EOIM-3) pallet on STS-46. It was Chemglas 250 GW-80, a bidirectionally woven fiberglass mat impregnated with poly(tetrafluoroethylene). Graphite bundles were substituted at 2-inch and 4-inch intervals in the warp and weft directions, respectively. This material was also flown in the Limited Duration Candidate Exposure (LDCE-3) pallet on STS-46, and was also ground tested at Physical Sciences, Inc. Three epoxy/fiber blends were also aboard the LDCE-3 pallet. They are MXB-7701/7781 (epoxy/E-glass), MXB-7976/6781 (epoxy/S-glass), and HMF-5-322/7714AC (epoxy/graphite).

The Chemglas 250GW-80 is a thermal control material used in thermal blankets on the Midcourse Space Experiment (MSX), a BMDO program. The purpose for testing this material was to ascertain the erosion potential at approximately 900 kilometers altitude, where MSX will orbit. The flight EOIM-3 sample showed no visible degradation, nor any mass loss. The LDCE-3 sample showed slight mass loss, equivalent to a reaction efficiency of 0.03×10^{-24} cc/atom; equivalent to data recorded by NASA from STS-8 for FEP. The ground test sample, exposed to atomic oxygen at Physical Sciences, Inc., showed visible degradation at 2000x magnification and mass loss equivalent to a reaction efficiency of 1.4×10^{-24} cc/atom, 47 times as large as the on-orbit reaction efficiency calculated for the LDCE-3 sample. Robert Krech of Physical Sciences, Inc. deduced a relationship between positive atomic oxygen ion concentration and FEP and PTFE erosion, which explains this disparity. Atomic force microscopy was used to image the surface of the Chemglas 250 GW-80, and showed no visible difference among the flight, ground test, and control samples. Based on an average atomic oxygen fluence of 6.85×10^{18} atoms/cm^2 over the lifetime of MSX, the projected erosion would be 3 nanometers, an insignificant amount.

The epoxy/fiber laminates all exhibited erosion that was visible to an unaided eye. The Erosion on the Fiberite epoxy/fiber blends was measured with a profilometer, and confirmed with mass measurements. The MXB-7976/6781 had an average erosion depth of 12.2 micrometers, and recorded mass gain. The erosion efficiency is therefore measured to be 5.3×10^{24} cc/atom. MXB-7701/7781 lost 9.9 micrometers of resin and 1.94 micrograms of mass. Both methods agree at about 4.3×10^{-24} cc/atom erosion rate. The HMF-5-322/7714AC material also showed predominantly resin erosion, despite the use of graphite fibers instead of glass fibers, as in the other two epoxy/fiber blends. The measured average erosion depth was 10.7 micrometers, and the mass loss was 2.31 milligrams. These values also agree well, with an erosion efficiency of 4.7×10^{-24} cc/atom. These values for reaction efficiency translate into a recession over the life of the MSX satellite of between 0.29 and 0.36 micrometers, which would not adversely affect the structural integrity of assemblies in which they are used.

POST TEST CHARACTERIZATION OF EOIM-3 SPECIMENS REPORT: HIGH TEMPERATURE COATINGS ON COMPOSITES

Richard Bohner
Applied Material Technologies, Inc.

Executive Summary

As part of a comprehensive material evaluation program to establish the performance parameters of candidate materials for application to BMDO interceptor structures, an evaluation of the effects of oxygen interaction on coating and substrate systems has been completed.

Initially, the material requirements for this program were to support the Brilliant Pebbles (BP) and Brilliant Eyes (BE) interceptor vehicle concepts. The candidate material systems proposed for these vehicles and requirements to support lightweight, high modulus structural designs and demonstrate nuclear survivability.

Martin Marietta was contacted by Applied Material Technologies (AMT), Santa Ana, CA, to perform post-test optical and surface characterization of candidate spacecraft materials and coatings flown on the Evaluation of Oxygen Interactions with Materials (EOIM) III experiment aboard Space Shuttle 46. Four material designs were subjected to a low earth space environment as part of the Jet Propulsion Laboratory (JPL) experiment. The objective of the program was to quantify the degradation and changes experienced by the materials due to exposure to the atomic oxygen environment. The contract effort included sample surface characterization, physical characterization, and optical characterization.

The post flight characterization testing was necessary to quantify the potential damage and degradation to the material surface and optical properties of the advanced coated materials. Interaction with the low earth space environment can result in surface morphology changes (recession) and optical property degradation significantly affecting spacecraft coating, component, and system performance. The post test characterization was performed on the following coating and substrate material designs:

1. Alumina Coated Graphite PEEK Composite (Al_2O_3/PEEK)

2. Boron Nitride/Alumina Coated Graphite PEEK Composite (BN-Al_2O_3/PEEK)

3. Alumina Coated Silicon Carbide Aluminum Composite (Al_2O_3/SiC-Al)

4. Calcium Zirconate Coated Silicon Carbide Aluminum Composite ($CaZrO_3$/SiC-Al)

Post test characterization consisted of weight, total hemispherical reflectance, solar absorptance, and emittance measurements. Scanning electron microscopy (SEM) and x-ray photoelectron spectroscopy was also performed one each of the samples. The characterization revealed no damage to the coated composite design. The coating were very stable, adherent, and impermeable to the atomic oxygen environment. The flight and ground test exposed specimens were found to be contaminated with silicon, fluorine, sodium, and some traces of copper. In the cases of fluorine contamination, by-products of AlF_3 (on Al_2O_3 samples) and CaF_2 (on the Ca ZrO_3 samples) were formed on the sample surface as a result of the atomic oxygen exposure.

SDIO EOIM-3 TRAY SAMPLES POST FLIGHT ANALYSIS

Jon Cross
Los Alamos National Laboratory

HIGH TEMPERATURE SUPERCONDUCTOR SAMPLES
5K6 and 5K7

These samples were composed of Yt-Ba-Cu-Ox where the 5K6 sample was prepared oxygen deficient by thermally decomposing a high quality sample in argon. The 5K7 sample was prepared in the same manner and at the same time as the oxygen deficient sample but was not thermally decomposed. The flight sample was composed of two samples, one which viewed the ram direction and a reference sample mounted behind the ram sample and faced the tray. Resistance-temperature curves were taken before flight (ground reference) and after the EOIM-3 flight (flight reference, unexposed and flight exposed.

The original sample (5K7) transition was at $Tc \approx 91$ K with a width of ≈ 3 K which represents a high quality film (thickness ≈ 2000Å). It is quite evident that what ever processing occurred to the spacecraft before flight degraded the film to a very low quality as shown in the unexposed flight reference sample that has a transition temperature of ≈ 50K and a width of 10-15 K. If it is assumed that the flight exposed sample degraded similarly as the flight reference, it is concluded that the atomic oxygen exposure in orbit successfully annealed the low quality film back almost to its original state since $Tc \approx 85$K and width ≈ 4-5 K.

The oxygen deficient HTSC film 5K6 however did not show a dramatic increase in transition temperature when exposed to the LEO ram environment.

It is concluded that the HTSC film degradation occurred in the near-surface region and the low fluence ($2X10^{20}$ AO/cm^2) of atomic oxygen at low substrate temperature was sufficient to replenish this near surface region. The fully deoxygenated film however had oxygen removed through out the bulk of the film and the combination of low substrate temperature and low AO fluence was not sufficient for appreciable oxygen replenishment.

NPB Carbon Foil Samples 1K8 and 1K9

Coated particle beam neutralizer foils were exposed to both the orbital environment on EOIM-3 as well as a laboratory source of atomic oxygen at Los Alamos.

The flight experiment did not have *in situ* data recording, i.e., the foil resistance was measured before and after flight and the normalized conductance change was then computed. The samples contained two resistive strips each. The laboratory samples were of the same configuration. The laboratory results for the 50Å Al_2O_3 coating showed similar results for both carbon films while the flight results showed a large variation between the two films. The SiO_2 coated flight sample, which was received with one carbon film strip damaged (open), showed fair agreement with laboratory based results. Even though all the coatings showed variations in their protective ability, all protective coatings seem to protect the carbon foils up to a fluence of 10^{19} AO/cm^2. The thicker Al_2O_3 coatings though exhibited the best protective behavior up to a fluence of 10^{20} AO/cm^2.

The Effect on Coated, Pyroelectric Detectors from Exposure to the Low Earth Orbit Environment During the EOIM-3 Experiment

Peter C. La Delfe
Los Alamos National Laboratory

The Los Alamos National Laboratory (LANL) provided three samples for the EOIM-3 experiment.

Los Alamos has a continuing program to develop pyroelectric, optical radiation detectors intended to reside on the skin of satellites in low earth orbit. The objective of this experiment was to determine the sensitivity of these devices to the atomic oxygen found in that environment.

Sample Description

The detectors we supplied were constructed using commercially available polyvinylidene fluoride (PVDF) film. This film is supplied in a nominal thickness of nine micrometers with 100 nanometers of aluminum deposited on each side.[1] We removed the aluminum from one side. The bare side was then glued to a copper clad, glass-epoxy, circuit board. The copper thus provided one electrode of the detector, albeit with a series capacitor between it and the pyroelectric medium due to the glue layer. The exposed, and intact, aluminum layer provided the second electrode. By cutting through the copper, the entire detector could be divided into segments. Two of the three samples were one inch in diameter and were divided into four segments, each occupying one quadrant. The third sample was one-half inch in diameter and was segmented into halves.

The one-inch flight samples were designed 1K3A and 1K4A and the half-inch flight sample was designed 5K5A. The corresponding control samples were 1K3B, 1K4B, and 5K6B, respectively.

[1] The Auger depth profiles conducted as part of the post-flight analysis revealed a nickel layer between the PVDF and the aluminum.

Some of the detector segments were coated with various selective absorbers. These are interference coatings which enhance the responsivity within a spectral band. The coatings flown on EOIM-3 were designed to select one of two common laser lines; YAG at 1.06 micrometers or CO_2 at 10.6 micrometers.

Analysis

The spectral response of each detector was measured before and after the flight. The shape of the spectral response curve is a sensitive function of the coating design. Therefore, small modifications in the coating manifest observable changes in the spectral response.

Each detector was also examined using Auger electron spectroscopy (AES) and Auger depth profiling. The AES is a sensitive probe of contamination by elemental species. The depth profiling can find contamination in the bulk and can determine stoichiometric imbalance or chemical change in cases involving a mobile species. Auger spectroscopy cannot, however, be used to determine the chemical bonding state.

The use of electron spectroscopy for chemical analysis (ESCA) was considered to look for changes in the chemical bonding state. However, in each of the possible changes in our samples due to oxidation of the coating materials, the shift in the ESCA peak is smaller than the resolution of the technique. Therefore, ESCA was not pursued for the purpose.

Results

With one exception, discussed below, we found no functional differences in the detectors due to exposure to the low earth orbit environment. Pre-flight and post-flight spectra are identical in every case but one. All samples which have no surface silicon by design, show a silicon peak in the AES spectrum of the flight sample which has no corresponding peak in the control sample. This is purely a surface feature, disappearing as soon as the depth profile is started, and has no effect on the detector performance. Silicon in the surface layer of the design for some segments, masks this peak at those locations.

The single, obvious, visual effect of the low earth orbit is a bright blue patch covering about 10% of segment A, the lead telluride coating, of sample 1K3A. This area is also characterized by a number of parallel cracks in the surface. The spectral response of this quadrant shows a shift of approximately 3% toward shorter wavelengths indicating a general thinning of the lead telluride. This shift is measured using a beam which covers mst of the segment, not just the blue area. However, by using a small polychromatic beam, confined to the blue, we determined that the area shows little or no pyroelectric activity. Comparison of the AES spectra and Auger depth profiles taken within and outside the blue area and on the control sample (1K3B, segment A) show no differences. Based on these data, as well as visual examination of the affected area, we made the following conclusions.

1. The spectral shift is due to an erosion of the lead telluride, not an oxidation with the oxides remaining in place. The magnitude of the shift is not sufficient to degrade detector performance.

2. The casual defect is a failure in the adhesion between the PVDF and the copper. Improved fabrication and testing methods, developed since these detectors were made, are expected to prevent recurrence.

3. We cannot explain the blue color as it has no corresponding distinction in chemistry that is apparent.

Conclusion

These coatings are quite tolerant of atomic oxygen. The zinc sulfide/lead fluoride design, the lead telluride design, and the bare aluminum detectors were included in this experiment to provide some measure of how much degradation might be expected in ill-suited materials. The degradation was minimal or nonexistent. We conclude that designs using refractory oxides and silicon, with an oxide surface layer, can be used successfully in low earth orbit.

ADVANCED INTERCEPTOR TECHNOLOGIES PROGRAM EVALUATION OF OXYGEN INTERACTION WITH MATERIALS (EOIM-3) RESULTS

Robert Wendt and Tim Gillespie
Martin Marietta

Executive Summary

The Martin Marietta Advanced Interceptor Technologies (AIT) program's participation in Evaluation of Oxygen Interaction with Materials (EOIM-3) supports the validation of AIT system mission performance. If space environment induced changes occur, the response should occur in a graceful and predictable manner. In order to avoid system over-design, the material's end-of-life (EOL) characteristics must be thoroughly understood to allow the spacecraft designer to account for the reasonable worst case. Martin Marietta provided ten (10) materials for the EOIM-3 experiment with applications to the AIT structure, power and thermal control systems. The preliminary results reaffirm the importance of atomic oxygen (AO) protection of the external materials, and indicate very robust AO protection is provided by both plasma-sprayed and chemically vapor deposited (CVD) coatings. The results also raise concerns about the ability of current ground test facilities to simulate the actual flight response.

Flight and Ground Test Results Comparison

In addition to the flight response data, the other primary objective of the experiment was to establish correlations between the flight test data and available AO ground test facilities. The Physical Sciences Incorporated (PSI) facility, Andover, MA was selected as the primary ground test facility. In general, the correlation of the flight and ground test response was very good. The optical properties were consistent for both flight and ground tested specimens as shown in Table 2-2. The correlation of the reaction efficiencies is difficult because in most cases it was based on the weight loss data and the specimens were not handled in a consistent manner before weighing. Chemical characterization of the ground and flight tested materials, was slightly different primarily due to the contribution of F, Cu and Na, attributed to the ground test facility hardware and the Si contamination of the flight specimens.

The Glass/Teflon™ (1L2 series) and the Beta-Alumina ($Na_2O \bullet Al_2O_3$) coated 6061-T6 Al(5L3 series) showed significant differences between flight and ground. The flight tested

Glass/Teflon™ exhibited no obvious physical damage, but the ground tested specimen exhibited extensive surface texturing (Figure 6-1). The texturing may be due to interaction with the PSI facility's ionic oxygen component. Similar results have been demonstrated when an AO source has a strong UV component, although PSI has indicated that their facility generates only approximately 1 equivalent UV sun intensity during exposure. The reason for the obvious difference in the Glass/Teflon™ flight and ground test results has not been determined at this time.

The Beta-Alumina ($Na_2O \bullet Al_2O_3$) coated 6061-T6 Al (5L3 series) also exhibited a significantly different flight and ground test response. The ground tested specimen had a fibrous morphology after test (Figure 6-2). The flight tested material showed no obvious morphological changes or chemical differences. This morphology was not evident on either the flight or ground tested Beta-Alumina ($Na_2O \bullet Al_2O_3$) coated Carbon-Carbon (C-C) specimens (5L7 series). Both $Na_2O \bullet Al_2O_3$ coatings were applied using identical materials and processes. The only difference is the 6061-T6 versus the C-C substrate. Based on high resolution XPS of the 5L3 ground specimen, the Na on the Beta-Alumina had reacted with the F contamination from the teflon™ poppet valve and formed NaF. Therefore, the fibrous morphology is believed to be the newly formed NaF phase. The reason why the 5L7 ground test specimen was not affected is not known at this time.

Overall, the ground test facility appears to be a useful screening method for materials AO response, although the flight test is still considered to be the final validation of the materials.

Table 2-2. Visual Appearance and Optical Properties for Specimens Exposed to Atomic Oxygen On-orbit and at the PSI Ground Test Facility.

Material	Visual	Optical Properties (α_s / ε_N)		
		Flight	Ground	Control
1. TiC coated C/C	No Degradation	0.56/0.15	0.56/0.15	0.55/0.14
2. Glass/Teflon®	No Degradation	—	—	—
3. Beta-Alumina coated 6061 Al	No Degradation	0.30/0.90	0.29/0.90	0.29/0.90
4. Reaction Bonded SiC	No Degradation	0.78/0.61	0.77/0.62	0.76/0.61
5. Carbon/Carbon (C/C)	Eroded	0.97/0.75	0.99/0.69	0.82/0.57
6. Calcium Zirconate coated C/C	No Degradation	0.59/0.82	0.59/0.82	0.59/0.82
7. Beta-Alumina coated C/C	No Degradation	0.26/0.89	0.28/0.89	0.28/0.90
8. CuInSe2 Photovoltaic	Darkened	—	—	—
9. Nb Beryllide	Discolored	0.57/0.12	0.57/0.13	0.62/0.12
10. P75/Magnesium	No Degradation	—	—	—

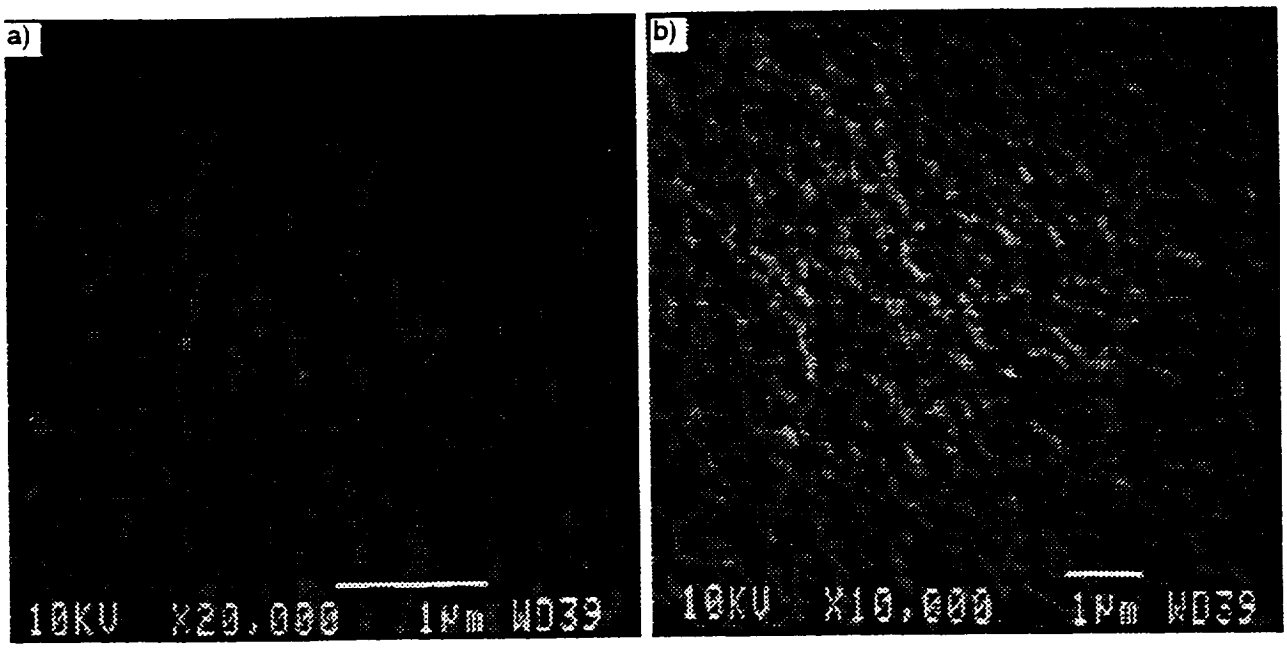

Figure 6-1. **High Magnification SEM Micrographs of the (a) Flight and (b) Ground Exposed Glass/Teflon™ Specimen.** The Glass/Teflon™ was not damaged in flight but the ground specimen appears to be severely eroded leaving a surface morphology consisting of deep pockets surrounded by less eroded fibrous colonies.

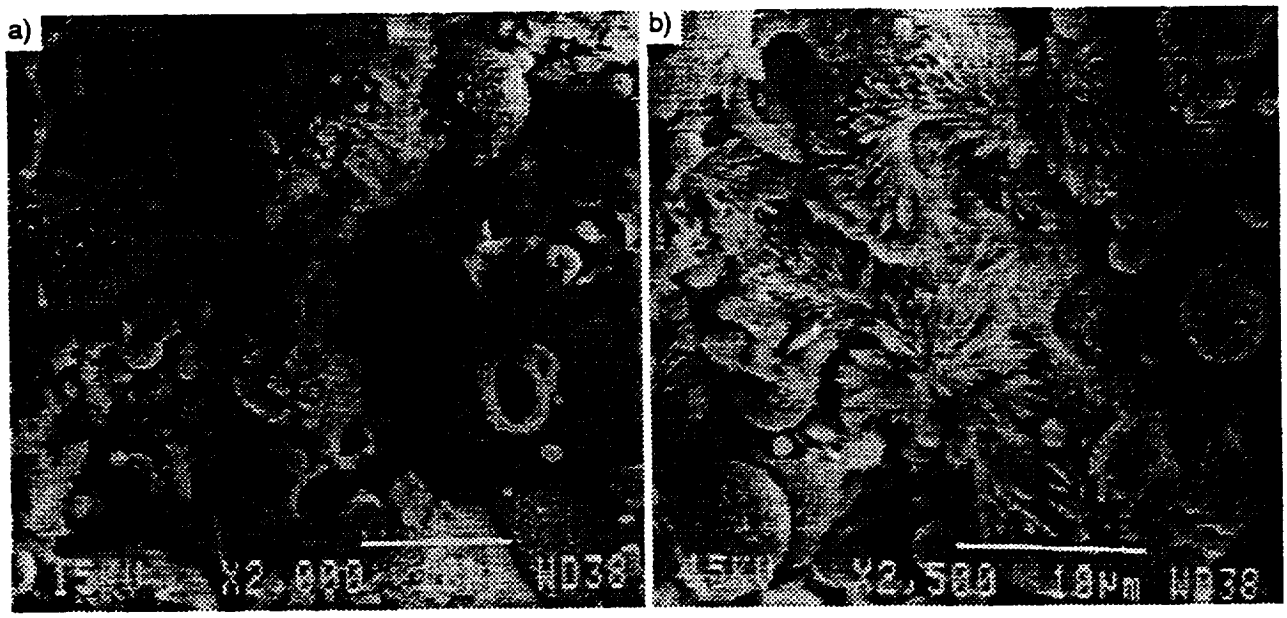

Figure 6-2. **High Magnification SEM Micrographs of the (a) and (b) Ground Exposed Beta-Alumina (5L3).** Several fibrous clusters were found in ground specimen exposed area that were not evident in the flight specimen. Based on high resolution XPS it appears.fibrous structure is NaF formed by reaction of the Na_2O with the F contamination from the Teflon™ poppet valve.

EOIM-3 RESULTS FOR NAWCWPNS DEVELOPMENTAL OPTICS

Linda Johnson, Karl Klemm, and Mark Moran
Physics Division, Research Department
Naval Air Warfare Center Weapons Division

Atomic-oxygen (AO) resistance is an important requirement for a space-based primary mirror in low Earth orbit (LEO). In previous years, the BMDO developmental optics community concentrated on the hostile nuclear survivability requirement. The EOIM-3 test provided an opportunity to validate the AO-resistance of the Si- and Al-based coating designs developed for radiation-hard primary mirror applications. In addition, the test provided an opportunity to measure AO-degradation of materials less suitable for LEO mirror applications. For example, enhanced reflectors with outer layers of BN, ZnS, or ZnSe were expected to perform poorly in the EOIM-3 flight test.

The boron nitride (BN)-overcoated mirror, concept 5M7, showed significant reflectance loss in the EOIM-3 experiment. The reflectance at $\lambda = 3.0\ \mu m$ dropped 4.57 and 2.71% for the flight and ground-test samples, respectively. In addition, the BN surface receded 75.0 and 131.4Å on the flight and ground-test samples, respectively. However, the RMS roughness values for the exposed and unexposed areas of the BN samples are the same suggesting the AO-degradation mechanism for BN is a chemical-oxidation rather than a mechanical-roughening or polishing effect.

The reflectance loss observed on the ZnS-based mirrors in the Long Duration Exposure Facility (LDEF) was not confirmed on similar mirrors in the Limited Duration Candidate Exposure (LDCE) experiment flown at the same time as EOIM-3. The ZnS- and ZnSe-based mirrors were located on the LDCE-3 tray and were more heavily contaminated than the mirrors flown on the EOIM-3 tray. The heavy contamination may have protected the underlying ZnS and ZnSe surfaces from AO.

Only one of the three broadband reflectors showed a small reflectance loss in the infrared. The reflectance from 2.8 to 5.2 μm was unchanged for the unprotected Al coating on Si, concept 5M8, and for the bare Be mirror, concept 1M13. The reflectance loss on the

$Al_2O_3/Al/\beta$-SiC ground-test sample, 1M12B-Al, increased from about 0.05% at 4.8 μm to about 0.35% at 2.8 μm. The 2000-Å-thick Al_2O_3 layer should have provided adequate protection against AO-degradation. The reflectance loss probably is related to the large amount of Cu contamination on this particular sample. The Cu contamination has been attributed to particulate debris from erosion of the nozzle in the ground-test chamber. No reflectance loss was observed on the $Al_2O_3/Al/\beta$-SiC flight-test sample, 1M12A-A1.

Contamination and debris prevented useful comparisons of the pre- and post-test total integrated scatter (TIS) at $\lambda = 3.39$ μm for many of the mirrors. Although the post-test TIS values were dominated by particulate debris, important conclusions about the optical scatter can be inferred from the Talystep roughness data. The pre- and post-test RMS roughness values were unchanged for all of the Si- and Al-based primary mirror designs. The TIS would have been unchanged for these mirrors if they had not been contaminated with debris.

An important candidate for a space-based primary mirror coating is the ion-beam-sputtered $(Si_3N_4/Al_2O_3)^n/Al$ design, concept 1M14. The superior thermal-shock resistance of this concept has been verified in several above-ground simulator tests at Blackjack 5 and in three underground nuclear tests. The EOIM-3 results show the design is also resistant to AO-degradation. The superior thermal-shock and AO resistance of the $(Si_3N_4/Al_2O_3)^n/Al$ design make it an excellent candidate for a space-based primary mirror.

The AO-exposure results were confounded by chemical and particulate contamination. The chemical-vapor-deposited (CVD) diamond surfaces, concepts 5M1 and 1M9, were expected to recede between 1000 and 2000Å. Silicone contamination protected the flight samples and prevented any discernible recession steps on the CVD diamond surfaces. However, recession steps were measured on the ground-test CVD diamond samples. Sample 5M1B receded 2138 $\pm$ 1150Å and sample 1M9B receded 1043 $\pm$ 59Å. In other words, the measured recession values for the ground-test CVD diamond samples were in the range of the predicted value.

The ground-test CVD diamond sample 1M9B was the only sample that showed a significant increase in microroughness. Preferential etching of the diamond grain boundaries is a possible explanation for the increase in RMS roughness from 58.6 to 263Å.

The (AlN/SiH) antireflection coating protected the underlying diamond from AO-degradation in sample 1M15B. No discernible recession steps were observed in the Talystep profiles. The microroughness was unchanged.

OPTICAL SAMPLES

Roland Seals and William Snyder
Oak Ridge National Laboratory

Forty-seven samples from eight material types were supplied by Oak Ridge National Laboratories for exposure on the EOIM-3 experiment. They were:

Baffle Coupons:	Mirror Coupons:
B/Be (6)	Be/Si/SiC (6)
Martin Black (6)	SPT Be/Be (6)
Be/Be Foam (5)	Polished Be/Be (6)
Black Etched Be/Be (8)	
B_4C/POCO (4)	

The B/Be Baffle Coupons are plasma sprayed (PS) boron on PS-Beryllium. Martin Black Baffle Coupons are an aluminum product supplied by Martin Marietta Denver Aerospace. Be/Be Foam Baffle Coupons are black-etched Be on Be Foam. The Be Foam was supplied by Brush-Wellman Co. Black Etched Be/Be Baffle Coupons are sputtered deposited Be (acid etched) on beryllium coupons. B_4C/POCO Baffle Coupons are CVD B_4C onto POCO graphite.

Be/Si/SiC Mirror Coupons are sputtered-deposited reflective beryllium coating (50 nm) on polished silicon on silicon-carbide substrates. The Si/SiC substrates were supplied by UTOS. SPT Be/Be Mirror Coupons are single point diamond turned sputtered-deposited beryllium on beryllium substrates. Polished Be/Be Mirror Coupons are polished sputtered-deposited beryllium on beryllium substrates.

Of the 47 samples fabricated, 18 randomly selected samples were post-exposure measured for BRDF, 11 for reflectance and 8 for mass change. The following is a summary of the pre- and post- test results.

Full in-plane scans of BRDF data at 0.633 and 10.6 μm wavelengths from eighteen optical baffle and mirror samples were measured and reviewed. All samples were pre-tested.

The observed variations in data are within normal experimental range for such BRDF measurements and any effect of AO is imperceptible.

PE 983G infrared reflectance data at 4 and 10 μm wavelengths from eleven baffle samples were reviewed. Of the eleven samples, all but two (Be Foams #3 & #9) of the observed variations in data are within normal experimental range for such reflectance measurements and any effect of AO is imperceptible. The Be Foams had a reflectance reduction of 54% and 19% (0.260 --> 0.120, 0.260 --> 0.210) which can not be explained by random error. Since baffles should have as low a reflectance as possible, these two changes can not be viewed as negative.

PE 983G infrared reflectance data at 4 and 10 μm wavelengths from seven mirror samples were reviewed. Of the seven samples, all of the observed variations in data are within normal experimental range for such reflectance measurements and any effect of AO is imperceptible.

The change in mass of one sample from each of the sample types was measured and reviewed. All of the observed variations in data are within normal experimental range for such mass measurements and any effect of AO is imperceptible.

In conclusion, 42 hours of atomic oxygen exposure did not degrade the optical performance of the baffle or mirror coupons analyzed.

ANALYSIS OF SPECIMEN 501

Walter Whatley
SPARTA, Inc.

Specimens of P-100 pitch fiber reinforced MR56-2 bismaleimide composites were submitted to JPL for Flight Ground Test and control specimens. All samples were machined from a single panel which was laminated and cured using standard composite processing techniques, and recommended processing schedules. The objective of the flight exposure was to characterize the erosion characteristics of both the fibers and matrix material. To assure that both matrix and reinforcement were exposed to the space environment, the surfaces of the specimens were grit blasted to expose the fibers, before being cleaned in preparation for flight.

Three of the six specimens were evaluated per the original plan for post flight analysis. One specimen was flown on the EOIM-3 experiment, and one specimen was exposed to an approximately equivalent AO fluence in a ground test facility. A third specimen, which was not exposed to any AO was analyzed as a control sample.

Both the flight specimen and the ground tested specimen showed very similar responses to atomic oxygen exposure. Chemical analysis of the surface of the AO exposed samples showed an increase in the amount of oxygen on the surface, and a small amount of silicon contamination. The surface morphology of the exposed samples was quite similar also. Both exposed samples showed extreme erosion of the polymer matrix. No matrix material was visible on the surface of the flight specimen. Fiber erosion was quite non-uniform on a microscopic level, and the effects of crystallinity and crystal orientation were readily apparent.

Analysis of the flight and ground test specimens indicate that for this type of material, the ground tests, provide a reasonable simulation of short term flight exposure. The mechanisms of material erosion appear to be similar in both specimens, although the amount of erosion is substantially different. It should be noted that extrapolation to longer term exposure at low AO flux (to achieve the same AO fluence) is questionable due to the uncertainties introduced by other aggressive elements of the space environment.

Response of the fibers tested to the AO flux indicate that crystallinity plays a large role in the ability of graphite fibers to resist erosion by atomic oxygen. Although this is not conclusive evidence, these results indicate that more highly crystalline fibers may be more suitable for use in applications where the composite will be exposed to AO.

Evaluation of Spacecraft Surface Materials in the Low Earth Orbital Environment
Evaluation of Oxygen Interactions with Materials (EOIM), Mission 3

Brian Blakkolb
TRW

Executive Summary

The sample set fielded for the Evaluation of Oxygen Interactions with Materials, mission 3 (EOIM-3) was composed of fifty-five specimens, consisting of ten material concepts, representative of thermal, optical, structural, and power subsystems of the Advanced Interceptor Technologies (Brilliant Pebbles) spacecraft. Participation in the BMDO sponsored EOIM-3 flight experiment was part of an overall technical risk mitigation strategy for the TRW AIT Program. The objectives of the TRW experiment on the EOIM-3 pallet were to take advantage of the opportunity to gain experience in handling new materials concepts and, to evaluate the performance of these materials in response to exposure to the low Earth orbital atomic oxygen environment. The objectives of the TRW experiment were met.

The sample set has legacy to AIT spacecraft designs in that the materials fielded for the EOIM-3 experiment were selected from those being considered for Low Earth orbital AIT space assets. The focus of the experiment was to gather engineering data with measurements and characterizations linked to key system parameters. Six examples of each sample material were produced to provide flight, ground test, and control specimens. The EOIM-3 experiment was flown aboard the Shuttle (STS-46). During the 42 hour experiment, the samples were exposed to a total fluence of $\approx 2 \times 10^{20}/cm^2$. Ground test specimens were exposed to a flight-equivalent fluence of atomic oxygen in the pulsed molecular beam facility at Physical Sciences, Inc.

TRW/EOIM-3 Sample Set

SAMPLE	DESCRIPTION	SUBSYSTEM
5P1	[Si/Al_2O_3]/Carbon/ SiC[Si/Al_2O_3]/Al/ Carbon/SC	Optical Pointing System
1P2	TiC/graphite cloth/C foam	Threat shielding
5P3	W/graphite cloth/C foam	Threat shielding
5P4	Al_2O_3/Aluminum	Optical Pointing System
1P5	CVD SiO_2/amorph Si cell	Solar array
5P6	Al_2O_3/thermoplastic	Structure/thermal control
5P7	Ge/Kapton	Thermal control
5P8	FEP/Ag/Inconel/Kapton	Thermal control
5P9	Microsheet/Ag	Thermal control
5P0	TiO_2/SiO_2/Si/Kapton	Thermal control

Overall, the materials performed as expected, indicating that initial design material selections were appropriate for the intended applications in the operational environment. Results of the flight exposure were consistent with preflight predictions; unprotected organic materials experienced measurable surface erosion, whereas inorganic materials and fluorinated polymers exhibited significantly less erosion. Optical mirror coatings exhibited no apparent damage from ram exposure, but particulate and molecular contamination originating from the Shuttle environment produced degradation of surface properties as measured by BRDF at 0.633 μm and spectral reflectance. No measurable change in the performance of the solar photovoltaic specimen was detected and no change in thermal properties, as assessed by integrated solar absorptance (α_s) and hemispherical emittance (ϵ_h) measurements, were observed in the thermal control samples. Synergistic interaction between atomic oxygen and ultraviolet radiation in the ground based AO source produced an accelerated erosion of the FEP/Ag/Kapton thermal blanket specimen compared to the flight-exposed specimen.

Optical Baffle Materials

Ed Johnson
SPIRE Corporation

The need for a space qualified baffle material is evident. Organic paints can outgas and are prone to atomic oxygen erosion. Metal blacks and acid bath anodized coatings change surface geometry, especially at knife-edges and tend to be fragile. Post-flight analysis of the textured metal baffle coupons shows no signs of damage due to exposure to the space environment.

In order for a baffle material to be space-qualified it must:

- Meet all optical specifications
- Survive launch without damage
- Be unaffected by exposure to space

Ground tests have shown that textured metal can be tuned to meet a wide variety of optical specifications. Simulated launch shock tests have shown that textured metals are not damaged by launch and do not produce particulate debris capable of obscuring sensitive optical components. The results of the EOIM-3 flight indicate that textured metals can now be specified for use in military or civilian space optical systems. Clementine, a joint NASA/DoD project, will launch (in 1994) with two Spire fabricated textured aluminum startracker baffles.

Four Spire samples were exposed to atomic oxygen on the ground after a 48 hour vacuum bake, two each textured aluminum and textured beryllium. Another two samples were kept as controls, one each textured aluminum and textured beryllium. Optical analysis of all six samples indicates that they were unaffected by ground exposure to atomic oxygen. BRDF scans at 30° incident angle, He:Ne wavelength for the four ground samples were performed, along with

control samples as reference. Corresponding visible/near IR total hemispherical reflectance (THR) scans were measures. Within the accuracy of the test equipment, no discernable difference can be seen between the controls and the exposed samples.

Optical Baffle Materials

Patrick Lamb
Battelle

Executive Summary

Battelle had submitted eight samples of an advanced infrared baffle material for inclusion in the EOIM-3 experiment. The baffle material was a plasma-sprayed magnesium oxide (MgO) coating on beryllium substrate. Characterizations performed under this task included visual inspection, ESCA, and raster-scan bi-directional reflectance distribution function (BRDF) measured at 10.6 μm.

Visual inspection indicated a large number of small chip-outs in the coating surface. These may have been caused by vibration during launch and re-entry, or by small particle impacts. The BRDF was improved (lowered) by about 10% on average, which may be attributed to additional surface texture created by the chipping. The sample weights changed by less than 0.1%, showing there was no significant coating erosion during the experiment. ESCA showed a significant increase in fluorine, probably because of external contamination; and a small shift in the magnesium peak location, which may be caused by the fluorine replacing oxygen in the coating.

Samples exposed to ground testing for atomic oxygen showed results comparable to the control samples. Based on these observations, the MgO coating did not appear to be oxidized or eroded by exposure to atomic oxygen. Surface damage was probably from mechanical causes.

APPENDIX B

BMDO EOIM-3 CO-INVESTIGATOR DIRECTORY

BMDO EOIM-3 Co-Investigator Directory

Richard Bohner
Applied Material Technologies, Inc.
3611 S. Harbor Blvd.
Suite 225
Santa Ana, CA 92704

PH: 714-454-8825
FAX: 714-545-2401

Pat Lamb
BATTELLE
7501 S. Memorial Parkway
Suite 101
Huntsville, AL 35802-2257

PH: 205-881-0262
FAX: 205-883-4442

Gary Pippin
Boeing
Defense and Space Group
2040 68 Avenue South
M/S 82-32
Kent, WA 98032

PH: 206-773-2846
FAX: 206-773-4946

Joseph Maly
CSA Engineering, Inc.
2850 W. Bayshore Rd.
Palo Alto, CA 94303-3843

PH: 415-494-7351
FAX: 415-494-8749

Susan Oldham
Hughes Aircraft Company
E-1 Mail Station F 157
2000 E. El Segundo Blvd.
El Segundo, CA 90245

PH: 310-616-8784
FAX: 310-616-2628

Jack Sanders
Johns Hopkins University
Applied Physics Lab
M/S13N216
Johns Hopkins Road
Off Route 29
Laurel, MD 20723-6099

PH: 410-792-6000 ext. 3055
FAX: 410-792-6119

Jon B. Cross
Los Alamos National Laboratory
CLS-2/MS J565
Los Alamos, NM 87545

PH: 505-667-0511
FAX: 505-665-4631

Peter C. LaDelfe
Los Alamos National Laboratory
MEE-3, MS J580
Los Alamos, NM 87545

PH: 505-667-1597
FAX: 505-665-3911

Tim Gillespie
Martin Marietta
Space & Threat Survivability DD-5
Mail Stop F4064
12257 State Highway 121
Littleton, CO 80127

PH: 303-971-3684
FAX: 303-971-6925

Linda Johnson
Naval Air Warfare Center
Weapons Division
Code 02316
China Lake, CA 93555-6001

PH: 619-939-1422
FAX: 619-939-1409

Roland Seals
Oak Ridge National Laboratory
Bldg. 9102-2, M/S 8039
Bear Creek Road
Oak Ridge, TN 37831-8039

PH: 615-574-0936
FAX: 615-574-9407

Michael Dugger
Sandia National Laboratory
Division 1832
1515 Eubank SE
Albuquerque, NM 87123

PH: 505-844-1091
FAX: 505-844-1543

Walter Whatley
SPARTA, Inc.
9455 Towne Centre Dr.
San Diego, CA 92121-1964

PH: 619-455-1650
FAX: 619-455-1698

Ed Johnson
SPIRE
One Patriots Park
Bedford, MA 01730-2396

PH: 617-275-6000
FAX: 617-275-7470

Brian Blakkolb
TRW
BE/BP Contamination
M/S 2/1534
One Space Park
Redondo Beach, CA 90278

PH: 310-814-9249
FAX: 310-814-6819

APPENDIX C

GUIDELINES AND RATIONALE FOR EOIM-III PASSIVE EXPOSURE SPECIMENS

Guidelines and Rationale for EOIM-III Passive Exposure Specimens

David E. Brinza and Ranty H. Liang
Jet Propulsion Laboratory
Pasadena, California

SUMMARY

This document provides guidelines and rationale for selection, characterization and preparation of materials specimens for flight testing on the NASA Evaluation of Oxygen Interactions with Materials (EOIM-3) experiment. A brief, general discussion of the exposure effects on materials witnessed in prior retrieved material missions is provided as a point of reference for developing strategies for the upcoming flight test opportunity. Specific requirements and specifications for potential materials test specimens are provided in this document. Some recommendations, based on prior flight testing experience, for sample and control preparation, handling, pre-flight and post-flight characterization are presented to help maximize the return of quality atomic oxygen effects testing data.

I. Introduction and Background

The NASA Evaluation of Oxygen Interactions with Materials (EOIM) experiments are an evolutionary series of investigations based on limited duration exposure of materials to substantial fluences of atomic oxygen (AO) in the low earth orbital environment. These low altitude shuttle-borne experiments are able to subject test materials to AO fluences equivalent to several months or even years of exposure at higher orbital altitudes. For example, EOIM-III is anticipated to bombard materials with approximately 2.5×10^{20} oxygen atoms per square centimeter during a 42-hour period. This is nearly the same fluence encountered by the Long Duration Exposure Facility (LDEF) after its first year on orbit. The EOIM-III experiment is intended to:

1) provide accurate reaction rate data for test materials by correlation of aeronometry data from an on-board mass spectrometer to ambient atmospheric models,

2) provide benchmarks for validation of ground-based testing methodologies via correlation of product molecular species detected by the mass spectrometer from selected materials with product yields in laboratory measurements, and

3) evaluate materials and coatings which have not been tested in flight previously including recently developed AO-resistant materials.

The selection of materials for evaluation on-board EOIM-3 shall be driven by these three goals in the above stated order of priority.

The database for on-orbit AO exposure effects at this time is rather limited. At this writing, very little quantitative data from LDEF has been disseminated with regards to materials erosion yields, although the gross effects of almost six years of AO bombardment were readily witnessed via casual inspection of the satellite recovered on STS-32 in January 1990. Many polymeric films were completely lost, some composite materials exhibited eroded plies and exposed fibers, several paints had lost the polymeric binders and pigment particles were easily dislodged from the surface, and teflon (FEP) films were visibly roughened and lost approximately 0.001" due to bombardment by almost 10^{22} atoms/cm^2. Teflon and Kapton materials were recovered from the Solar Maximum Satellite during the Solar Maximum Repair Mission (SMRM) on 41-C in April 1984 which also was the LDEF deployment mission. Kapton films (0.005") exhibited up to a 40% loss of thickness as a result of exposure to approximately 2×10^{21} atoms/cm^2 during 50 months on-orbit. Silver/teflon materials exhibited obvious degradation, especially in regions exposed both to AO and solar radiation.

Results from the prior EOIM missions on STS-5 and STS-8 provide most of the quantitative AO erosion data for a wide variety of materials. The STS-5 experiment, flown in November 1982, exposed a rather limited set of materials to an estimated AO fluence of nearly 10^{20} atoms/cm^2. Results from this early experiment have been summarized by Leger, *et al.* in AIAA Paper 83-2361 (1983). The STS-8 experiment (August 1983) provided an opportunity to expose over 300 material specimens to an AO fluence estimated at 3.5×10^{20} atoms/cm^2. A detailed review of several key investigations for these experiments were compiled by James Visentine (NASA/JSC) in the three-volume NASA Technical Memorandum 100459. A more complete description of AO-related research (flight experiments, chemical mechanisms, ground simulations, etc.) may be found in the "Proceedings of the NASA Workshop on Atomic Oxygen Effects" (JPL Publication 87-14), edited by D. E. Brinza. Key observations in prior flight experiments were that material recession was essentially proportional to AO fluence, which allows the establishment of material-specific "reaction efficiency" parameters, the development of textured surfaces similar to the erosion morphologies witnessed in directed-beam sputtering targets, and changes in the chemical composition of exposed surfaces due to oxidation. Reaction efficiency parameters allow an estimation of the recession in a given mission to be made for a material by multiplication with the anticipated mission AO fluence. Table 1 provides a few representative reaction efficiencies determined in prior EOIM experiments.

The discrepancy in reaction efficiencies of the fluorocarbon FEP in LDEF and EOIM exposures is attributed to the synergistic interaction of the solar vacuum ultraviolet radiation and AO on LDEF which dramatically increases the susceptibility of fluorocarbons to AO attack. Silicones are known to form a self-protective SiO_x glass-like film which resists AO attack. For this reason, the EOIM experiments are quite sensitive to contamination, especially from silicone or fluorocarbon oils, greases, and release agents. Special attention is required to prevent contamination effects from invalidating test results. The handling procedures and pre-flight characterizations described in Sections III and IV were established to minimize and quantify contamination effects on the EOIM-3 experiment.

Table 1. Atomic Oxygen Reaction Efficiencies for Several Materials

Material	Reaction Efficiency ($\times 10^{-24}$ cm^3/atom)
Kapton	3.0
Tedlar	3.2
Mylar	3.4
Polyethylene	3.7
Graphite/Epoxies: 5208/T300 1034C	 2.6 2.1
Carbon (various forms)	0.5 - 1.3
FEP Teflon (EOIM)	< 0.05
FEP Teflon (LDEF)	0.25
Silicones: RTV-560 DC6-1104	 0.02 * 0.02 *

*Units of mg/cm^2, loss assumed to occur in early part of exposure on STS-8 mission.

II. Passive Sample Specifications

Exposure test specimens for the passive tray facility shall consist of either 1" or 1/2" disk specimens which shall conform to the dimensions provided in the following illustration.

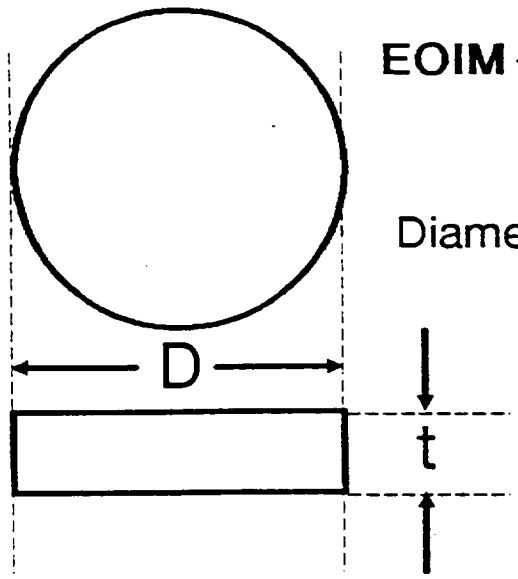

EOIM – 3 Passive Sample Disk

Diameter and thickness specification

Disk	D	t
1"	.995" +.000" −.005"	.032" to .250"
1/2"	.495" +.000" −.005"	.032" to .250"

Specimens will be retained within the passive exposure tray as indicated in the sketch below:

SAMPLE CONFIGURATION

(EOIM – 3 Passive Exposure Tray)

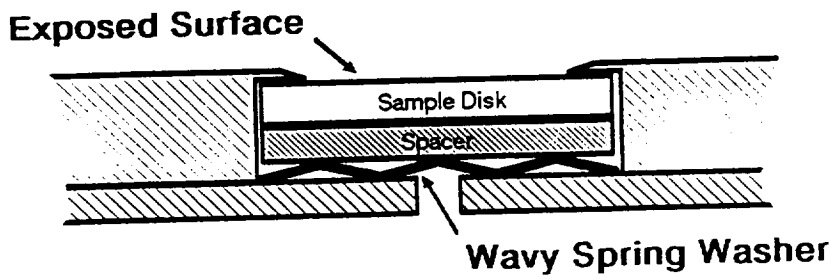

Thin film specimens may be adhesively mounted to a flat rigid substrate to facilitate handling and post-flight recession measurements. Use of a qualified, low-outgassing, non-silicone based adhesive such as 3135/7111 Epoxy (Crest Products Corp.) is recommended in such applications. Alternatively, unmounted film specimens can be installed with an aluminum spacer employed to secure the specimen within the holder. Note that the maximum allowable thickness for any material/substrate combination is 0.250".

Outgassing characteristics of test materials are of particular concern for this flight test. Materials which have the potential for producing significant quantities of volatile condensable material (VCM) will be scrutinized by the NASA Principal Investigator. All materials are required to be subjected to a thermal/vacuum cycle of 150°F for 48 hours at 10^{-6} torr or better prior to integration into the passive tray. A formal ASTM E-595 outgassing test will be required for curable, multi-component coating and adhesive materials after post-cure treatment to verify compliance with the standard screening limits of <1% for total mass loss (TML) and <0.1% for VCM. Materials which approach or exceed these limits may be subjected to extended thermal/vacuum conditioning, more extensive outgassing tests and may ultimately be rejected if the material fails to meet the above stated limits. Silicone or silane-containing materials may be subjected to more stringent outgassing requirements, with analysis of VCM performed due to the sensitivity of AO erosion to contamination by these materials.

III. Specimen Preparation Recommendations

Specimens for the flight test should be a representative sample of the intended flight application material with a known pedigree (batch/lot number, processing conditions, handling history, etc.). At least two each flight test specimens, ground test and control test specimens

should be prepared for each candidate material. Generally only one specimen of each bulk or film material or two specimens of each surface coating will be flown to provide flight exposed and flight control surfaces. Multiple flight specimens of a given material will not be accomodated unless processing variability, statistical or specific testing needs and available space dictate otherwise. The material specimens should be designated as "Flight", "Flight Back-up", "Control A" and "Control B". The selection of material, processing, and handling for each of these specimens should be carried out in as similar of a manner as possible in order to isolate space environmental effects from ground-handling and aging induced artifacts.

Cleaning of the test specimens should be performed after processing of the materials to dimensional specifications. Any loose debris (dust, metal chips, overspray particles, etc.) should be removed by oil-free compressed gas (Dust-Off, etc.). Any adhering particles or contaminant films should be removed by inert solvents (solvents which swell, dissolve or react with test materials should obviously be avoided). Solvents selected for cleaning should contain minimal amounts (< 10 ppm) of non-volatile residue (NVR). A certified, low-NVR (≈ 1 ppm) azeotrope of 1,1,1-trichloroethane and ethanol is available from Thermal Analytical Research Laboratories, Monrovia, California and is recommended for final cleaning of materials inert to this solvent mixture. Test specimens should be subjected to thermal/vacuum conditions to remove solvents, moisture, or other outgassing components prior to placing into containers. Cleaned, low-outgassing covered dishes (Fluoroware, Inc.) are available from JPL as the preferred storage containers for the test specimens. The cleaned test specimens should be carefully placed in individual storage containers and subsequently bagged in cleaned (MIL-STD-1246B level 100) chlorotrifluoroethylene (CTFE), 3M2100 or fluoroethylenepropylene (FEP) Teflon heat-sealed bags. The use of polyethylene bags is to be avoided since these are typically impregnated with anti-static oils or release agents. The final cleaning and packaging procedures should be carefully performed in a clean room or clean bench environment in order to minimize contamination effects.

IV. Measurement Strategies

This section provides basic guidelines for measurements relevant for characterization of space environmental effects on materials in the EOIM-3 mission. Methods for the generation of data for reactivity efficiency, surface morphological change, surface chemical change and bulk property changes are discussed. The sequence of measurements to be performed is also addressed in order to prevent the inadvertent loss or invalidation of data. Careful planning of both the types and sequence of tests to be performed on the test specimens is essential to maximize the data return from flight experiments.

The preferred method of determination of reaction efficiency for small material specimens is via surface recession measurements. Weight-loss measurements are subject to a number of errors, including moisture loss/gain, particle contamination, balance calibration, etc. Recession measurements may be obtained near the masked edge region of the sample or masking bars of a non-reactive material (i.e. gold) may be deposited across the surface to provide protected and exposed regions across the material surface. The use of stylus profilometry is recommended for rigid materials with large anticipated surface recession whereas atomic force microscopy (AFM) or scanning electron microscopy (SEM)

measurements should be performed on flexible materials or materials with low anticipated surface recession.

Various methods exist for the determination of changes in surface morphology. Light-scattering measurements such as bi-directional reflectance distribution function (BRDF) or bi-directional transmittance distribution function (BTDF) are non-destructive techniques which generate directly applicable optical properties for materials. There are several microscopic techniques available to image surface features. Scanning tunneling microscopy (STM) utilizes a fine tip tunneling-current probe rastered over the surface to generate surface topographic images with resolution available to the atomic scale. Atomic force microscopy (AFM) operates in a similar fashion, but requires no surface conductivity, hence no metallization, to produce images. Scanning electron microscopy (SEM) has long been used to image features to the submicron scale, but suffers from the potential for damaging of surface features by the electron beam and the requirement for surface electrical conductivity to avoid charging. AFM is the preferred method for producing detailed images of the surface morphology for insulating materials since it does not require the application of a conductive coating prior to imaging.

Changes in surface chemical composition may be characterized by several techniques. Electron spectroscopy for chemical analysis (ESCA) is a very sensitive technique capable of probing the elemental composition for the outer 100-200 Å of the test material surface. High-resolution ESCA is able to distinguish various levels of oxidation of carbon routinely. Composition-depth profiling can be performed using either Auger electron spectroscopy (AES) or secondary ion mass spectrometry (SIMS). AES is generally not well suited for insulating materials due to charging problems. SIMS, a technique in which material is sputtered from the test material surface with concurrent mass spectrometry of the ejected material provides chemical information as well as elemental composition as a function of depth in the material. Traditional spectroscopic techniques (UV/VIS, IR, ATR) are generally of lower sensitivity and lower cost than the above methods. These techniques have been used to detect qualitative changes in surface chemical composition due to oxidation or loss of organic material. The use of integrating spheres coupled with visible/near-IR spectrometers permits accurate determination of post-exposure solar absorptance of thermal control materials. Hemispherical emittance measurement are also routinely measured in the laboratory of such materials. Electron spin resonance (ESR) is able to detect low concentrations of radical species (i.e. photofragments in polymer chains) but has not yet been exploited for characterization of space exposed materials. Non-microscopic characterization of surface energy via contact angle techniques, etc. has also been performed on materials which were exposed to AO and were found to be effective in the detection of surface oxidation.

In the past, standard tests of modulus, strength, viscoelastic properties have been performed on large exposed material strips. Dynamic modulus testing devices are now able to characterize mechanical properties of films as a function of temperature of small (1" x 1/4") film material specimens. Unfortunately, the small specimen sizes available on the passive sample tray are not compatible with the usual test article sizes required for mechanical properties characterization of structural composite materials.

The above paragraphs outline some of the various techniques available to investigators for characterization of space exposed and control materials. In general, the characterization of the flight and control specimens should be performed with the same test instruments.

Some of the tests are purely non-intrusive while others are considered destructive. SEM is a surface destructive technique since the gold shadowing required for insulating materials will preclude subsequent surface spectroscopic measurements. AFM, on the other hand, does not require any modification of the surface to perform the measurements, nor does it significantly alter the surface. ESCA is extremely sensitive to minute amounts of surface contamination (even sub-monolayer coverage is detectable) hence requires careful handling of test and control specimens to avoid artifacts. Pre-flight ESCA analysis of materials may reveal the presence of surface contaminants (i.e. silicones, fluorocarbons) which may invalidate the flight test for the material and is recommended for materials in which the handling history or contamination control procedures are not well known. In summary, the value of the data from the flight test will be strongly influenced by the handling and characterization of the control and flight material specimens.

APPENDIX D

INSTRUCTIONS FOR SAMPLE DELIVERY TO JPL

Instructions for Sample Delivery to JPL

The enclosed shipping kits include double-bagged, cleaned Fluoroware containers which have been marked with identification codes. The containers are packaged in sets of six for each material for testing. The following guidelines for handling and packaging of test specimens should be adhered to as closely as possible to minimize risk of contamination and subsequent invalidation of test results.

NOTE: HANDLING OF CONTAINERS AND TEST SPECIMENS SHOULD BE DONE IN A CLEAN ROOM ENVIRONMENT USING POWDER-FREE GLOVES.

1. Select specimens which are representative of material to be tested - avoid specimens with obvious flaws or contaminants.

2. Open shipping kits in clean environment only when specimens are ready for packing. Avoid unnecessary handling of inner bags or containers. Do not discard 3M-2110 zip-lock bags.

3. Fluoroware containers are opened by rotating the top CLOCKWISE. Remove "spider-spring".

4. Inspect specimens and containers for dust or lint. If needed, remove particles with filtered dry nitrogen.

5. Place test specimen in tray FACE DOWN. Place "spring" over specimen. Replace cover. Secure by turning COUNTERCLOCKWISE.

6. Return containers to inner bag. Seal zip-lock. Place kit in outer bag and seal.

7. Return kit(s) to shipping box, affix mailing label, and return to:

   Shirley Chung
   Bldg. 67 Room 214
   Jet Propulsion Laboratory
   4800 Oak Grove Drive
   Pasadena, California 91109

APPENDIX E

PROCEDURES FOR ASSEMBLY OF DISK SAMPLE SPECIMENS INTO A PASSIVE SAMPLE CARRIER

National Aeronautics and
Space Administration

JSC-22054

Lyndon B. Johnson Space Center
Houston, Texas 77058

EVALUATION OF OXYGEN INTERACTION WITH MATERIALS-III EXPERIMENT

PROCEDURES

FOR

ASSEMBLY OF DISK SAMPLE SPECIMENS INTO PASSIVE SAMPLE CARRIER

Materials Branch

Structures and Mechanics Division

Lyndon B. Johnson Space Center

Houston, Texas

February 1986

JSC-22054

EVALUATION OF OXYGEN INTERACTION WITH MATERIALS-III EXPERIMENT

PROCEDURES
FOR
ASSEMBLY OF DISK SAMPLE SPECIMENS
INTO PASSIVE SAMPLE CARRIER

Prepared by:

JAMES T. VISENTINE
Senior Materials Science Technologist
Materials Branch (ES5)

Approved by:

LUBERT J. LEGER
Head, Non-Metallic Materials Section
Materials Branch (ES5)

Structures and Mechanics Division

Lyndon B. Johnson Space Center

Houston, Texas

EVALUATION OF OXYGEN INTERACTION WITH MATERIALS-III EXPERIMENT

ASSEMBLY OF DISK SAMPLE SPECIMENS INTO PASSIVE SAMPLE CARRIER

1.0 INTRODUCTION

The following procedures apply to assembly of disk sample specimens into the sample carriers for use on the Evaluation of Oxygen Interaction with Materials-III (EOIM-III) experiment. The procedures apply equally to the 1-inch (25.4 mm) samples and to the .5-inch (12.7 mm) samples to be assembled into the carriers. Figure 1 depicts the appearance of the assembled sample disk aperture.

2.0 COMPONENTS AND PARTS REQUIRED

2.1 CARRIER COMPONENTS

Two separate passive sample carrier assemblies are covered by these instructions - the single-size disk carrier has provisions for 46 sample disks, 1-inch (25.4 mm) in diameter, while the dual-size disk sample carrier has provisions for 27 sample disks, 1-inch (25.4 mm) in diameter together with 55 sample disks, .5-inch (12.7 mm) in diameter. The part numbers for the sample carrier components are:

a. Single-size disk carrier (SED39118361-301 Assembly):

   1) SED39118359-701 - Sample Carrier

   2) SDD39118360-001 - Retainer Plate

   3) MS51959-28 - Assembly screws

   4) SED39118186-701 - Protective cover

b. Dual-size disk carrier (SED39117947-301 Assembly):

   1) SED39118183-701 - Sample Carrier

   2) SDD39118185-001 - Retainer Plate

   3) MS51959-28 - Assembly screws

   4) SED39118186-701 - Protective cover

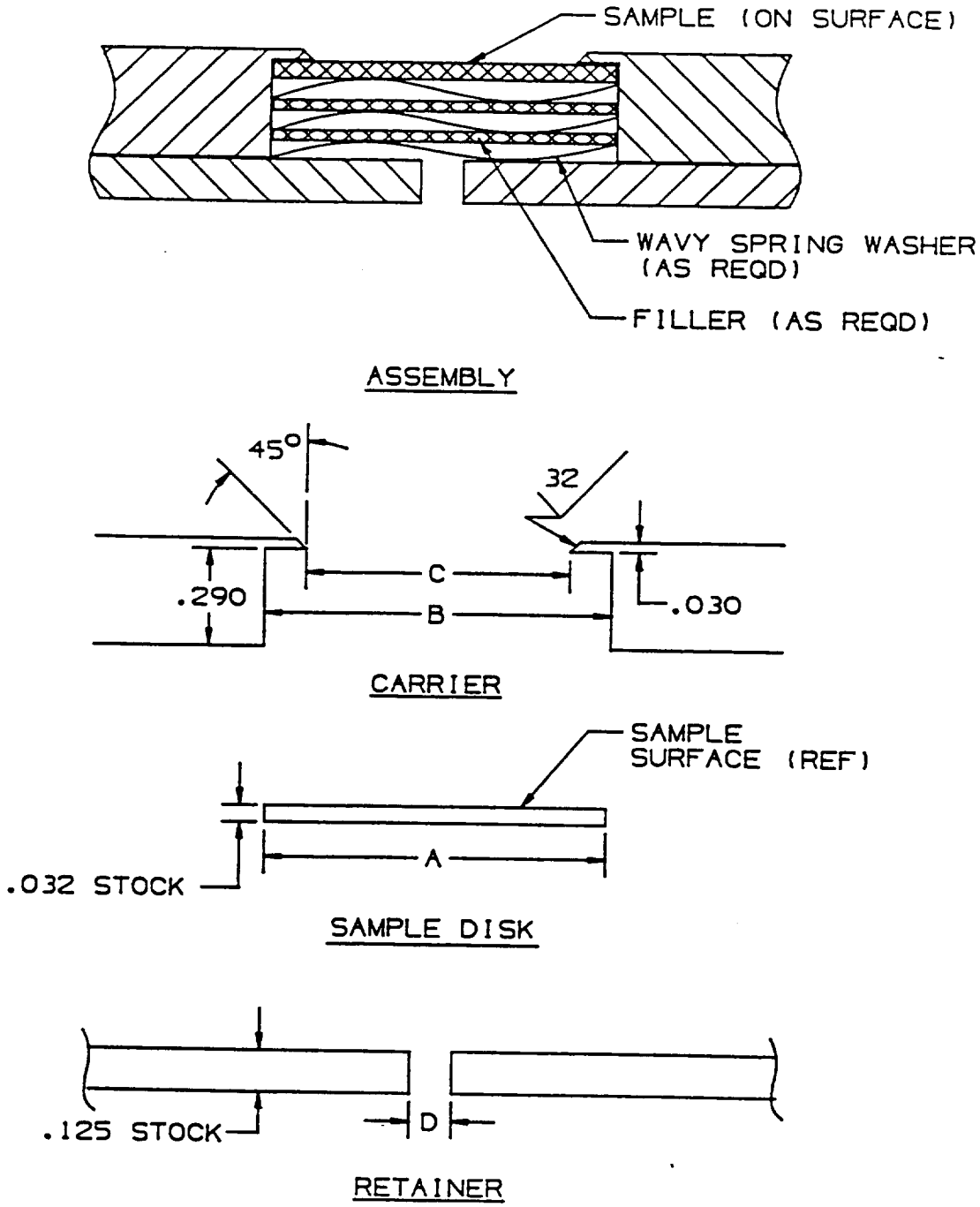

	A	B	C	D
1" DISK	.995 +000 -005	1.020 ±005	.813 ±010	.125 ±01
1/2" DISK	.495 +000 -005	.520 ±005	.375 ±010	.125 ±01

Figure 1 Assembly of Sample Disks

2.2 SAMPLE DISKS, FILLERS, AND SPRINGS

The same disk part number is used as substrate, carrier, or backup for the thin-film and coated specimens and for the fillers used to fill the sample apertures behind the sample disks; in selecting disks to be used as substrates, any of the identically-numbered parts may be used. The part numbers for the disks and for the wave springs used in the apertures are:

a. SDD39118184-001 - Sample Disk, 1" (25.4 mm) diameter

b. SDD39118184-003 - Sample Disk, .5" (12.5 mm) diameter

c. SDD39118177-001 - Spring, 1" (nominal) diameter

d. SDD39118177-003 - Spring, .5" (nominal) diameter

2.3 ACCESSORY ITEMS

Two accessory items are furnished for use during the sample-loading procedure; these items, and the purposes for each, are:

a. Template - This is used for identification of the apertures into which the sample specimen disks are inserted, and to facilitate the necessary record-keeping. The template for the single-size disk carrier is depicted in Figure 2, and the template for the dual-size disk carrier is depicted in Figure 3; the templates are reduced in size for the illustrations.

b. Sample Record - This is a tabular form to be used for recording the identification of the sample specimens inserted into each of the separate disk apertures in the sample carrier.

3.0 PREPARATION OF SAMPLE CARRIERS AND DISKS

3.1 CLEANING

Prior to start of the assembly process, the sample carriers, retainer plates, sample disks, fillers, springs, and assembly screws must be cleaned in accordance with procedures prescribed in the Appendix to this Procedure.

3.2 APPLICATION OF SAMPLE SPECIMENS

The thin-film and coated specimens shall be furnished, prepared, and installed by the Investigator.

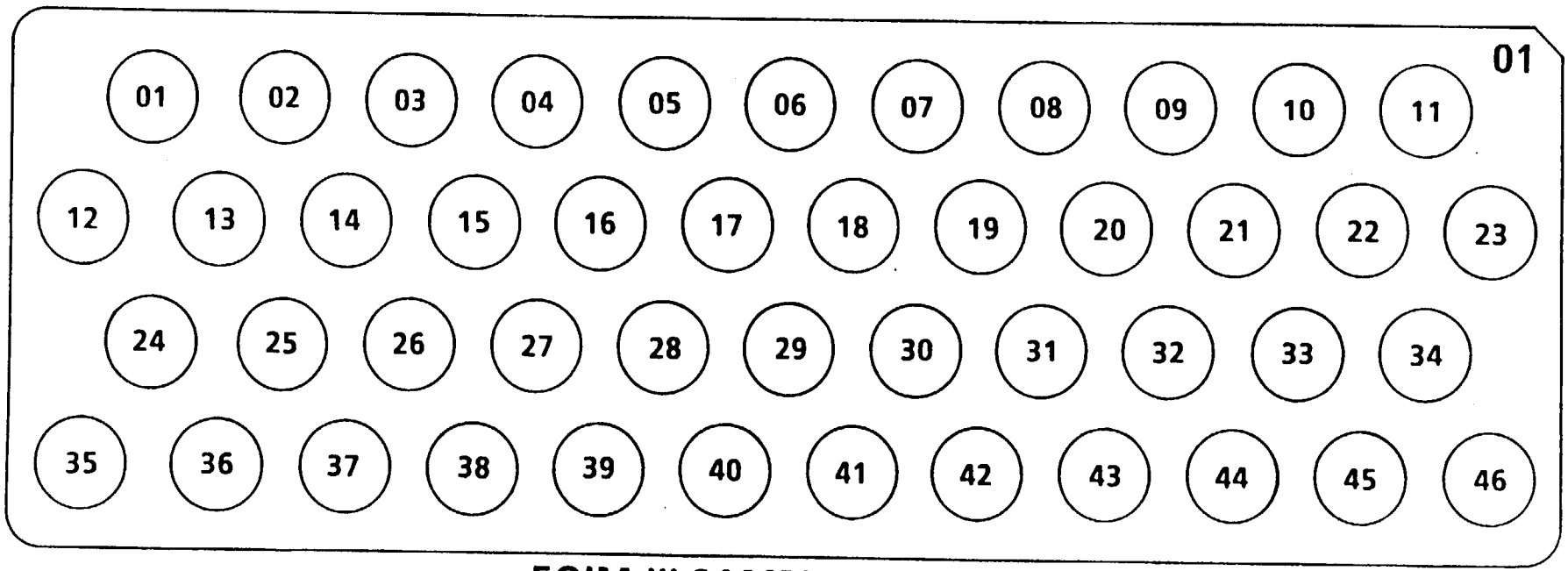

EOIM-III SAMPLE CARRIER

VIEWED IN THE INVERTED (LOADING) POSITION

Figure 2 Single-Size Carrier Template

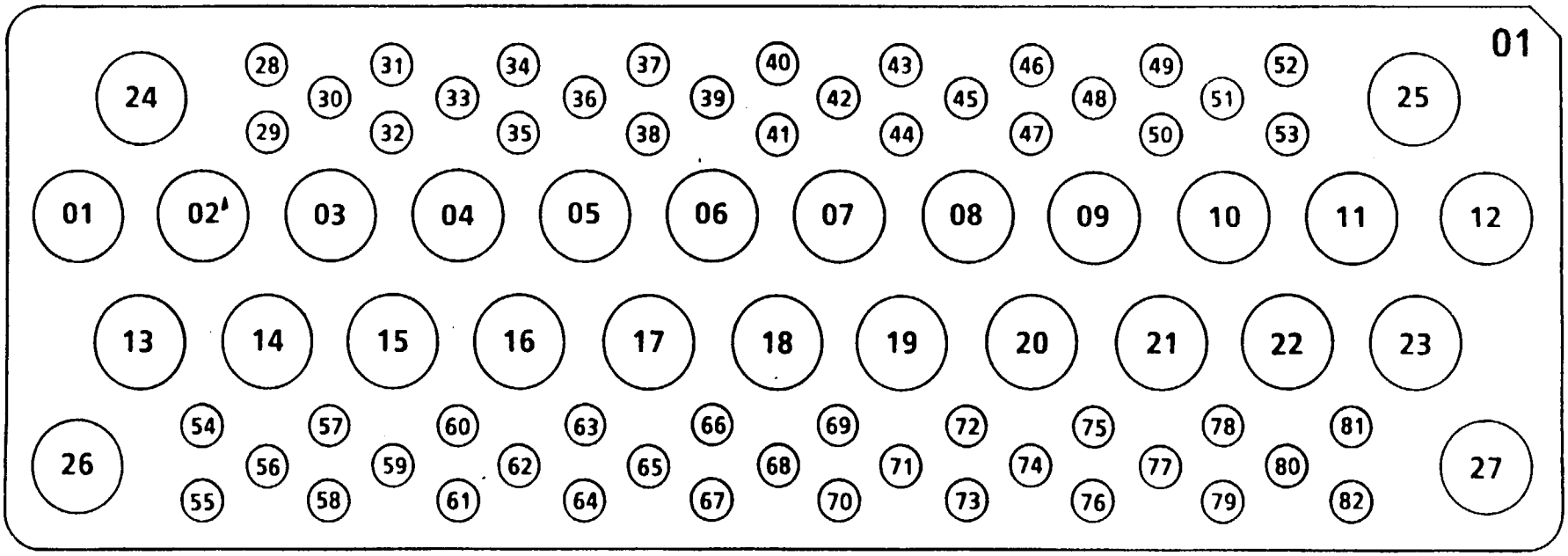

EOIM-III SAMPLE CARRIER

VIEWED IN THE INVERTED (LOADING) POSITION

Figure 3 Dual-Size Carrier Template

4.0 ASSEMBLY PROCEDURE

a. Collect the components for a single sample carrier assembly, assuring that one of each of the major components (i. e., items a.1 through a.4, or b.1 through b.4, as appropriate, as shown in paragraph 2.1, above) is available, and that the identity numbers on all are matched. (NOTE: The thin-film specimens and coated disks should have been obtained for the assembly task before this step is begun, and should be ready for assembly into the carrier.)

b. Collect the wave spring washers and the disk fillers in sufficient quantity; four of each per disk aperture should suffice for a start.

c. Remove the protective cover from the sample carrier, and set aside.

d. Invert the sample carrier (i.e., aperture rims with the chamfers should be downward), and remove the eleven (11) MS51959-28 (6-32 x 3/8-inch) assembly screws that hold the sample retainer plate; set the screws and retainer plate to one side.

e. Place the sample carrier over the template so that the aperture numbers are visible through the sample apertures; assure that the corner of the carrier having the chamfer and identity number is aligned with the comparable corner on the template.

f. Enter the identity number of the sample carrier on the Sample Record.

g. Insert the samples into the disk apertures in sequential order, with the surface to be exposed facing downward, toward the template. Unmounted thin-film specimens should have a sample disk inserted immediately behind the specimen, as a backup. Identification of the sample specimen should be entered at the aperture identification line on the Sample Record at this time.

h. After each coated disk or backup disk has been inserted in the disk aperture, insert one wave spring washer atop the disk, followed by a filler disk. Continue inserting wave spring washers and filler disks, alternately, until the disk aperture is filled to an approximate level <u>slightly</u> above the surface of the sample carrier. NOTE: The last-inserted item, spring washer or filler disk, should project <u>slightly</u> above the surface of the sample carrier, but not so much that it could slide out of place.

i. Disk apertures that are not used need not have disks, fillers, or spring washers inserted.

j. When all sample specimen disks have been inserted, and the disk apertures filled with spring washers and fillers, the retainer plate should be placed on the back surface of the sample carrier, taking care not to disturb the contents of the disk

apertures. Assure that the identity number of the sample retainer matches that of the sample carrier, and that the chamferred corner is aligned with that of the sample carrier.

k. Insert the assembly screws (removed in step "d", above) through the holes in the retainer; tighten the screws, taking care to prevent damaging the screwdriver slot or shearing the screw.

l. When all screws have been inserted and tightened, re-invert the sample carrier so that the sample specimen surfaces face upward, then install the protective cover and tighten the retaining screws finger-tight. Assure that the identity number of the protective cover matches that of the sample carrier.

m. Verify that the Sample Record includes all information pertinent to the samples inserted into the particular sample carrier, before installing the protective cover on the carrier.

5.0 PREPARATION FOR DELIVERY

When the foregoing steps have been completed, the sample carrier is ready for installation on the EOIM-III pallet. To maintain cleanliness, the assembled sample carrier must be protected by double-bagging the assembly in suitable materials. Instructions for delivery and disposition of the assembled sample carriers will be found in Section 5.0 of JSC-22053, Design, Fabrication, and Processing Guidelines for the EOIM-III Hardware.

APPENDIX F

MASS AND ESCA DATA

TABLE OF CONTENTS

TABLE OF CONTENTS (continued)

TABLE OF CONTENTS (continued)

TABLE OF CONTENTS (continued)

1A1 MoS_2-Ni lubricant on steel, Ovonic

1A1A	As Received	Post-Bake	Post-Flight	Difference
Mass	4.62700	4.62700	4.62695	-0.00005

1A1C	Pre-Ground	Post-Ground	Difference
Mass(g)	4.6374	4.6375	0.0001

Electron Spectroscopy for Chemical Analysis (ESCA)

Element	1A1D As Received Atom %	1A1D Post-Bake Atom %	1A1A Post-Flight Atom %
C	41.82	51.35	-----
O	19.63	18.64	-----
S	19.40	15.50	-----
Mo	16.93	14.51	-----
F	2.22	0.00	-----

1A2 MoS_2-Ni lubricant on steel, Ovonic

1A2A	As Received	Post-Bake	Post-Flight	Difference
Mass	4.65977	4.65977	4.65973	-0.00004

1A2C	Pre-Ground	Post-Ground	Difference
Mass(g)	4.6095	4.6094	-0.0001

Electron Spectroscopy for Chemical Analysis (ESCA)

Element	1A2D As Received Atom %	1A2D Post-Bake Atom %	1A2A Post-Flight Atom %
C	43.27	51.61	-----
O	20.78	20.96	-----
S	17.28	13.55	-----
Mo	16.10	13.88	-----
F	2.57	0.00	-----

1A3 MoS_2-SbO_x lubricant on steel, Hohman

1A3A	As Received	Post-Bake	Post-Flight	Difference
Mass	4.66989	4.66988	4.66992	0.00004

1A3C	Pre-Ground	Post-Ground	Difference
Mass(g)	4.6427	4.6427	0.0000

Electron Spectroscopy for Chemical Analysis (ESCA)

Element	1A3D As Received Atom %	1A3D Post-Bake Atom %	1A3A Post-Flight Atom %
C	31.53	47.94	-----
Sb	15.65	15.91	-----
S	29.42	21.25	-----
Mo	19.95	14.90	-----
F	3.45	0.00	-----

1A4 MoS_2-SbO_x lubricant on steel, Hohman

1A4A	As Received	Post-Bake	Post-Flight	Difference
Mass	4.65406	4.65408	4.65424	0.00016

1A4C	Pre-Ground	Post-Ground	Difference
Mass(g)	4.6574	4.6573	-0.0001

Electron Spectroscopy for Chemical Analysis (ESCA)

Element	1A4D As Received Atom %	1A4D Post-Bake Atom %	1A4A Post-Flight Atom %
C	31.79	46.80	-----
Sb	16.64	11.53	-----
S	31.11	24.89	-----
Mo	20.46	16.77	-----

1B1 SiO_2-doped Al_2O_3/SiO_2 multilayer on fused SiO_2

1B1A	As Received	Post-Bake	Post-Flight	Difference
Mass(g)	1.74563	1.74569	1.74570	0.00001

1B1C	Pre-Ground	Post-Ground	Difference
Mass(g)	1.7549	1.7549	0.0000

Electron Spectroscopy for Chemical Analysis (ESCA)

Element	1B1E As Received Atom %	1B1E Post-Bake Atom %	1B1A Post-Flight Atom %
Si	3.26	3.72	-----
C	31.62	34.39	-----
O	40.05	37.72	-----
Al	21.58	21.60	-----
F	3.49	2.57	-----

1B2 TiN (1000 Å) on fused SiO_2

1B2A	As Received	Post-Bake	Post-Flight	Difference
Mass(g)	1.72806	1.72798	1.72801	0.00003

1B2C	Pre-Ground	Post-Ground	Difference
Mass(g)	1.7282	1.7283	0.0001

Electron Spectroscopy for Chemical Analysis (ESCA)

Element	1B2F As Received Atom %	1B2F Post-Bake Atom %	1B2A Post-Flight Atom %
C	31.91	38.08	-----
O	28.95	27.65	-----
Ti	13.75	12.70	-----
N	14.03	12.45	-----
Al	4.66	6.12	-----
F	6.71	3.01	-----

5C1 T300/934 composite, LDEF trailing edge

5C1A	As Received	Post-Bake	Post-Flight	Difference
Mass(g)	0.60046	0.59963	0.60091	0.00128

5C1B	Pre-Ground	Post-Ground	Difference
Mass(g)	0.5974	0.5972	-0.0002

Electron Spectroscopy for Chemical Analysis (ESCA)

Element	5C1C As Received Atom %	5C1C Post-Bake Atom %	5C1A Post-Flight Atom %	5C1B Post-Ground Atom %
Si	13.47	13.88	24.01	14.63
C	49.06	47.35	17.94	24.67
O	35.57	36.42	54.57	45.92
N	1.90	1.91	2.31	4.99
S	0.00	0.00	1.18	3.99
Na	0.00	0.44	0.00	1.10
Al	0.00	0.00	0.00	2.25
F	0.00	0.00	0.00	1.97
Cu	0.00	0.00	0.00	0.47

5C2 T300/934 composite, adjacent to 5C1 on LDEF

5C2A	As Received	Post-Bake	Post-Flight	Difference
Mass(g)	0.59216	0.59096	0.59201	0.00105

5C2B	Pre-Ground	Post-Ground	Difference
Mass(g)	0.5933	0.5927	-0.0006

Electron Spectroscopy for Chemical Analysis (ESCA)

Element	5C2C As Received Atom %	5C2C Post-Bake Atom %	5C2A Post-Flight Atom %	5C2B Post-Ground Atom %
Si	7.28	6.89	2.26	2.28
C	49.54	46.27	56.30	45.75
O	24.87	24.63	28.65	35.61
N	3.62	3.53	8.43	6.98
S	1.13	0.50	3.57	6.42
F	13.24	17.83	0.80	0.00
Sn	0.31	0.34	0.00	0.00
Na	0.00	0.00	0.00	2.68
Cu	0.00	0.00	0.00	0.28

5C4 Polyethylene ring, anodized aluminum cover ring on aluminum base coated with silver oxide

5C4A	As Received	Post-Bake	Post-Flight	Difference
Mass(g) (disk)	0.16033	0.16048	0.16044	-0.00004

5C4C	Pre-Ground	Post-Ground	Difference
Mass(g)	0.7185	0.7185	0.0000

Electron Spectroscopy for Chemical Analysis (ESCA)

Element	5C4E As Received Atom %	5C4E Post-Bake Atom %	5C4A Post-Flight Atom %	5C4C Post-Ground Atom %
C	48.90	51.32	33.35	36.94
O	27.76	24.80	34.40	27.19
Ag	23.34	22.08	32.24	26.33
Cl	0.00	1.80	0.00	0.00
F	0.00	0.00	0.00	8.20
S	0.00	0.00	0.00	1.33

5C5 Polyethylene ring, anodized aluminum cover ring on anodized aluminum base

5C5A	As Received	Post-Bake	Post-Flight	Difference
Mass(g) (disk)	0.16313	0.16322	0.16321	-0.00001

5C5C	Pre-Ground	Post-Ground	Difference
Mass(g)	0.7097	0.7097	0.0000

Electron Spectroscopy for Chemical Analysis (ESCA)

Element	5C5E As Received Atom %	5C5E Post-Bake Atom %	5C5A Post-Flight Atom %	5C5C Post-Ground Atom %
Si	0.00	0.00	5.12	0.00
C	20.31	29.21	12.68	17.23
O	55.88	44.83	52.87	47.38
Al	18.56	18.45	23.47	19.25
P	3.88	0.00	0.00	2.50
Cr	1.37	1.30	0.00	1.21
B	0.00	6.20	4.76	0.00
F	0.00	0.00	1.10	8.66
S	0.00	0.00	0.00	2.60
N	0.00	0.00	0.00	1.18

5D1 3M Y9469 acrylic transfer tape

5D1A	As Received	Post-Bake	Post-Flight	Difference
Mass(g)	0.79515	0.79514	0.79434	-0.00080

5D1C	Pre-Ground	Post-Ground	Difference
Mass(g)	0.7940	0.7934	-0.0006

Electron Spectroscopy for Chemical Analysis (ESCA)

Element	5D1F As Received Atom %	5D1F Post-Bake Atom %	5D1A Post-Flight Atom %	5D1C Post-Ground Atom %
Si	5.24	5.81	2.06	4.88
C	76.48	76.44	77.23	45.88
O	18.28	17.75	20.35	35.15
Sn	0.00	0.00	0.37	5.10
F	0.00	0.00	0.00	4.44
N	0.00	0.00	0.00	1.95
S	0.00	0.00	0.00	1.32
Cu	0.00	0.00	0.00	1.27

5E1 HRG-3/AB epoxy silane (HAC)

5E1A	As Received	Post-Bake	Post-Flight	Difference
Mass(g)	0.12665	0.12657	0.12669	0.00012

5E1C	Pre-Ground	Post-Ground	Difference
Mass(g)	0.125685	0.125672	-0.000013

Electron Spectroscopy for Chemical Analysis (ESCA)

Element	5E1F As Received Atom %	5E1F Post-Bake Atom %	5E1A Post-Flight Atom %	5E1C Post-Ground Atom %
Si	6.88	7.25	29.11	24.41
C	77.19	76.90	15.16	14.34
O	12.56	12.21	54.48	54.73
N	2.69	2.64	1.26	1.78
Al	0.67	0.00	0.00	0.00
F	0.00	1.00	0.00	4.75

5E2 HRG-3/AB epoxy silane (vendor)

5E2A	As Received	Post-Bake	Post-Flight	Difference
Mass(g)	0.12403	0.12396	0.12402	0.00006

5E2C	Pre-Ground	Post-Ground	Difference
Mass(g)	0.124065	0.124060	-0.000005

Electron Spectroscopy for Chemical Analysis (ESCA)

Element	5E2F As Received Atom %	5E2F Post-Bake Atom %	5E2A Post-Flight Atom %	5E2C Post-Ground Atom %
Si	7.07	6.52	27.90	22.84
C	75.51	75.43	16.32	15.04
O	14.36	14.88	54.28	54.00
N	3.05	3.17	1.50	1.63
F	0.00	0.00	0.00	5.01
Cu	0.00	0.00	0.00	0.87
Na	0.00	0.00	0.00	0.62

5F1 Diamond film on silicon wafer

5F1A	As Received	Post-Bake	Post-Flight	Difference
Mass(g)	0.25013	0.25006	0.25005	-0.00001

5F1B	Pre-Ground	Post-Ground	Difference
Mass(g)	0.2544	0.2543	-0.0001

Electron Spectroscopy for Chemical Analysis (ESCA)

Element	5F1C As Received Atom %	5F1C Post-Bake Atom %	5F1A Post-Flight Atom %	5F1B Post-Ground Atom %
Si	4.45	5.16	9.76	0.00
C	86.29	85.73	61.12	86.61
O	8.66	9.11	28.40	11.52
F	0.60	0.00	0.72	0.99
Cu	0.00	0.00	0.00	0.89

5F2 Diamond film on silicon wafer

5F2A	As Received	Post-Bake	Post-Flight	Difference
Mass(g)	0.24678	0.24680	0.24680	0.00000

5F2B	Pre-Ground	Post-Ground	Difference
Mass(g)	0.2465	0.2465	0.0000

Electron Spectroscopy for Chemical Analysis (ESCA)

Element	5F2C As Received Atom %	5F2C Post-Bake Atom %	5F2A Post-Flight Atom %	5F2B Post-Ground Atom %
Si	4.45	5.16	9.37	0.89
C	86.29	85.73	60.23	83.37
O	8.66	9.11	28.16	13.24
F	0.60	0.00	0.74	1.27
N	0.00	0.00	1.50	0.00
Cu	0.00	0.00	0.00	0.95
S	0.00	0.00	0.00	0.28

5G1 Beta-cloth, graphite interwoven (Chemglas 250 GW-80)

5G1A	As Received	Post-Bake	Post-Flight	Difference
Mass(g)	0.03285	0.03286	0.03289	0.00003

5G1C	Pre-Ground	Post-Ground	Difference
Mass(g)	0.032668	0.032168	-0.000500

Electron Spectroscopy for Chemical Analysis (ESCA)

Element	5G1F As Received Atom %	5G1F Post-Bake Atom %	5G1A Post-Flight Atom %	5G1C Post-Ground Atom %
Si	0.82	0.00	3.69	2.24
C	30.45	32.66	29.65	30.97
O	1.15	1.25	7.78	5.10
F	67.58	66.09	58.88	61.69

5H1 SiC/Al composite, $CaZrO_3$ coating

5H1A	As Received	Post-Bake	Post-Flight	Difference
Mass(g)	0.32116	0.32112	0.32111	-0.00001

5H1C	Pre-Ground	Post-Ground	Difference
Mass(g)	0.3184	0.3185	0.0001

Electron Spectroscopy for Chemical Analysis (ESCA)

Element	5H1F As Received Atom %	5H1F Post-Bake Atom %	5H1A Post-Flight Atom %	5H1C Post-Ground Atom %
Si	2.40	2.64	9.76	2.65
C	31.53	37.35	17.45	16.25
O	47.22	43.36	48.84	37.47
F	0.00	0.00	7.31	20.05
Ca	15.08	13.42	12.16	11.24
Zr	3.78	3.22	4.50	7.33
Cu	0.00	0.00	0.00	3.92
S	0.00	0.00	0.00	1.07

5H2 SiC/Al composite, Al_2O_3 coating

5H2A	As Received	Post-Bake	Post-Flight	Difference
Mass(g)	0.33720	0.33722	0.33715	-0.00007

5H2C	Pre-Ground	Post-Ground	Difference
Mass(g)	0.3397	0.3396	-0.0001

Electron Spectroscopy for Chemical Analysis (ESCA)

Element	5H2F As Received Atom %	5H2F Post-Bake Atom %	5H2A Post-Flight Atom %	5H2C Post-Ground Atom %
Si	0.00	0.00	6.12	0.00
C	14.66	21.93	11.27	14.73
O	52.07	47.99	50.13	38.58
F	0.00	0.00	3.73	14.77
Al	31.44	28.47	25.01	28.27
Na	1.83	1.61	3.74	0.73
Cu	0.00	0.00	0.00	1.90
Na	0.00	0.00	0.00	0.73

5H3 IM7/PEEK, Al_2O_3 coating

5H3A	As Received	Post-Bake	Post-Flight	Difference
Mass(g)	0.20577	0.20562	0.20577	0.00015

5H3C	Pre-Ground	Post-Ground	Difference
Mass(g)	0.198571	0.198550	-0.000021

Electron Spectroscopy for Chemical Analysis (ESCA)

Element	5H3F As Received Atom %	5H3F Post-Bake Atom %	5H3A Post-Flight Atom %	5H3C Post-Ground Atom %
Si	0.00	0.00	4.87	0.00
C	17.13	25.96	9.62	11.89
O	52.03	46.58	51.33	40.19
F	0.00	0.00	4.18	18.02
Al	29.20	26.26	25.68	27.61
Na	1.64	1.20	4.31	1.15
Cu	0.00	0.00	0.00	1.14

5H4 IM7/PEEK, BN/Al_2O_3 coating

5H4A	As Received	Post-Bake	Post-Flight	Difference
Mass(g)	0.18585	0.18580	0.18585	0.00005

5H4C	Pre-Ground	Post-Ground	Difference
Mass(g)	0.183384	0.183362	-0.000022

Electron Spectroscopy for Chemical Analysis (ESCA)

Element	5H4F As Received Atom %	5H4F Post-Bake Atom %	5H4A Post-Flight Atom %	5H4C Post-Ground Atom %
Si	0.00	0.00	7.56	0.00
C	17.77	23.21	10.56	5.91
O	52.01	47.35	53.09	42.65
F	0.00	0.00	2.33	17.03
Al	30.22	28.59	25.50	29.74
Na	0.00	0.00	0.96	1.48
N	0.00	0.85	0.00	0.00
Cu	0.00	0.00	0.00	1.90
K	0.00	0.00	0.00	1.28

1K3 Four coatings on Al/PVDF/circuit board (mass data only)

1K3A	As Received	Post-Bake	Post-Flight	Difference
Mass(g)	1.67881	1.67770	-------	-------

1K3C	Pre-Ground	Post-Ground	Difference
Mass(g)	1.6528	1.6528	0.0000

1K4 Four coatings on Al/PVDF/circuit board

1K4A	As Received	Post-Bake	Post-Flight	Difference
Mass(g)	1.56511	1.56400	-------	-------

1K4C	Pre-Ground	Post-Ground	Difference
Mass(g)	1.7034	1.7034	0.0000

1K3 Four coatings on Al/PVDF/circuit board, Quadrants #1 and #2 clockwise from notch

Electron Spectroscopy for Chemical Analysis (ESCA)

Quadrant #1 clockwise from notch (Ni/PbTe)

Element	1K3F As Received Atom %	1K3F Post-Bake Atom %	1K3A Post-Flight Atom %	1K3C Post-Ground Atom %
C	40.85	38.75	-----	25.58
O	32.52	31.56	-----	42.91
Pb	14.80	14.60	-----	14.51
Te	11.83	10.95	-----	9.20
Cl	0.00	4.14	-----	0.00
F	0.00	0.00	-----	5.00
Cu	0.00	0.00	-----	2.81

Quadrant #2 clockwise from notch (Ni/Si/SiO_2)

Element	1K3F As Received Atom %	1K3F Post-Bake Atom %	1K3A Post-Flight Atom %	1K3C Post-Ground Atom %
Si	29.39	28.04	-----	29.08
C	17.77	20.03	-----	4.77
O	52.84	51.94	-----	57.35
F	0.00	0.00	-----	5.09
Na	0.00	0.00	-----	1.96
Cu	0.00	0.00	-----	1.06
K	0.00	0.00	-----	0.70

1K3 Four coatings on Al/PVDF/circuit board, Quadrants #3 and #4 clockwise from notch

Electron Spectroscopy for Chemical Analysis (ESCA)

Quadrant #3 clockwise from notch (Ni/SiO_2)

Element	1K3F As Received Atom %	1K3F Post-Bake Atom %	1K3A Post-Flight Atom %	1K3C Post-Ground Atom %
Si	31.10	30.96	-----	29.27
C	14.38	16.59	-----	6.97
O	54.51	52.45	-----	58.62
F	0.00	0.00	-----	4.03
Cu	0.00	0.00	-----	1.10

Quadrant #4 clockwise from notch ($Ni/ZnS/PbF_2/ZnS$)

Element	1K3F As Received Atom %	1K3F Post-Bake Atom %	1K3A Post-Flight Atom %	1K3C Post-Ground Atom %
C	47.26	52.45	-----	18.36
O	14.93	15.20	-----	37.51
S	22.65	17.93	-----	6.35
Zn	12.52	11.22	-----	20.25
F	2.65	0.00	-----	14.39
N	0.00	3.20	-----	0.00
Cu	0.00	0.00	-----	3.15

1K4 Four coatings on Al/PVDF/circuit board (mass data only)

1K4A	As Received	Post-Bake	Post-Flight	Difference
Mass(g)	1.56511	1.56400	-------	-------

1K4C	Pre-Ground	Post-Ground	Difference
Mass(g)	1.7034	1.7034	0.0000

1K4 Four coatings on Al/PVDF/circuit board, Quadrants #1 and #2 clockwise from notch

Electron Spectroscopy for Chemical Analysis (ESCA)

Quadrant #1 clockwise from notch ($Mo/Si/SiO_2$)

Element	1K4F As Received Atom %	1K4F Post-Bake Atom %	1K4A Post-Flight Atom %	1K4C Post-Ground Atom %
Si	28.30	25.40	-----	29.01
C	13.34	22.69	-----	9.44
O	55.56	50.21	-----	56.07
F	2.79	1.70	-----	3.88
Na	0.00	0.00	-----	0.86
Cu	0.00	0.00	-----	0.74

Quadrant #2 clockwise from notch ($No/TiO_2/Al_2O_3/TiO_2$)

Element	1K4F As Received Atom %	1K4F Post-Bake Atom %	1K4A Post-Flight Atom %	1K4C Post-Ground Atom %
Si	0.00	1.66	-----	2.39
C	30.71	38.87	-----	22.40
O	45.16	43.78	-----	49.22
Ti	14.23	10.89	-----	10.01
F	8.20	4.81	-----	10.26
N	1.70	0.00	-----	0.00
Cu	0.00	0.00	-----	3.66
S	0.00	0.00	-----	2.07

1K4 Four coatings on Al/PVDF/circuit board, Quadrants #3 and #4 clockwise from notch

Electron Spectroscopy for Chemical Analysis (ESCA)

Quadrant #3 clockwise from notch ($Mo/TiO_2/Al_2O_3/TiO_2$)

Element	1K4F As Received Atom %	1K4F Post-Bake Atom %	1K4A Post-Flight Atom %	1K4C Post-Ground Atom %
Si	0.00	0.00	-----	2.27
C	39.91	49.64	-----	17.74
O	44.10	41.61	-----	53.16
Ti	8.89	6.46	-----	13.95
F	5.61	2.30	-----	6.27
N	1.49	0.00	-----	0.00
Cu	0.00	0.00	-----	3.34
S	0.00	0.00	-----	3.27

Quadrant #4 clockwise from notch (bare)

Element	1K4F As Received Atom %	1K4F Post-Bake Atom %	1K4A Post-Flight Atom %	1K4C Post-Ground Atom %
Si	3.94	4.05	-----	0.00
C	27.82	29.72	-----	17.36
O	37.70	36.29	-----	29.13
Al	22.28	23.82	-----	26.61
F	7.76	5.59	-----	21.47
Ca	0.50	0.53	-----	0.52
Na	0.00	0.00	-----	0.73
Cu	0.00	0.00	-----	4.18

5K5 Vendor aluminum electrode/PVDF film

5K5A	As Received	Post-Bake	Post-Flight	Difference
Mass(g)	0.37411	0.37378	0.37432	0.00054

5K5C	Pre-Ground	Post-Ground	Difference
Mass(g)	0.3820	0.3818	-0.0002

Electron Spectroscopy for Chemical Analysis (ESCA)

Element	5K5F As Received Atom %	5K5F Post-Bake Atom %	5K5A Post-Flight Atom %	5K5C Post-Ground Atom %
Si	0.00	0.00	9.71	1.53
C	30.89	34.28	21.74	26.12
O	37.80	33.69	41.29	27.72
Al	26.21	27.43	19.77	28.72
F	4.41	4.60	5.73	12.23
Na	0.69	0.00	0.84	1.51
Ca	0.00	0.00	0.56	0.00
Cu	0.00	0.00	0.37	2.17

5K6 Y-Ba-Cu-O High temperature superconductor, oxygen deficient

5K6A	As Received	Post-Bake	Post-Flight	Difference
Mass(g)	0.41368	0.41372	0.41371	-0.00001

5K6B	Pre-Ground	Post-Ground	Difference
Mass(g)	0.4130	0.4131	0.0001

Electron Spectroscopy for Chemical Analysis (ESCA)

Element	5K6C As Received Atom %	5K6C Post-Bake Atom %	5K6A Post-Flight Atom %	5K6B Post-Ground Atom %
Si	0.00	0.00	11.72	0.00
C	34.50	44.90	23.98	18.19
O	45.23	38.93	43.36	35.54
Y	4.89	3.77	1.78	2.61
Ba	6.77	5.59	6.62	9.41
Cu	8.62	6.81	9.24	10.21
F	0.00	0.00	3.30	22.27
S	0.00	0.00	0.00	1.76

5K7 Y-Ba-Cu-O High temperature superconductor, fully oxygenated

5K7A	As Received	Post-Bake	Post-Flight	Difference
Mass(g)	0.41560	0.41538	0.41535	-0.00003

5K7B	Pre-Ground	Post-Ground	Difference
Mass(g)	0.4122	0.4124	0.0002

Electron Spectroscopy for Chemical Analysis (ESCA)

Element	5K7C As Received Atom %	5K7C Post-Bake Atom %	5K7A Post-Flight Atom %	5K7B Post-Ground Atom %
Si	0.00	0.00	11.09	0.00
C	52.28	52.07	27.28	21.43
O	34.39	34.40	42.80	36.60
Y	1.99	1.81	1.33	2.02
Ba	5.88	5.73	7.04	8.42
Cu	5.47	6.00	6.65	12.27
F	0.00	0.00	3.81	19.26

1K8 Al_2O_3/NPB carbon foil on sapphire, Al holder

	As Received	Post-Bake	Post-Flight	Difference
Mass(g)	4.94819	4.94805	-------	-------

Electron Spectroscopy for Chemical Analysis (ESCA)

Element	1K8A As Received Atom %	1K8A Post-Bake Atom %	1K8A Post-Flight Atom %
Si	0.97	17.22	-----
C	39.50	53.11	-----
O	40.46	25.62	-----
Al	16.68	0.00	-----
F	1.45	0.00	-----
S	0.94	0.00	-----
W	0.00	4.05	-----

1K9 SiO_x/NPB carbon foil on sapphire, Al holder

	As Received	Post-Bake	Post-Flight	Difference
Mass(g)	4.86856	4.86784	4.86851	0.00067

Electron Spectroscopy for Chemical Analysis (ESCA)

Element	1K9A As Received Atom %	1K9A Post-Bake Atom %	1K9A Post-Flight Atom %
Si	22.63	22.03	19.45
C	19.64	20.41	25.71
O	48.82	50.38	45.03
Al	3.65	3.39	2.93
F	4.27	2.79	2.97
N	0.00	0.00	1.12
Na	0.00	0.00	2.78

1L1 TiC-coated carbon/carbon

1L1A	As Received	Post-Bake	Post-Flight	Difference
Mass(g)	0.28591	0.28589	0.28450	-0.00005

1L1C	Pre-Ground	Post-Ground	Difference
Mass(g)	0.2859	0.2858	-0.0001

Electron Spectroscopy for Chemical Analysis (ESCA)

Element	1L1F As Received Atom %	1L1F Post-Bake Atom %	1L1A Post-Flight Atom %	1L1C Post-Ground Atom %
Si	0.00	0.00	13.29	0.00
C	51.99	51.72	19.31	10.10
O	24.28	30.18	55.58	45.21
Ti	17.68	13.75	9.66	13.22
F	6.05	4.36	0.00	18.40
N	0.00	0.00	2.16	0.78
Na	0.00	0.00	0.00	6.58
Cu	0.00	0.00	0.00	3.23
K	0.00	0.00	0.00	1.96
Zn	0.00	0.00	0.00	0.52

1L2 Glass fiber/Teflon composite

1L2A	As Received	Post-Bake	Post-Flight	Difference
Mass(g)	0.16428	0.16430	0.16416	-0.00014

1L2C	Pre-Ground	Post-Ground	Difference
Mass(g)	0.164398	0.164371	-0.000027

Electron Spectroscopy for Chemical Analysis (ESCA)

Element	1L2F As Received Atom %	1L2F Post-Bake Atom %	1L2A Post-Flight Atom %	1L2C Post-Ground Atom %
Si	0.00	0.00	2.03	0.00
C	31.76	32.28	30.35	31.77
O	0.00	0.00	4.02	2.57
F	68.24	67.72	63.60	64.00

5L3 Beta-alumina (.002") coated aluminum

5L3A	As Received	Post-Bake	Post-Flight	Difference
Mass(g)	0.53069	0.53053	0.53064	0.00011

5L3C	Pre-Ground	Post-Ground	Difference
Mass(g)	0.5372	0.5372	0.0000

Electron Spectroscopy for Chemical Analysis (ESCA)

Element	5L3D As Received Atom %	5L3D Post-Bake Atom %	5L3A Post-Flight Atom %	5L3C Post-Ground Atom %
Si	0.00	0.00	4.57	3.19
C	17.64	22.61	16.04	6.29
O	60.15	56.71	52.40	29.99
Al	17.65	16.53	14.01	10.75
Na	4.56	4.14	10.39	21.13
F	0.00	0.00	2.59	28.65

5L4 Silicon carbide ceramic

5L4A	As Received	Post-Bake	Post-Flight	Difference
Mass(g)	1.01769	1.01763	1.01760	-0.00003

5L4C	Pre-Ground	Post-Ground	Difference
Mass(g)	1.0046	1.0045	-0.0001

Electron Spectroscopy for Chemical Analysis (ESCA)

Element	5L4D As Received Atom %	5L4D Post-Bake Atom %	5L4A Post-Flight Atom %	5L4C Post-Ground Atom %
Si	28.63	29.59	30.48	24.40
C	47.71	45.87	12.79	8.08
O	21.88	23.10	54.82	45.14
Na	0.00	0.56	1.18	3.78
F	0.95	0.88	0.73	13.40
Ca	0.57	0.00	0.00	0.00
Zn	0.25	0.00	0.00	0.00
Cu	0.00	0.00	0.00	3.00
K	0.00	0.00	0.00	2.19

5L5 Carbon/carbon composite

5L5A	As Received	Post-Bake	Post-Flight	Difference
Mass(g)	0.51996	0.51908	0.52166	0.00258

5L5C	Pre-Ground	Post-Ground	Difference
Mass(g)	0.4873	0.4866	-0.0007

Electron Spectroscopy for Chemical Analysis (ESCA)

Element	5L5F As Received Atom %	5L5F Post-Bake Atom %	5L5A Post-Flight Atom %	5L5C Post-Ground Atom %
Si	0.00	0.00	2.55	0.00
C	83.98	85.61	80.10	73.19
O	14.46	13.38	15.19	15.62
Na	0.90	0.58	0.00	1.62
N	0.00	0.00	2.17	0.00
S,Cl	0.66	0.00	0.00	0.00
F	0.00	0.00	0.00	7.67
Cu	0.00	0.00	0.00	1.90

5L6 Calcium zirconate coated carbon/carbon

5L6A	As Received	Post-Bake	Post-Flight	Difference
Mass(g)	0.56149	0.56043	0.56310	0.00267

5L6C	Pre-Ground	Post-Ground	Difference
Mass(g)	0.5491	0.5488	-0.0003

Electron Spectroscopy for Chemical Analysis (ESCA)

Element	5L6D As Received Atom %	5L6D Post-Bake Atom %	5L6A Post-Flight Atom %	5L6C Post-Ground Atom %
Si	0.00	1.19	9.62	0.00
C	29.59	34.12	19.39	13.24
O	49.92	45.20	44.29	33.60
Ca	15.13	15.18	12.54	15.23
Zr	5.36	4.31	6.84	7.88
F	0.00	0.00	7.31	24.35
Cu	0.00	0.00	0.00	2.93
Na	0.00	0.00	0.00	2.77

5L7 Beta-alumina on carbon/carbon

5L7A	As Received	Post-Bake	Post-Flight	Difference
Mass(g)	0.56882	0.56766	0.57056	0.00290

5L7C	Pre-Ground	Post-Ground	Difference
Mass(g)	0.5687	0.5684	-0.0003

Electron Spectroscopy for Chemical Analysis (ESCA)

Element	5L7D As Received Atom %	5L7D Post-Bake Atom %	5L7A Post-Flight Atom %	5L7C Post-Ground Atom %
Si	0.00	0.00	6.51	0.00
C	16.33	22.24	12.01	6.66
O	60.32	55.73	52.53	29.66
Al	18.71	16.62	17.27	12.19
Na	4.64	5.41	7.91	22.72
F	0.00	0.00	3.76	28.51
Cu	0.00	0.00	0.00	0.26

5L8 Copper indium diselenide($CuInSe_2$)-photovoltaic

5L8A	As Received	Post-Bake	Post-Flight	Difference
Mass(g)	0.03965	0.03700	0.03683	-0.00017

5L8C	Pre-Ground	Post-Ground	Difference
Mass(g)	0.0357	0.0357	0.0000

Electron Spectroscopy for Chemical Analysis (ESCA)

Element	5L8D As Received Atom %	5L8D Post-Bake Atom %	5L8A Post-Flight Atom %	5L8C Post-Ground Atom %
Si	0.00	0.00	10.78	0.00
C	48.44	57.80	16.41	12.81
O	34.84	27.45	44.79	33.39
Zn	8.06	8.21	20.06	18.75
Cl	3.07	0.00	1.20	0.00
N	3.43	0.00	2.32	14.46
Ni	2.16	0.00	0.00	0.00
Se	0.00	3.30	0.00	0.00
In	0.00	1.90	0.00	1.39
Cd	0.00	1.34	0.00	0.00
F	0.00	0.00	4.44	13.15
Cu	0.00	0.00	0.00	6.05

5L9 Niobium beryllide, high temperature alloy

5L9A	As Received	Post-Bake	Post-Flight	Difference
Mass(g)	1.53320	1.53323	1.53324	0.00001

5L9C	Pre-Ground	Post-Ground	Difference
Mass(g)	1.5985	1.5985	0.0000

Electron Spectroscopy for Chemical Analysis (ESCA)

Element	5L9D As Received Atom %	5L9D Post-Bake Atom %	5L9A Post-Flight Atom %	5L9C Post-Ground Atom %
Si	0.00	0.00	12.64	0.00
C	37.63	53.34	20.76	21.36
O	45.56	33.92	55.17	49.53
Fe	7.85	5.51	4.04	7.72
Cu	4.76	3.34	2.66	11.42
Cl	1.51	0.00	0.00	0.00
Ar	0.79	0.00	0.00	0.00
F	1.90	0.00	0.00	9.97
S	0.00	3.89	0.00	0.00
N	0.00	0.00	2.86	0.00
Na	0.00	0.00	1.87	0.00

5L0 P75 graphite/magnesium vacuum cast composite

5L0A	As Received	Post-Bake	Post-Flight	Difference
Mass(g)	0.41955	0.41955	0.42006	0.00051

5L0C	Pre-Ground	Post-Ground	Difference
Mass(g)	0.3804	0.3804	0.0000

Electron Spectroscopy for Chemical Analysis (ESCA)

Element	5L0F As Received Atom %	5L0F Post-Bake Atom %	5L0A Post-Flight Atom %	5L0C Post-Ground Atom %
C	40.46	43.06	31.94	12.15
O	38.05	36.94	42.04	22.26
Mg	20.83	17.95	22.36	24.63
S	0.66	0.00	0.00	0.00
F	0.00	1.23	2.79	36.19
Ar	0.00	0.82	0.88	0.00
Cu	0.00	0.00	0.00	3.82
Na	0.00	0.00	0.00	0.95

5M1 CVD diamond on silicon

5M1B	Pre-Ground	Post-Ground	Difference
Mass(g)	0.5163	0.5160	-0.0003

Electron Spectroscopy for Chemical Analysis (ESCA)

Element	5M1C As Received Atom %	5M1C Post-Bake Atom %	5M1A Post-Flight Atom %	5M1B Post-Ground Atom %
Si	0.00	0.40	10.75	0.00
C	96.02	96.56	58.15	88.52
O	2.89	2.33	30.58	10.43
F	0.75	0.50	0.52	0.00
Cu	0.00	0.00	0.00	1.05
S,Na,Cl	0.35	0.21	0.00	0.00

5M2 $(SiC/SiO_2)(SiH/SiO_2)^5/Si$, MWIR-tuned reflector

5M2B	Pre-Ground	Post-Ground	Difference
Mass(g)	0.5269	0.5268	-0.0001

Electron Spectroscopy for Chemical Analysis (ESCA)

Element	5M2C As Received Atom %	5M2C Post-Bake Atom %	5M2A Post-Flight Atom %	5M2B Post-Ground Atom %
Si	37.18	33.18	32.05	23.67
C	38.24	44.12	10.97	11.39
O	24.59	22.70	56.98	49.29
F	0.00	0.00	0.00	7.36
Cu	0.00	0.00	0.00	5.05
Na	0.00	0.00	0.00	2.59
K	0.00	0.00	0.00	0.66

5M3 $(Si_3N_4/SiO_2)^6/Si$, MWIR-tuned reflector

5M3B	Pre-Ground	Post-Ground	Difference
Mass(g)	0.5039	0.5038	-0.0001

Electron Spectroscopy for Chemical Analysis (ESCA)

Element	5M3C As Received Atom %	5M3C Post-Bake Atom %	5M3A Post-Flight Atom %	5M3B Post-Ground Atom %
Si	35.23	31.38	31.81	21.34
C	13.20	23.08	7.87	10.65
O	16.58	15.21	54.30	42.72
N	34.99	29.37	6.03	6.32
F	0.00	0.96	0.00	9.15
Cu	0.00	0.00	0.00	4.22
Na	0.00	0.00	0.00	3.57
K	0.00	0.00	0.00	2.03

5M4 $(AlN/Al_2O_3)^6/Si$, visible-wavelength-tuned reflector

5M4B	Pre-Ground	Post-Ground	Difference
Mass(g)	0.5042	0.5042	0.0000

Electron Spectroscopy for Chemical Analysis (ESCA)

Element	5M4C As Received Atom %	5M4C Post-Bake Atom %	5M4A Post-Flight Atom %	5M4B Post-Ground Atom %
Si	1.59	0.00	10.59	0.00
C	28.85	40.12	16.56	16.17
O	26.84	24.79	47.32	26.52
N	14.64	11.76	3.35	3.39
Al	26.74	22.42	18.71	21.98
Cu	1.34	0.91	0.67	2.26
F	0.00	0.00	2.80	21.51
Na	0.00	0.00	0.00	5.97
K	0.00	0.00	0.00	2.20

5M5 $(Si/SiO_2)^5/Si$, MWIR-tuned reflector

5M5B	Pre-Ground	Post-Ground	Difference
Mass(g)	0.5288	0.5286	-0.0002

Electron Spectroscopy for Chemical Analysis (ESCA)

Element	5M5C As Received Atom %	5M5C Post-Bake Atom %	5M5A Post-Flight Atom %	5M5B Post-Ground Atom %
Si	53.73	44.12	34.04	21.71
C	11.27	24.51	6.53	9.42
O	33.80	29.72	59.43	42.80
Ar	1.20	1.66	0.00	0.00
F	0.00	0.00	0.00	15.35
Na	0.00	0.00	0.00	5.48
K	0.00	0.00	0.00	2.82
Cu	0.00	0.00	0.00	2.43

5M6 $(SiH/SiO_2)^5/Si$, MWIR-tuned reflector

5M6B	Pre-Ground	Post-Ground	Difference
Mass(g)	0.5054	0.5051	-0.0003

Electron Spectroscopy for Chemical Analysis (ESCA)

Element	5M6C As Received Atom %	5M6C Post-Bake Atom %	5M6A Post-Flight Atom %	5M6B Post-Ground Atom %
Si	46.83	41.79	33.62	22.11
C	16.90	26.63	8.82	8.98
O	34.65	30.06	57.11	41.96
Ar	1.63	1.52	0.00	0.00
Na	0.00	0.00	0.45	6.86
F	0.00	0.00	0.00	15.29
K	0.00	0.00	0.00	2.99
Cu	0.00	0.00	0.00	1.81

5M7 $(BN/SiO_2)(SiH/SiO_2)^5/Si$, MWIR-tuned reflector

5M7B	Pre-Ground	Post-Ground	Difference
Mass(g)	0.5173	0.5170	-0.0003

Electron Spectroscopy for Chemical Analysis (ESCA)

Element	5M7C As Received Atom %	5M7C Post-Bake Atom %	5M7A Post-Flight Atom %	5M7B Post-Ground Atom %
Si	0.56	0.43	10.59	1.71
C	22.69	32.16	14.70	11.49
O	15.10	13.87	36.39	30.38
B	44.58	37.77	27.80	31.64
N	15.92	13.62	9.56	9.66
Ar	0.93	0.90	0.00	0.00
F	0.00	0.93	0.96	6.60
S	0.22	0.33	0.00	0.00
Cu	0.00	0.00	0.00	5.21
Na	0.00	0.00	0.00	2.05
K	0.00	0.00	0.00	1.27

5M8 Unprotected aluminum on silicon, broadband reflector

5M8B	Pre-Ground	Post-Ground	Difference
Mass(g)	0.5168	0.5166	-0.0002

Electron Spectroscopy for Chemical Analysis (ESCA)

Element	5M8C As Received Atom %	5M8C Post-Bake Atom %	5M8A Post-Flight Atom %	5M8B Post-Ground Atom %
Si	3.02	2.75	9.68	0.00
C	24.68	36.00	16.20	7.94
O	42.61	35.63	48.91	28.89
Al	29.54	25.45	21.28	26.95
N	0.00	0.00	1.00	0.00
F	0.00	0.00	2.92	25.29
Cu	0.15	0.16	0.00	2.17
Na	0.00	0.00	0.00	5.18
K	0.00	0.00	0.00	3.59

1M9 CVD Diamond brazed to a ZnS window

1M9B	Pre-Ground	Post-Ground	Difference
Mass(g)	6.7174	6.7171	-0.0003

Electron Spectroscopy for Chemical Analysis (ESCA)

Element	1M9C As Received Atom %	1M9C Post-Bake Atom %	1M9A Post-Flight Atom %	1M9B Post-Ground Atom %
Si	3.02	3.29	13.90	0.00
C	85.06	84.62	48.99	89.01
O	10.68	11.08	37.11	10.34
F	1.24	1.01	0.00	0.65

1M10 $(SiC/SiO_2)^6/Si$, MWIR-tuned reflector

1M10B	Pre-Ground	Post-Ground	Difference
Mass(g)	3.6576	3.6574	-0.0002

Electron Spectroscopy for Chemical Analysis (ESCA)

Element	1M10C As Received Atom %	1M10C Post-Bake Atom %	1M10A Post-Flight Atom %	1M10B Post-Ground Atom %
Si	40.68	32.60	30.79	16.30
C	45.86	52.12	9.93	9.32
O	13.46	13.59	59.28	53.02
F	0.00	1.69	0.00	11.74
Cu	0.00	0.00	0.00	4.38
Na	0.00	0.00	0.00	3.44
K	0.00	0.00	0.00	1.79

1M11 $(Si_3N_4/Al_2O_3)^6$/Ag/fused silica, beam splitter

1M11B	Pre-Ground	Post-Ground	Difference
Mass(g)	1.7599	1.7598	-0.0001

Electron Spectroscopy for Chemical Analysis (ESCA)

Element	1M11C As Received Atom %	1M11C Post-Bake Atom %	1M11A Post-Flight Atom %	1M11B Post-Ground Atom %
Si	34.51	34.05	31.42	21.29
C	13.72	13.92	7.71	5.70
O	23.14	22.59	55.16	38.66
N	28.64	29.44	5.70	4.72
F	0.00	0.00	0.00	17.52
Na	0.00	0.00	0.00	6.96
K	0.00	0.00	0.00	3.61
Cu	0.00	0.00	0.00	1.54

1M12 Al_2O_3/Al half-coated on β-SiC

1M12B	Pre-Ground	Post-Ground	Difference
Mass(g)	5.0762	5.0760	-0.0002

Electron Spectroscopy for Chemical Analysis (ESCA)

(coated side)

Element	1M12C As Received Atom %	1M12C Post-Bake Atom %	1M12A Post-Flight Atom %	1M12B Post-Ground Atom %
Si	2.18	4.46	10.36	0.00
C	28.36	29.37	16.01	9.43
O	42.27	41.14	50.35	34.63
Al	27.19	25.03	18.35	23.15
N	0.00	0.00	1.73	0.00
F	0.00	0.00	3.21	22.84
Cu	0.00	0.00	0.00	6.38
Na	0.00	0.00	0.00	2.12
K	0.00	0.00	0.00	1.45

(uncoated side)

Element	As Received Atom %	Post-Bake Atom %	Post-Flight Atom %	Post-Ground Atom %
Si	36.26	36.88	32.55	24.46
C	36.86	36.30	10.62	9.04
O	26.88	26.81	56.83	46.75
F	0.00	0.00	0.00	10.49
Cu	0.00	0.00	0.00	4.37
Na	0.00	0.00	0.00	3.22
K	0.00	0.00	0.00	1.68

1M13 Uncoated HIP I-70 beryllium, broadband reflector

1M13B	Pre-Ground	Post-Ground	Difference
Mass(g)	5.7974	5.7974	0.0000

Electron Spectroscopy for Chemical Analysis (ESCA)

Element	1M13C As Received Atom %	1M13C Post-Bake Atom %	1M13A Post-Flight Atom %	1M13B Post-Ground Atom %
Be	39.10	29.19	28.59	27.49
Si	0.00	2.70	7.45	1.29
C	28.15	36.31	15.05	7.89
O	32.75	30.09	44.32	30.80
Al	0.00	1.01	0.00	0.00
Na	0.00	0.69	0.00	2.62
N	0.00	0.00	1.43	0.00
F	0.00	0.00	3.15	24.52
Cu	0.00	0.00	0.00	3.59
K	0.00	0.00	0.00	1.79

1M14 $(Si_3N_4/Al_2O_3)^2/Al/Si$, MWIR-tuned reflector

1M14B	Pre-Ground	Post-Ground	Difference
Mass(g)	3.6782	3.6786	0.0004

Electron Spectroscopy for Chemical Analysis (ESCA)

Element	1M14C As Received Atom %	1M14C Post-Bake Atom %	1M14A Post-Flight Atom %	1M14B Post-Ground Atom %
Si	36.52	33.04	32.22	20.00
C	12.65	19.83	7.13	9.39
O	21.82	21.30	54.57	36.96
N	29.01	25.82	6.08	4.55
F	0.00	0.00	0.00	18.04
Na	0.00	0.00	0.00	5.08
K	0.00	0.00	0.00	3.99
Cu	0.00	0.00	0.00	1.98

1M15 AlN/SiH/CVD diamond/ZnS

1M15B	Pre-Ground	Post-Ground	Difference
Mass(g)	6.7942	6.7935	-0.0007

Electron Spectroscopy for Chemical Analysis (ESCA)

Element	1M15C As Received Atom %	1M15C Post-Bake Atom %	1M15A Post-Flight Atom %	1M15B Post-Ground Atom %
Al	26.94	22.87	22.27	29.98
Si	0.00	0.00	7.18	0.00
C	20.78	30.94	15.12	8.30
O	38.25	31.84	45.02	29.15
N	11.86	10.16	7.14	8.40
S	2.17	1.82	0.00	0.00
F	0.00	0.00	3.27	18.18
B	0.00	2.38	0.00	0.00
Cu	0.00	0.00	0.00	2.56
Na	0.00	0.00	0.00	2.05
K	0.00	0.00	0.00	1.37

1M16 $(Si/SiO_2)^4/Al/Si$, MWIR-tuned reflector

1M16B	Pre-Ground	Post-Ground	Difference
Mass(g)	3.6486	3.6485	-0.0001

Electron Spectroscopy for Chemical Analysis (ESCA)

Element	1M16C As Received Atom %	1M16C Post-Bake Atom %	1M16A Post-Flight Atom %	1M16B Post-Ground Atom %
Si	43.72	40.96	34.14	21.48
C	17.54	22.89	6.89	14.86
O	38.74	35.00	57.75	44.28
N	0.00	0.00	1.23	0.00
F	0.00	1.15	0.00	10.26
Cu	0.00	0.00	0.00	5.53
Na	0.00	0.00	0.00	2.15
K	0.00	0.00	0.00	1.45

5N1 Beryllium, diamond turned, on beryllium

5N1A	As Received	Post-Bake	Post-Flight	Difference
Mass(g)	0.59574	0.59567	0.59565	-0.00002

5N1C	Pre-Ground	Post-Ground	Difference
Mass(g)	0.5887	0.5886	-0.0001

Electron Spectroscopy for Chemical Analysis (ESCA)

Element	5N1F As Received Atom %	5N1F Post-Bake Atom %	5N1A Post-Flight Atom %	5N1C Post-Ground Atom %
Si	8.94	6.38	10.35	6.97
C	51.55	48.19	41.82	8.79
O	19.57	20.35	28.59	38.13
Be	19.94	24.68	18.47	26.72
F	0.00	0.00	0.77	13.47
Cl	0.00	0.40	0.00	0.00
Cu	0.00	0.00	0.00	2.18
Na	0.00	0.00	0.00	1.65
S	0.00	0.00	0.00	1.00
K	0.00	0.00	0.00	0.71
Ca	0.00	0.00	0.00	0.38

5N2 Beryllium, conventional polished, on beryllium

5N2A	As Received	Post-Bake	Post-Flight	Difference
Mass(g)	0.57233	0.57226	0.57238	0.00012

5N2C	Pre-Ground	Post-Ground	Difference
Mass(g)	0.5804	0.5804	0.0000

Electron Spectroscopy for Chemical Analysis (ESCA)

Element	5N2F As Received Atom %	5N2F Post-Bake Atom %	5N2A Post-Flight Atom %	5N2C Post-Ground Atom %
Si	2.52	6.62	11.93	5.61
C	29.73	40.43	32.68	14.12
O	26.45	22.85	31.32	32.69
Be	41.29	30.10	22.54	28.93
F	0.00	0.00	1.54	13.73
Cu	0.00	0.00	0.00	1.88
S	0.00	0.00	0.00	1.59
Na	0.00	0.00	0.00	0.89
K	0.00	0.00	0.00	0.56

5N3 Beryllium/silicon/silicon-carbide substrate

5N3A	As Received	Post-Bake	Post-Flight	Difference
Mass(g)	1.11414	1.11420	1.11418	-0.00002

5N3C	Pre-Ground	Post-Ground	Difference
Mass(g)	1.1160	1.1162	0.0002

Electron Spectroscopy for Chemical Analysis (ESCA)

Element	5N3F As Received Atom %	5N3F Post-Bake Atom %	5N3A Post-Flight Atom %	5N3C Post-Ground Atom %
Si	2.25	2.02	6.58	1.93
C	24.31	28.12	15.58	9.81
O	29.06	27.59	41.13	30.25
Be	44.38	42.27	33.84	34.99
F	0.00	0.00	2.33	17.87
N	0.00	0.00	0.53	0.73
K	0.00	0.00	0.00	1.53
Cu	0.00	0.00	0.00	1.18
Na	0.00	0.00	0.00	0.88
S	0.00	0.00	0.00	0.83

1N4 Beryllium (black-etched) on beryllium foam

1N4A	As Received	Post-Bake	Post-Flight	Difference
Mass(g)	2.17168	2.17149	2.17093	-0.00056

1N4D	Pre-Ground	Post-Ground	Difference
Mass(g)	0.7241	0.7234	-0.0007

Electron Spectroscopy for Chemical Analysis (ESCA)

Element	1N4F As Received Atom %	1N4F Post-Bake Atom %	1N4A Post-Flight Atom %	1N4D Post-Ground Atom %
Si	0.00	0.00	2.88	0.00
C	11.86	16.61	8.77	5.95
O	40.38	36.81	42.24	34.24
Be	30.17	31.59	35.01	38.40
F	13.62	14.99	11.10	20.34
B	3.98	0.00	0.00	0.00
S	0.00	0.00	0.00	0.66
Cu	0.00	0.00	0.00	0.41

1N5 Boron (plasma sprayed) on beryllium

1N5A	As Received	Post-Bake	Post-Flight	Difference
Mass(g)	0.49497	0.49467	1.55320	1.05853

1N5C	Pre-Ground	Post-Ground	Difference
Mass(g)	0.4862	0.4862	0.0000

Electron Spectroscopy for Chemical Analysis (ESCA)

Element	1N5F As Received Atom %	1N5F Post-Bake Atom %	1N5A Post-Flight Atom %	1N5C Post-Ground Atom %
Si	3.58	3.67	8.16	6.37
C	28.69	30.75	13.14	9.91
O	31.51	30.08	39.43	38.67
B	34.38	35.50	36.98	37.97
N	1.73	0.00	1.38	0.00
Ca	0.00	0.00	0.90	0.76
W	0.11	0.00	0.00	0.00
F	0.00	0.00	0.00	5.66
Cu	0.00	0.00	0.00	0.66

1N6 Martin Black on aluminum

1N6A	As Received	Post-Bake	Post-Flight	Difference
Mass(g)	4.14826	4.14793	4.14794	0.00001

1N6C	Pre-Ground	Post-Ground	Difference
Mass(g)	4.1493	4.1490	-0.0003

Electron Spectroscopy for Chemical Analysis (ESCA)

Element	1N6F As Received Atom %	1N6F Post-Bake Atom %	1N6A Post-Flight Atom %	1N6C Post-Ground Atom %
Si	0.00	0.00	4.41	0.00
C	43.30	48.09	16.01	11.71
O	33.45	32.27	53.73	46.95
Al	10.30	12.04	19.24	23.18
B	4.03	0.00	0.00	0.00
N	4.69	4.62	1.65	1.12
F	1.43	0.00	1.70	13.17
S	2.81	2.98	3.26	2.76
Cu	0.00	0.00	0.00	1.12

501 P-100 graphite fiber/MR 56-2 (bismaleimide)

501A	As Received	Post-Bake	Post-Flight	Difference
Mass(g)	0.41494	0.41460	0.41480-95	0.00020-35

501C	Pre-Ground	Post-Ground	Difference
Mass(g)	0.4122	0.4119	-0.0003

Electron Spectroscopy for Chemical Analysis (ESCA)

Element	501F As Received Atom %	501F Post-Bake Atom %	501A Post-Flight Atom %	501C Post-Ground Atom %
Si	0.00	0.00	2.40	1.35
C	84.80	84.54	75.77	54.69
O	10.28	11.48	18.32	22.61
Na	2.36	1.97	3.09	9.52
N	1.97	2.01	0.00	0.00
P	0.59	0.00	0.41	0.97
F	0.00	0.00	0.00	7.78
S	0.00	0.00	0.00	1.81
Cu	0.00	0.00	0.00	1.26

5P1 Two coatings on Vit-C/SiC substrate

5P1A	As Received	Post-Bake	Post-Flight	Difference
Mass(g)	0.76622	0.76622	0.76617	-0.00005

5P1C	Pre-Ground	Post-Ground	Difference
Mass(g)	0.7636	0.7634	-0.0002

Electron Spectroscopy for Chemical Analysis (ESCA)

Si/Al_2O_3 (light blue circle)

Element	5P1E As Received Atom %	5P1E Post-Bake Atom %	5P1A Post-Flight Atom %	5P1C Post-Ground Atom %
Si	----	12.10	18.42	9.15
C	----	39.34	14.92	7.69
O	----	36.43	52.15	34.52
Al	----	8.65	9.12	26.73
N	----	1.37	3.55	0.91
F	----	2.10	1.84	15.85
Cu	----	0.00	0.00	4.33
Na	----	0.00	0.00	0.82

Si/Al_2O_3/enhanced MLD (lower, dark blue circle)

Element	As Received Atom %	Post-Bake Atom %	Post-Flight Atom %	Post-Ground Atom %
Si	46.02	41.56	33.74	25.20
C	10.99	22.42	8.07	8.32
O	38.42	34.68	57.29	51.68
F	4.57	1.34	0.90	6.07
Cu	0.00	0.00	0.00	7.39
Na	0.00	0.00	0.00	1.33

1P2 Tungsten/graphite cloth/carbon foam

1P2A	As Received	Post-Bake	Post-Flight	Difference
Mass(g)	1.45018	1.44792	1.45178	-0.00014

1P2C	Pre-Ground	Post-Ground	Difference
Mass(g)	0.8703	0.8696	-0.0007

Electron Spectroscopy for Chemical Analysis (ESCA)

Element	1P2F As Received Atom %	1P2F Post-Bake Atom %	1P2A Post-Flight Atom %	1P2C Post-Ground Atom %
Si	11.74	17.13	23.87	0.00
C	46.14	48.86	21.46	17.00
O	28.26	26.55	48.87	54.34
W	8.17	7.45	5.80	18.51
N	5.68	0.00	0.00	0.00
F	0.00	0.00	0.00	4.69
Cu	0.00	0.00		

5P3 CVD TiC/graphite cloth/carbon foam

5P3A	As Received	Post-Bake	Post-Flight	Difference
Mass(g)	0.16636	0.16636	0.16581	-0.00055

5P3C	Pre-Ground	Post-Ground	Difference
Mass(g)	0.1673	0.1658	-0.0015

Electron Spectroscopy for Chemical Analysis (ESCA)

Element	5P3F As Received Atom %	5P3F Post-Bake Atom %	5P3A Post-Flight Atom %	5P3C Post-Ground Atom %
Si	0.00	0.00	13.25	0.00
C	44.81	48.69	16.72	18.41
O	32.71	32.39	58.40	45.07
Ti	19.04	16.52	9.04	11.45
N	3.44	2.40	2.59	0.00
F	0.00	0.00	0.00	13.45
K	0.00	0.00	0.00	4.84
B	0.00	0.00	0.00	3.42
Cu	0.00	0.00	0.00	3.36

5P4 Alumina on aluminum substrate

5P4A	As Received	Post-Bake	Post-Flight	Difference
Mass(g)	1.01047	1.01039	1.01041	0.00002

5P4C	Pre-Ground	Post-Ground	Difference
Mass(g)	1.0022	1.0021	-0.0001

Electron Spectroscopy for Chemical Analysis (ESCA)

Element	5P4F As Received Atom %	5P4F Post-Bake Atom %	5P4A Post-Flight Atom %	5P4C Post-Ground Atom %
Si	0.00	0.00	10.67	0.00
C	30.74	39.12	16.17	12.31
O	41.70	37.11	48.75	31.04
Al	26.09	23.77	19.96	26.32
F	1.47	0.00	3.01	21.48
N	0.00	0.00	1.44	0.00
Na	0.00	0.00	0.00	4.31
Cu	0.00	0.00	0.00	2.54
K	0.00	0.00	0.00	1.99

1P5 Solar cell

	As Received	Post-Bake	Post-Flight	Difference
Mass(g)	3.33187	3.33168	3.33150	-0.00018

Electron Spectroscopy for Chemical Analysis (ESCA)

Element	1P5A As Received Atom %	1P5A Post-Bake Atom %	1P5A Post-Flight Atom %
Si	19.71	11.82	20.57
C	44.47	36.57	11.55
O	30.73	40.48	52.79
Al	5.10	9.86	10.66
F	0.00	0.00	2.43
N	0.00	1.26	1.99

5P6 Al_2O_3/graphite composite

5P6A	As Received	Post-Bake	Post-Flight	Difference
Mass(g)	0.45261	0.45238	-------	-------

5P6C	Pre-Ground	Post-Ground	Difference
Mass(g)	0.4608	0.4601	-0.0007

Electron Spectroscopy for Chemical Analysis (ESCA)

Uncoated (Black area)

Element	5P6F As Received Atom %	5P6F Post-Bake Atom %	5P6A Post-Flight Atom %	5P6C Post-Ground Atom %
Si	3.89	4.74	8.67	4.79
C	66.72	65.22	52.39	56.84
O	24.15	23.88	32.21	28.84
F	1.06	1.05	0.00	2.14
N	2.14	1.76	2.61	2.42
S	2.05	2.16	4.12	2.82
Cl	0.00	0.59	0.00	0.00
Na	0.00	0.59	0.00	0.91
Cu	0.00	0.00	0.00	1.14

Al_2O_3 coating (white area)

Element	As Received Atom %	Post-Bake Atom %	Post-Flight Atom %	Post-Ground Atom %
Si	15.34	14.40	20.14	0.00
C	28.08	27.62	4.98	11.37
O	39.40	40.37	54.96	33.46
Al	17.18	17.61	17.52	33.61
F	0.00	0.00	0.95	14.55
Na	0.00	0.00	1.45	1.17
Cu	0.00	0.00	0.00	5.20

5P7 Germanium/Kapton

5P7A	As Received	Post-Bake	Post-Flight	Difference
Mass(g)	0.86534	0.86520	0.86529	0.00009

5P7C	Pre-Ground	Post-Ground	Difference
Mass(g)	0.8653	0.8650	-0.0003

Electron Spectroscopy for Chemical Analysis (ESCA)

Element	5P7F As Received Atom %	5P7F Post-Bake Atom %	5P7A Post-Flight Atom %	5P7C Post-Ground Atom %
Si	0.00	0.00	11.26	4.48
C	33.07	38.48	11.63	7.50
O	32.16	34.11	54.16	44.80
Ge	29.95	27.41	22.96	23.77
F	3.03	0.00	0.00	11.06
Na	1.79	0.00	0.00	5.14
K	0.00	0.00	0.00	3.25

5P8 Indium tin oxide/Teflon/VDA/Kapton

5P8A	As Received	Post-Bake	Post-Flight	Difference
Mass(g)	0.87846	0.87829	0.87841	0.00012

5P8C	Pre-Ground	Post-Ground	Difference
Mass(g)	0.8749	0.8747	-0.0002

Electron Spectroscopy for Chemical Analysis (ESCA)

(Central Spot)

Element	58PF As Received Atom %	5P8F Post-Bake Atom %	5P8A Post-Flight Atom %	5P8C Post-Ground Atom %
Si	7.42	9.07	6.73	2.56
C	70.49	65.93	63.44	31.38
O	21.81	23.46	29.11	36.58
In	0.28	0.51	0.28	10.19
F	0.00	1.04	0.00	14.82
Sn	0.00	0.00	0.44	0.96
Cu	0.00	0.00	0.00	2.19
S	0.00	0.00	0.00	1.33

(Away from central spot)

Element	As Received Atom %	Post-Bake Atom %	Post-Flight Atom %	Post-Ground Atom %
Si	0.00	0.00	11.31	0.00
C	45.29	48.95	16.50	15.44
O	30.86	25.78	52.88	36.06
In	14.14	11.96	18.04	20.69
F	8.77	12.54	0.00	22.45
Sn	0.94	0.77	1.26	1.68
Cu	0.00	0.00	0.00	3.68

5P9 Microsheet/Ag/Y966/Al

5P9A	As Received	Post-Bake	Post-Flight	Difference
Mass(g)	0.86892	0.86884	0.86898	0.00014

5P9C	Pre-Ground	Post-Ground	Difference
Mass(g)	0.8697	0.8694	-0.0003

Electron Spectroscopy for Chemical Analysis (ESCA)

Element	5P9F As Received Atom %	5P9F Post-Bake Atom %	5P9A Post-Flight Atom %	5P9C Post-Ground Atom %
Si	22.04	24.77	27.65	25.76
C	23.26	17.42	12.39	3.77
O	49.68	53.84	58.16	60.83
N	0.00	0.00	1.15	0.00
Na	1.16	1.65	0.66	1.37
Ag	0.07	0.70	0.00	0.00
Zn	0.70	0.92	0.00	0.00
K	1.39	0.99	0.00	1.80
Al	1.44	0.00	0.00	0.00
Ti	0.26	0.00	0.00	0.00
F	0.00	0.00	0.00	5.23
Cu	0.00	0.00	0.00	1.23

5P0 (Si/SiO_2)/(TiO_2/SiO_2)/Kapton

5P0A	As Received	Post-Bake	Post-Flight	Difference
Mass(g)	0.87000	0.86991	0.86999	0.00008

5P0C	Pre-Ground	Post-Ground	Difference
Mass(g)	0.8708	0.8706	-0.0002

Electron Spectroscopy for Chemical Analysis (ESCA)

Element	5P0F As Received Atom %	5P0F Post-Bake Atom %	5P0A Post-Flight Atom %	5P0C Post-Ground Atom %
Si	3.30	4.35	12.13	0.00
C	41.56	47.37	17.86	17.12
O	38.59	37.60	57.90	51.39
Ti	11.09	8.72	9.74	11.24
N	2.09	1.96	2.36	0.00
F	3.37	0.00	0.00	12.42
Cu	0.00	0.00	0.00	6.63
K	0.00	0.00	0.00	1.20

5Q1 Aluminum, textured

5Q1A	As Received	Post-Bake	Post-Flight	Difference
Mass(g)	0.26172	0.26179	0.26179	0.00000

5Q1C	Pre-Ground	Post-Ground	Difference
Mass(g)	0.2618	0.2616	-0.0002

Electron Spectroscopy for Chemical Analysis (ESCA)

Element	5Q1D As Received Atom %	5Q1D Post-Bake Atom %	5Q1A Post-Flight Atom %	5Q1C Post-Ground Atom %
Si	0.00	0.00	5.07	0.00
C	19.64	22.99	13.06	6.71
O	44.56	42.42	51.85	44.65
Al	30.68	29.81	25.45	30.60
F	5.13	4.78	3.38	13.60
N	0.00	0.00	1.19	0.00
Cu	0.00	0.00	0.00	4.43

5Q2 Aluminum, textured

5Q2A	As Received	Post-Bake	Post-Flight	Difference
Mass(g)	0.26475	0.26468	0.26465-8	-0.00003-0

5Q2C	Pre-Ground	Post-Ground	Difference
Mass(g)	0.2612	0.2612	0.0000

Electron Spectroscopy for Chemical Analysis (ESCA)

Element	5Q2D As Received Atom %	5Q2D Post-Bake Atom %	5Q2A Post-Flight Atom %	5Q2C Post-Ground Atom %
Si	0.00	0.00	5.28	0.00
C	20.40	22.76	12.20	8.79
O	44.32	42.80	53.15	42.76
Al	29.97	29.62	25.91	28.04
F	5.31	4.82	3.45	14.08
Cu	0.00	0.00	0.00	4.73
Na	0.00	0.00	0.00	0.86
K	0.00	0.00	0.00	0.75

5Q3 Beryllium, textured, 100 μm, on aluminum

5Q3A	As Received	Post-Bake	Post-Flight	Difference
Mass(g)	0.30155	0.30150	0.30147	-0.00003

5Q3C	Pre-Ground	Post-Ground	Difference
Mass(g)	0.2992	0.2990	-0.0002

Electron Spectroscopy for Chemical Analysis (ESCA)

Element	5Q3D As Received Atom %	5Q3D Post-Bake Atom %	5Q3A Post-Flight Atom %	5Q3C Post-Ground Atom %
Si	0.00	0.00	3.23	0.00
C	9.40	15.53	7.69	12.53
O	40.07	34.50	41.57	32.95
Be	48.36	47.77	44.65	38.31
F	1.71	1.66	2.86	14.05
Ar	0.46	0.46	0.00	0.00
S	0.00	0.00	0.00	1.31
Na	0.00	0.00	0.00	0.51
Cu	0.00	0.00	0.00	0.33

5Q4 Beryllium, textured, 100 μm, on aluminum

5Q4A	As Received	Post-Bake	Post-Flight	Difference
Mass(g)	0.29927	0.29935	0.29927	-0.00008

5Q4C	Pre-Ground	Post-Ground	Difference
Mass(g)	0.3046	0.3044	-0.0002

Electron Spectroscopy for Chemical Analysis (ESCA)

Element	5Q4D As Received Atom %	5Q4D Post-Bake Atom %	5Q4A Post-Flight Atom %	5Q4C Post-Ground Atom %
Si	0.00	0.00	3.98	0.00
C	10.24	16.40	9.96	8.34
O	38.42	32.87	41.81	30.47
Be	49.31	49.03	40.67	44.80
F	1.54	1.37	2.84	13.87
N	0.00	0.00	0.74	0.00
Ar	0.49	0.33	0.00	0.00
S	0.00	0.00	0.00	1.11
Cu	0.00	0.00	0.00	0.49
Na	0.00	0.00	0.00	0.47
K	0.00	0.00	0.00	0.46

5Q5 Beryllium, black-etched, on beryllium

	As Received	Post-Bake	Post-Flight	Difference
Mass(g)	0.38214	0.38204	0.38213	0.00009

Electron Spectroscopy for Chemical Analysis (ESCA)

Element	5Q5D As Received Atom %	5Q5D Post-Bake Atom %	5Q5A Post-Flight Atom %
Si	0.00	0.00	2.60
C	18.86	19.77	9.75
O	34.76	34.31	42.19
Be	31.70	31.81	32.27
F	14.68	14.11	12.39
N	0.00	0.00	0.81

5Q6 Beryllium, black-etched, on beryllium

5Q6A	As Received	Post-Bake	Post-Flight	Difference
Mass(g)	0.34820	0.34824	0.34828	0.00004

5Q6B	Pre-Ground	Post-Ground	Difference
Mass(g)	0.3813	0.3812	-0.0002

Electron Spectroscopy for Chemical Analysis (ESCA)

Element	5Q5D As Received Atom %	5Q5D Post-Bake Atom %	5Q6A Post-Flight Atom %	5Q6B Post-Ground Atom %
Si	0.00	0.00	3.09	0.00
C	18.86	19.77	10.18	5.25
O	34.76	34.31	41.68	36.09
Be	31.70	31.81	32.34	36.86
F	14.68	14.11	12.12	19.93
N	0.00	0.00	0.60	0.00
S	0.00	0.00	0.00	1.02
Cu	0.00	0.00	0.00	0.84

5Q7 CVD B_4C on POCO graphite

5Q7A	As Received	Post-Bake	Post-Flight	Difference
Mass(g)	1.17709	1.17721	1.17718	-0.00003

5Q7B	Pre-Ground	Post-Ground	Difference
Mass(g)	1.1315	1.1315	0.0000

Electron Spectroscopy for Chemical Analysis (ESCA)

Element	5Q8B As Received Atom %	5Q8B Post-Bake Atom %	5Q7A Post-Flight Atom %	5Q7B Post-Ground Atom %
Si	3.58	2.63	4.44	4.60
C	31.86	32.35	19.62	15.33
O	11.36	10.66	18.83	30.01
B	50.95	54.06	54.86	40.11
N	1.75	0.00	0.00	0.00
S	0.50	0.30	0.00	1.34
F	0.00	0.00	1.27	3.13
Na	0.00	0.00	0.97	2.14
Cu	0.00	0.00	0.00	2.06
K	0.00	0.00	0.00	1.29

5Q8 CVD B_4C on POCO graphite

	As Received	Post-Bake	Post-Flight	Difference
Mass(g)	1.21724	1.21726	1.21735	0.00009

Electron Spectroscopy for Chemical Analysis (ESCA)

Element	5Q8B As Received Atom %	5Q8B Post-Bake Atom %	5Q8A Post-Flight Atom %
Si	3.58	2.63	3.45
C	31.86	32.35	36.29
O	11.36	10.66	27.71
B	50.95	54.06	16.72
N	1.75	0.00	7.49
S	0.50	0.30	0.00
Na	0.00	0.00	5.46
K	0.00	0.00	1.98
Ca	0.00	0.00	0.90

5Q9 Magnesium oxide on beryllium

5Q9A	As Received	Post-Bake	Post-Flight	Difference
Mass(g)	0.23987	0.23983	0.23984	0.00001

5Q9C	Pre-Ground	Post-Ground	Difference
Mass(g)	0.2429	0.2428	-0.0001

Electron Spectroscopy for Chemical Analysis (ESCA)

Element	5Q9D As Received Atom %	5Q9D Post-Bake Atom %	5Q9A Post-Flight Atom %	5Q9C Post-Ground Atom %
Si	6.72	5.98	6.70	7.15
C	26.49	35.04	16.94	11.44
O	39.00	34.79	43.12	31.07
Mg	24.51	21.95	26.94	28.52
Cl	1.77	1.15	0.00	0.00
Ar	1.51	1.10	0.00	0.00
F	0.00	0.00	6.31	21.82

5Q0 Magnesium oxide on beryllium

5Q0A	As Received	Post-Bake	Post-Flight	Difference
Mass(g)	0.23994	0.23996	0.23998	0.00002

5Q0C	Pre-Ground	Post-Ground	Difference
Mass(g)	0.2376	0.2376	0.0000

Electron Spectroscopy for Chemical Analysis (ESCA)

Element	5Q0D As Received Atom %	5Q0D Post-Bake Atom %	5Q0A Post-Flight Atom %	5Q0C Post-Ground Atom %
Si	2.79	3.84	5.50	2.03
C	26.34	34.55	18.63	12.25
O	41.86	35.20	42.97	27.90
Mg	26.23	25.03	27.28	29.07
Cl	1.51	0.00	0.00	0.00
Ar	1.28	1.37	0.00	0.00
F	0.00	0.00	5.61	27.62
S	0.00	0.00	0.00	1.13

Kapton HN

A	As Received	Post-Bake	Post-Flight	Difference
Mass(g)	0.03413	0.03412	0.03112	-0.00300

C	Pre-Ground	Post-Ground	Difference
Mass(g)	0.033665	0.028385	-0.005280

Electron Spectroscopy for Chemical Analysis (ESCA)

Element	F As Received Atom %	F Post-Bake Atom %	A Post-Flight Atom %	C Post-Ground Atom %
Si	0.00	1.37	2.73	0.00
C	77.30	76.90	63.53	56.08
O	16.24	15.75	25.04	27.60
N	6.46	5.99	6.72	5.72
Na	0.00	0.00	1.98	2.99
F	0.00	0.00	0.00	5.99
Cu	0.00	0.00	0.00	1.18
S	0.00	0.00	0.00	0.45

MgF_2 on aluminum mirror, glass substrate

	As Received	Post-Bake	Post-Flight	Difference
Mass(g)	6.53705	6.53700	-------	-------

Electron Spectroscopy for Chemical Analysis (ESCA)

Element	A As Received Atom %	A Post-Bake Atom %	A Post-Flight Atom %
C	38.70	51.50	-----
O	29.99	25.43	-----
Mg	11.18	7.54	-----
Al	12.20	11.27	-----
F	6.20	4.26	-----
P	1.73	0.00	-----

APPENDIX G

PROPOSED FORMAT FOR M/VISION ATOMIC OXYGEN DATABASE

SEE DATABASE

The SEE Program co-investigators are providing AO interaction results from the flight and ground-based elements of their experiments. These results will be reviewed for completeness and installed in the SEE AO database. Once installed, the BMDO SEE Program's data will be available to NASA, DOD, universities, and industry through an on-line database.

Providing quality AO data for design work is the goal of the database task. Data will be collected from controlled, documented SEE experiments and evaluated by technical experts for inclusion in the database. The database will contain sufficient supporting information to identify the AO source, the exposure environment and conditions, material processing history, and other information deemed necessary to characterize the experiment.

The database will contain all AO data generated by the ground-based and flight experiments. Science and engineering data produced directly by or derived from the experiments will be carefully screened for installation in the database. Pedigree information about each material and component of the experiments is documented and will be included in the database. A well documented pedigree ensures that users can select data applicable to their particular design or analysis problem and be confident that they are suitable for their circumstances. Database entities also contain information on the statistical basis or confidence status of the included engineering data. Users can use this information and confidently apply appropriate design factors of safety for their specific application.

The SEE database is part of a relational database system and will be available to users nationwide over Internet. It gives all sectors of an engineering organization the capability to access the evaluated data. The M/VISION software enables users to query, reduce, compare and analyze the data. The database stores text and graphics data. The graphics data include digitized photographs, ESCA plots, charts, and other graphical representations. Where raw data exist for charts and graphs, the database system stores the data and recreates the charts and graphs if given simple user command input.

The database is designed to be compatible with other NASA systems such as MAPTIS. This compatibility ensures the ability to transfer the SEE data to other databases in the future.

The following is a proposed format for the M/VISION atomic oxygen database.

```
                  __Structural materials
                  |__Optical materials
                  |__Optical coatings
AO_________       |__Thermal materials
                  |__Thermal coatings
                  |__Tribological
                  |__Detectors
                  |__AO-protective coatings
                  |__High-temperature superconductors
```

Some materials may appear in several categories, e.g., Al_2O_3 is a thermal bulk material and an AO-protective coating. Within each category, information will be stored in a typical M/VISION hierarchy. The typical M/VISION metadata structure is:

```
Material
   |
Specimen
   |
  Test
   |
Property
```

All information is stored in named attributes, e.g., an attribute CNAME might contain the common name of the material: CNAME="Kapton." Each level contains several attributes. Numerical data may be stored as single numbers, e.g., an emittance could be EMIT=0.2. They may also be stored as x-y data, e.g., an absorption spectrum:

280	0.1
290	0.2
300	0.5

Digitized photographs are stored in a matrix; the integer in a bitmap value contains the color and brightness of the corresponding pixel in a bitmap, e.g.,

127	30	3	...
57	11	8	...
..	..	.	...

Where applicable, use standard M/VISION attribute names, e.g., G13T for a shear modulus. In the "Type" column, C denotes a text (character) attribute, I a single integer, R a

single real number, X an x-y array of real numbers, and M a matrix of integers. In the "Units" column, "°C; K" means that M/VISION will store and display temperature as °C, but a conversion factor will be supplied if the user wants K. Attributes should be defined with the same name, description, and units in all categories where they appear.

More information about the typical M/VISION metadata structure follows.

Material: Description, manufacturers, and composition. The attributes apply to each category:

Attribute	Type	Description of attribute	Example of attribute
COMMAT	C	Comments on material	Poor AO resistance
MATSPC	C	Material specification	QQ-A-250/11
MATPRC	C	Material processing specification	CVD
CNAME	C	Common name	Graphite/polysulfone
TNAME	C	Trade name	
CHNAME	C	Chemical name	Graphite/poly(diphenylsulfone)
FORMUL	C	Chemical formula	$C/[-(Ph_2CSO_2)-]_n$
MANUF	C	Manufacturer	DuPont
SUPPL	C	Supplier name & address	Bruce Banks,...
PMC	C	Polymer matrix composite code	U00CA123PSU4567

Specimen: Identifying numbers, geometry, and processing and handling procedures. The same attributes apply to each category. M/VISION can accept data in scientific notation: 1E-5 denotes 1×10^{-5}.

Attribute	Type	Description of attribute	Example of attribute	Units
COMMSP	C	Comments on specimen	Pinholes	
JPLID	C	JPL sample ID	1A1C	
SHAPE	C	Shape	Disk	
BAKCND	C	Baking conditions	48 h, 1E-5 torr, 60°C	
CONRH	R	Conditioning RH, pre-weighing	50	%
CONTEM	R	Conditioning temp.	25	°C; K
CONTIM	R	Conditioning time	6	h
GTHICK	R	Sample thickness	0.01	cm; in.
GWID	R	Sample width (of rectangle)	1	cm; in.
GLEN	R	Sample length (of rectangle)	1	cm; in.
GDIA	R	Sample diameter (of disk)	0.8	cm; in.
GAREA	R	Sample area	0.5	cm^2; $in.^2$

Test: Test site (ground-based or flight), contact names, AO source, test conditions. The same attributes apply to each category.

Attribute	Type	Description of attribute	Example of attribute	Units
SETCOND	C	Test conditions		
FACIL	C	Test facility	JPL Minton; EOIM-3	
PINAME	C	PI's name	Minton; Leger	
PIADDR	C	PI's address	JPL 67-201...	
PITEL	C	PI's tel #; FAX #	(818) 354-8580 (818) 393-6869	
TNAME	C	Test title		
FACILT	C	Test facility type	"Pulsed valve" or "flight"	
AOMETH	C	Method of determining AO efficiency	Profilometry	
DURAT	C	Test duration	40	h
LAUNCH	C	Flight launch date	May 8, 1992 13:30:12 EST	
PERIGE	R	Orbit perigee	250	km; nmi
APOGEE	R	Orbit apogee	300	km; nmi
INCLIN	R	Orbit inclination	28	°
TTEMP	R	Test temperature	60	°C; K
FLUENC	R	Test AO fluence	2E20	cm^{-2}
FLUX	R	Test AO flux	1.2E15	$cm^{-2}\ s^{-1}$
TDUR	R	Test duration	50	h
AOEN	R	Mean AO energy	3	eV
NUMSPC	I	# of specimens tested	1	

Properties: Pre-test and post-test data will be recorded where appropriate, e.g., MASSBT = mass before test, MASSAT = mass after test. M/VISION can calculate and display differences between pre- and post-test values.

The uncertainties in numeric data may be recorded more conveniently as text comments than as a large set of numeric attributes.

The following attributes will be the same for each category:

Attribute	Type	Description of attribute	Example of attribute	Units
COMMPR	C	Comments on errors, properties, etc.	all masses +/- 0.1 mg(1 s.d.)	
MASSBB	R	Mass before baking	0.5083	g
MASSBT	R	Mass before test	0.5081	g
MASSAT	R	Mass after test	0.5051	g
ESCABVSEN	X	ESCA graph pre-test		Intensity vs. energy/eV
ESCAAVSEN	X	ESCA graph post-test		Intensity vs. energy/eV
ESCABT	C	ESCA table pre-test		
ESCAAT	C	ESCA table post-test		
PHOTBT	M	Photo before test		
PHOTAT	M	Photo after test		

Each category will have the additional attributes listed on the following pages:

Structural materials:

Attribute	Type	Description of attribute	Example of attribute	Units
MICROC	C	Microcracking	Slight	
SPECGR	R	Specific gravity	3	None
FIBERC	R	Fiber content volume/volume	30	%
US11T	R	Ultimate strength in 11 direction in tension	83	MPa; ksi
US12T	R	Ultimate strength in 12 direction	56	MPa; ksi
US11C	R	Ultimate strength in compression, 11 direction	58	MPa; ksi
US11F	R	Ultimate strength in flexure	48	MPa; ksi
US11SP	R	Ultimate strength in punch shear	35	MPa; ksi
E11T...	R	Extension (Young's) modulus	2	GPa; Msi
G13T...	R	Shear modulus, 13 direction	1	GPa; Msi
ELONG	R	Elongation after test	5	%
CTE	R	Coefficient of thermal exp.	2.8	ppm K^{-1}
CTC	R	Coefficient of thermal con.	5	W m^{-2} K^{-1}
CP	R	Specific heat at constant pressure	1	J kg^{-1} K^{-1}; cal g^{-1} $°C^{-1}$
TMIN	R	Minimum use temperature	-20	°C; K
TG	R	Glass transition temperature	60	°C; K
TMAX	R	Maximum use temperature	150	°C; K
TD	R	Decomposition temperature	200	°C; K

Structural materials (continued):

Attribute	Type	Description of attribute	Example of attribute	Units
VOLAT	C	Gaseous products from baking	CO, water	
EMIT	R	Emittance	0.7	None
ABS	R	Absorbance	0.8	None
HEMIR	R	Hemispherical infrared		
AOEFF	R	AO reaction efficiency	4E-24	cm^3 $atom^{-1}$
SEM	M	SEM photograph		
STEM	M	STEM photograph		

Optical materials:

Attribute	Type	Description of attribute	Example of attribute	Units
EMISSV	R	Normal emissivity	0.7	None
ABSSOL	R	Solar absorbance	0.8	None
REFL	R	Reflectance	0.97	None
REFLW	R	REFL wavelength	3.1	μm
REFLPK	R	Peak reflectance	0.99	None
REFLPW	R	REFLPK wavelength	3.4	μm
TIS	R	Total integrated scatter	0.97	None
TISW	R	TIS wavelength	632	nm
REFL VS WAVE	X	Reflectance spectrum		None vs. nm
BRDF VS DEG	X	Bidirectional reflectance distribution function		None vs. °
BRDFR	M	BRDF raster scan		
BRDFW	R	BRDF wavelength	10.6	μm
PROF VS DIST	X	Profilometer trace		μm vs. mm
STEP VS DIST	X	Talystep roughness trace		μm vs. mm
EDS VS EN	X	Electron dispersion spectrum		Counts vs. channel #
SEM	M	SEM photograph		
STEM	M	STEM photograph		
AFM	M	AFM photograph		

Optical coatings:

Attribute	Type	Description of attribute	Example of attribute	Units
REFL	R	Reflectance	0.97	None
REFLW	R	REFL wavelength	3.1	μm
REFLPK	R	Peak reflectance	0.99	None
REFLPW	R	REFLPK wavelength	3.4	μm
REFL VS WAVE	X	Reflectance spectrum		None vs. nm
BRDFR	M	BRDF raster scan		
BRDFW	R	BRDF wavelength	10.6	μm
BRDF VS DEG	X	Bidirectional reflectance distribution function		None vs. °
TIS	R	Total integrated scatter	0.97	None
TISW	R	TIS wavelength	632	nm
STEP VS DIST	X	Talystep roughness trace		μm vs. mm
EDS VS EN	X	Electron dispersion spectrum		Counts vs. channel #
SEM	M	SEM photograph		
TEM	M	TEM photograph		
AFM	M	AFM photograph		

Thermal materials:

Attribute	Type	Description of attribute	Example of attribute	Units
EMIT	R	Normal emittance	0.7	None
ABSSOL	R	Solar absorbance	0.8	None
PROF VS DIST	X	Profilometer trace		μm vs. mm
SEM	M	SEM photograph		
STEM	M	STEM photograph		
MICOPT	M	Optical microphotograph		
MICIR	M	Infrared microphotograph		

Thermal coatings:

Attribute	Type	Description of attribute	Example of attribute	Units
EMIT	R	Normal emittance	0.7	None
ABSSOL	R	Solar absorbance	0.8	None
SEM	M	SEM photograph		
STEM	M	STEM photograph		

Tribological:

Attribute	Type	Description of attribute	Example of attribute	Units
MU	R	Coefficient of rolling or sliding friction, μ	0.1	None
RAMANW	R	Raman laser wavelength	430	nm; angstrom
RAMAN VS WAVE	X	Raman spectrum		None vs. cm^{-1}
AES VS EV	X	AES spectrum		Counts vs. eV
XPS VS EV	X	XPS spectrum		Counts vs. eV

Detectors:

Attribute	Type	Description of attribute	Example of attribute	Units
RES	R	Sample resistance	28	Ω
VRESP	R	Voltage responsivity	1	mV W^{-1}
VRESPF	R	VRESP frequency	60	Hz
IRESP VS WAVE	X	Current responsivity vs. wavelength		μA W^{-1} vs. μm
RBS VS DEG	X	Rutherford backscattering		Intensity vs. °
SEM	M	SEM photograph		

AO-protective coatings:

Attribute	Type	Description of attribute	Example of attribute	Units
EMISSV	R	Normal emissivity	0.7	None
ABSSOL	R	Solar absorbance	0.8	None
REFL	R	Reflectance	0.97	None
REFLW	R	REFL wavelength	3.1	μm
REFLPK	R	Peak reflectance	0.99	None
REFLPW	R	REFLPK wavelength	3.4	μm
REFL VS WAVE	X	Reflectance spectrum		None vs. nm
BRDF VS DEG	X	Bidirectional reflectance distribution function		None vs. °
BRDFR	M	BRDF raster scan		
BRDFW	R	BRDF wavelength	10.6	μm
TIS	R	Total integrated scatter	0.97	None
TISW	R	TIS wavelength	632	nm
STEP VS DIST	X	Talystep roughness trace		μm vs. mm
SEM	M	SEM photograph		
STEM	M	STEM photograph		

High-temperature superconductors:

Attribute	Type	Description of attribute	Example of attribute	Units
TC	R	Transition temperature, T_c	91	K
TCW	R	Width of transition	3	K
RVST	X	Resistance vs. temperature		Ω vs. K

TECHNICAL REPORT STANDARD TITLE PAGE

1. Report No. 93-31	2. Government Accession No.	3. Recipient's Catalog No.
4. Title and Subtitle Flight- and Ground-Test Correlation Study of BMDO SDS Materials: Phase I Report		5. Report Date December 1993 6. Performing Organization Code
7. Author(s) S. Y. Chung, D. E. Brinza, T. K. Minton, A. E. Stiegman, J. T. Kenny, and R. H. Liang		8. Performing Organization Report No.
9. Performing Organization Name and Address JET PROPULSION LABORATORY California Institute of Technology 4800 Oak Grove Drive Pasadena, California 91109		10. Work Unit No. 11. Contract or Grant No. NAS7-918 13. Type of Report and Period Covered JPL Publication
12. Sponsoring Agency Name and Address NATIONAL AERONAUTICS AND SPACE ADMINISTRATION Washington, D.C. 20546		14. Sponsoring Agency Code RE 182 PX-644-11-00-06-62
15. Supplementary Notes		

16. Abstract

The NASA Evaluation of Oxygen Interactions with Materials-3 (EOIM-3) experiment served as a testbed for a variety of materials that are candidates for Ballistic Missile Defense Organization (BMDO) space assets. The materials evaluated on this flight experiment were provided by BMDO contractors and technology laboratories. A parallel ground exposure evaluation was conducted using the FAST atomic-oxygen simulation facility at Physical Sciences, Inc. The EOIM-3 materials were exposed to an atomic oxygen fluence of approximately 2.3 x 10^{20} atoms/cm^2. The ground-exposed materials' fluence of 2.0 - 2.5 x 10^{20} atoms/cm^2 permits direct comparison of ground-exposed materials' performance with that of the flight-exposed specimens. The results from the flight test conducted aboard STS-46 and the correlative ground exposure are presented in this publication.

17. Key Words (Selected by Author(s)) Spacecraft Design, Testing, and Performance Materials (General) Laboratories, Test Facilities, and Test Equipment Space Radiation		18. Distribution Statement Unclassified; unlimited	
19. Security Classif. (of this report) Unclassified	20. Security Classif. (of this page) Unclassified	21. No. of Pages 246	22. Price

JPL 0184 R 9/83